SYNTHESIS OF FUNCTIONAL ZEOLITIC ADSORBENTS USING RICE HUSK ASH-DERIVED SiO_2 VIA DRY-GEL CONVERSION METHOD FOR REMOVAL OF POLLUTANTS FROM WATER

A Doctoral Dissertation by

Vanpaseuth PHOUTHAVONG

MARCH 2024

DEPARTMENT OF CHEMICAL SYSTEMS ENGINEERING

GRADUATE SCHOOL OF ENGINEERING

NAGOYA UNIVERSITY

Table of Content

CHAPTER 1

Introduction

Anthropogenic activities including rapid industrialization and agriculture are the main sources of environmental contamination, especially water pollution, arising due to the huge growth in global population. The Food and Agricultural Organization of the United Nations estimated that approximately 1.9 billion people will be affected by lacking of clean water sources by 2050 [1]. Unfortunately, various organic and inorganic compounds have been improperly discharged from industrial effluents, agricultural and daily activities as shown in Figure 1.1 [2]. Contamination of these compounds in water at unsafe levels led to water pollution which severely threatens human health and ecosystems. Development of effective removal tools of water contaminations are therefore necessary to support the large increasing in global clean water demand that may happen in near future.

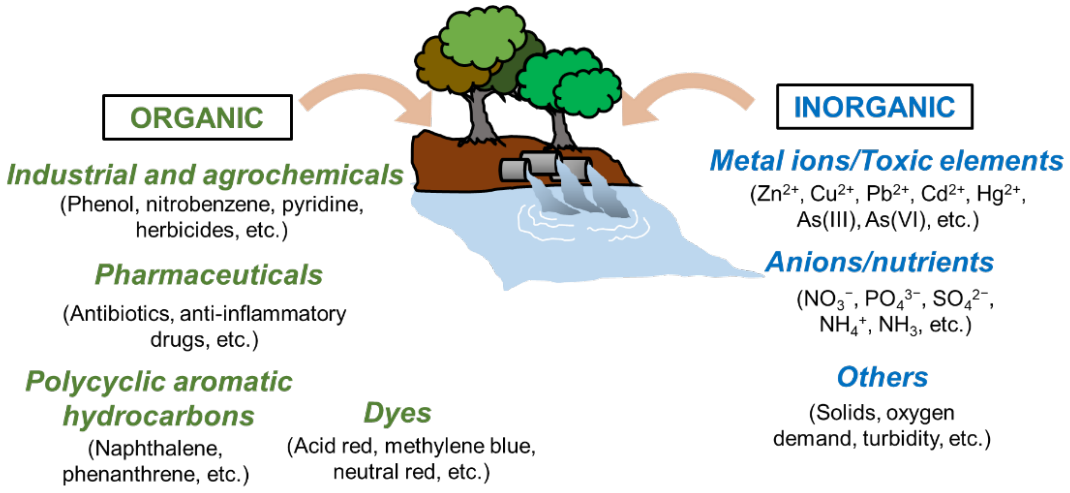

Figure 1.1 Various organic and inorganic pollutants discharged in water

Besides industry, it is reported that agriculture has become a leading source of water pollution [3]. In modern agricultural activities, huge amounts of agrochemicals are consumed in order to increase crops and livestock products for supplying the global food demand. Use of agrochemicals is not only accountable for improving crop and livestock production but for releasing harmful substances, i.e., inorganic cations (heavy metals) [4]

and anions (nitrogen and phosphorus) [5], pesticides (including herbicides and insecticides) [6], and contaminants of emerging concern (CECs), i.e., antibiotics and hormones, into waterbodies as well. Contamination of these substances in water sources definitely threatens human health and ecosystems [3,7]. Removal of these contaminants from water is consequently necessary which can be done by physical, chemical and biological methods [8]. The physical method, i.e., adsorption using adsorbents, is said to be the most effective way in that the diversity in adsorbents make this method suitable for attracting various types of pollutants with relative high removal efficiency. Moreover, handling of the adsorbents becomes simpler when the adsorbents are integrated with magnetic particles because the collection of the adsorbents can be accelerated by a magnetic field. This feature makes adsorbents more attractive and cost-effective. Among various adsorbents, microporous aluminosilicate materials, i.e., zeolites, is focused in this dissertation owing to their wide range adsorption abilities for organic and inorganic pollutants and stability, which play essential roles in wastewater treatment [9].

Laos is said to be one of the agriculture-based countries in that the economy and society rely on agriculture, accounting for approximately one fourth of Gross Domestic Product [10]. More than 90% of the agricultural area is used for rice production, especially sticky rice which is a typical food in daily meals for Lao people. Moreover, the land is also used for growing other essential crops such as cassava, soybeans, cotton, sugarcane, coffee, etc. Therefore, a large quantity of agricultural wastes, including rice husk, sugarcane tops, and cassava stalks, is produced annually, reaching approximately twelve million tons in 2016 [11]. Besides crop productions, livestock manufacturing is also potentially growing in Laos which consequently leads to increasing the consumption of antibiotics and generation of livestock manures [11,12]. Since waste management capacities in Laos are reported to be insufficient, handling of an overloaded amount of waste is therefore problematic. Utilizing of agricultural wastes as biomass for producing green energy mainly leave behind residue as secondary wastes. Ash that left behind from the incineration of rice husk is an example of the aforementioned problem. On the other hand, rice husk ash is said to have highly silica (SiO_2) content (approximately 90% [13]) which can be further utilized as a lower-cost SiO_2

source for preparing SiO_2-based advanced materials, such as magnetic zeolite composites. The application of such recycled waste as a SiO_2 source in the conventional hydrothermal methods yet causes environmental issue since a large amount of solvent is consumed in the synthesis and to wash the products, resulting in vast amount of wastewater. Dry-gel conversion method is considered as a promising route for synthesis of magnetic zeolite composites since it provides uniform crystalline products with higher yield compared to the conventional hydrothermal route [14]. This method practically requires no washing of the product after synthesis which means generation of waste becomes less. Thus, dry-gel conversion is environmentally friendly method. Moreover, if the agricultural waste-derived materials, i.e., rice husk ash-derived SiO_2, can be directly utilized as a SiO_2 source in dry-gel conversion method, the synthesis route of zeolites shall be more sustainable and eco-friendlier. The magnetic zeolite composites obtained from the proposed method can be exploited as adsorbents for removal of contaminants from water that is affected from using agrochemicals. This shall be implemented not only in Laos but for global community in order to reduce water pollution.

Figure 1.2 illustrates the overall concept of this doctoral research theme which aims for addressing the sustainability of utilizing and circulating materials which comply with the Sustainable Development Goals (SDGs). Scope of this doctoral research is to develop an environmentally friendly and sustainable synthesis method for magnetic zeolite composites by:

(i) utilizing agricultural waste-derived materials, i.e., rice husk ash-derived SiO_2, as a low-cost ingredient in synthesizing magnetic zeolite composites via dry-gel conversion method, and

(ii) evaluating adsorption performance of the composites for removal of agrochemical contaminants from water.

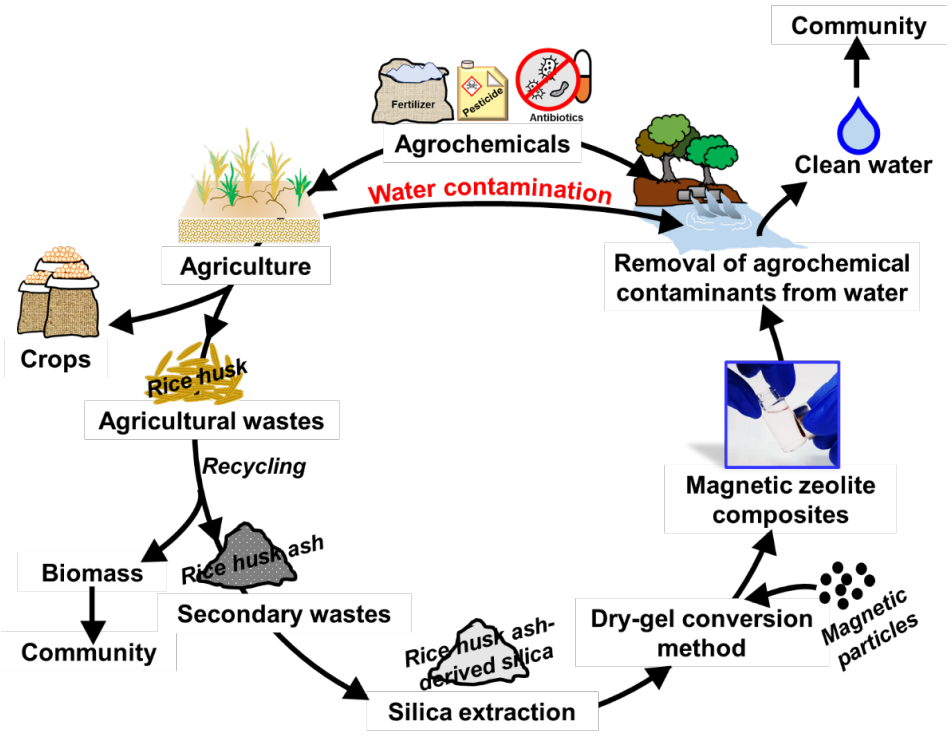

Figure 1.2 Overall concept of this doctoral research theme.

1.1 Removal of pollutants in water by adsorption

Adsorption in wastewater treatment is a process that the target pollutant(s) (adsorbate(s)) is transferred from the water phase to the surface of adsorbent through attractive forces [15]. Types of interaction taken place between the adsorbate(s) and the adsorbent surface vary depending on nature of the pollutant(s) and adsorbent. The interaction can be categorized based on the activation energy of adsorption. Ones with lower energy than 40 kJ/mol [16] are classified as physisorption such as Van Der Waals and dipole-dipole forces [17], or interactions that do not alter the electronic state of the adsorbate(s), i.e., electrostatic interaction and chelation [18]. Whereas chemisorption takes place via stronger interactions with higher energy than this energy level [16]. During the adsorption, transferring of the target pollutant(s) to the adsorbent surface generally takes place via three kinetic steps as shown in Figure 1.3. In step 1, the adsorbate(s) diffuses from the bulk solution through the external boundary layer, called external diffusion. Then, the adsorbate(s) diffuses in pores of the adsorbent which located inside the adsorbent. Therefore,

this step is called internal diffusion, pore-diffusion [19] or intraparticle diffusion [20]. Finally, the adsorbate(s) interacts with the active sites of the adsorbent through surface reaction [19].

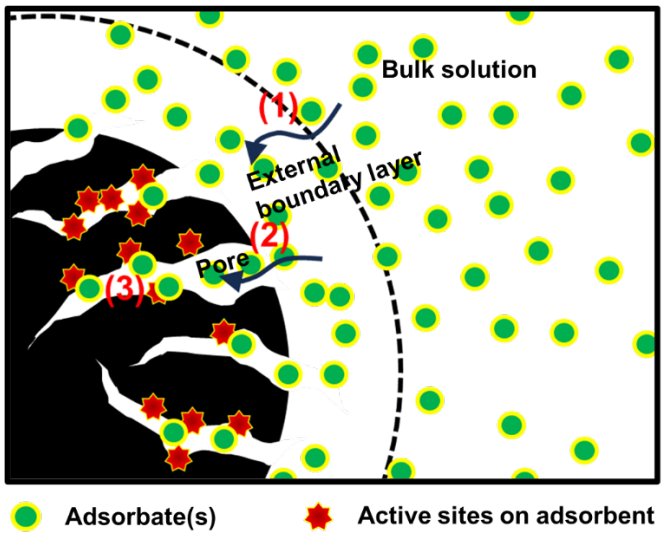

Figure 1.3 Three kinetic steps take place during adsorption on porous materials [20].

Several factors regarding the properties of adsorbents define the effectiveness of adsorption, such as surface area, surface functional groups, pore sizes, pore dimension, and pore distribution [21]. Moreover, economic factors such as synthesis cost and reusability are also of importance. However, when compared with various wastewater treatment techniques, adsorption is considered as a simple, cost-effective, and ecofriendly physical process which shows pollutant removal efficiency up to 99.9%. The high efficiency makes it the best water treatment technique according to the United States Environmental Protection Agency [8].

Types of adsorbents are actually diverse. Classification of adsorbents used in wastewater treatment is thus ambiguous because there is unclear boundary among them. Adsorbents that have been widely used in wastewater treatment for decades such as activated carbon, ion exchange polymeric resin, and zeolites are classified as conventional adsorbents [22]. Owing to the variety in emerging pollutants, many novel adsorbents, such as new materials, modification or combination of conventional adsorbents with different

functional materials as composites, have been developed. Many types of adsorbents have also been developed and employed in removal of agrochemical contaminants from water. Some examples of the adsorbents reported in the literatures are shown in Table 1.1. Among various adsorbents, zeolites are a group of aluminosilicate compounds with well-defined pore sizes, synthesizable with tunable composition, and thermally stable [23]. They show excellent adsorption properties toward a broad range of target substances. For these reasons, zeolites have received attention in this doctoral research.

Table 1.1 Adsorbents used in removal of potential agrochemicals from wastewater

Pollutants	Examples of adsorbents
Pesticides (including herbicides, insecticides, and fungicides)	Carbonaceous materials (activated carbon, biochar, etc.) [24], biopolymers [24], graphene-based materials [24], metal organic frameworks (MOFs) [24], fly ash [24], *zeolites* [24], agricultural-waste biosorbents [6], clays [6]
Heavy metals	Carbonaceous materials (activated carbon, biochar, carbon nanotubes (CNTs), and graphene oxide-based materials) [25,26], MOFs [27], covalent organic frameworks (COFs) [28], layered double hydroxides (LDHs) [29], agricultural-waste biosorbents [30], *zeolites* [31], clays [32], mesoporous SiO_2 [33]
Antibiotics	Carbonaceous materials (including activated carbon, biochar and their composites, etc.) [34], MOFs [34], clays [34], agricultural-waste biosorbents [34], biopolymers [34], *zeolites* [35], metal oxides [36], COFs [36], molecular imprinted polymers [37], polymer of intrinsic microporosity [38]
Hormones	Carbonaceous materials (including activated carbon, biochar, carbon nanotubes) [39], LDHs [39], biopolymers [39], agricultural-waste biosorbents [39], *zeolites* [40]

1.2 Zeolites and their environmental applications

Zeolites, named as "boiling stones" in 1756 by a Swedish mineralogist Axel Fredrik Cronsted [23], who firstly observed steam released when the material was heated, are naturally generated as a result of thousand-of-year reaction between hot magma erupted from volcano and sea water [41]. Zeolites are crystalline materials that are generally composed of silicon (Si), aluminum (Al), and oxygen (O) as the so-called aluminosilicate compounds. The Si–O and Al–O bonds form tetrahedral $[SiO_4]^{4-}$ and $[AlO_4]^{5-}$ primary building units (PBU), respectively, and connect to each other by a shared O atom as T–O–T, where T represents Si or Al (Figure 1.4), with a general chemical formula: $M_{a/b}[(AlO_2)_a(SiO_2)_y]\cdot cH_2O$. In the formula of a unit cell, M is the counter cation i.e., Na^+, K^+. Ca^{2+}, H^+, etc., which balances the negative charge on $[AlO_2]^-$, *a* is the number of $[AlO_4]^{5-}$, *b* is the valence of the cation, *y* is the number of $[SiO_4]^{4-}$, and *c* is the amount of water molecule per unit cell [42,43].

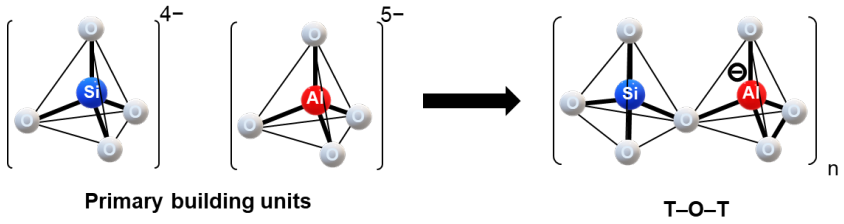

Figure 1.4 Tetrahedral $[SiO_4]^{4-}$ and $[AlO_4]^{5-}$ primary building units and their connection as T–O–T.

The linkage of PBUs in a unit cell create various secondary building units (SBUs) which further connect with each other to form tertiary units or to build polyhedra. These building units periodically connect with each other, yielding more than 220 various and uniform porous zeolite structures including natural and synthetic ones [44,45]. An example of LTA zeolite formation is illustrated in Figure 1.5.

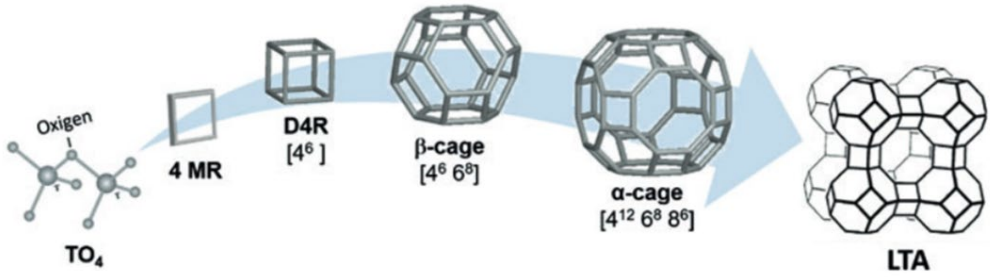

Figure 1.5 Formation of LTA zeolite from PBUs, SBUs (4MR), and tertiary units (D4R). TO_4 represents SiO_4 or AlO_4. Reprinted with permission from Schwanke, A.J., Balzer, R., Pergher, S. (2019). Microporous and Mesoporous Materials from Natural and Inexpensive Sources. In: Martínez, L., Kharissova, O., Kharisov, B. (eds) Handbook of Ecomaterials. Springer, Cham. [46], Springer Nature.

Zeolites were firstly discovered as naturally occurred compounds, until 1862 the first synthetic zeolite, levyne, was synthesized by Sainte-Claire-Deville M. H. [23,47]. Some well-known zeolite structures are illustrated in Figure 1.6, and more framework types can be found in the International Zeolite Association website: http://www.iza-online.org/.

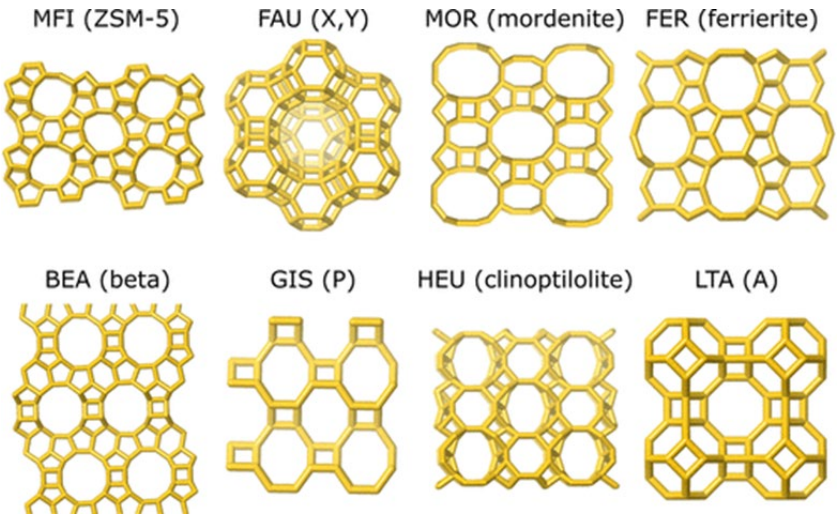

Figure 1.6 Structures of some well-known zeolites. Reprinted with permission from E. Pérez-Botella, S. Valencia, F. Rey [23], American Chemical Society, under the terms and conditions of the Creative Commons Attribution 4.0 (CC BY 4.0) license.

Zeolites can be classified based on their pore size ranges and Si/Al ratios. Basically, pore size of a unit zeolite crystal is below 2 nm which assigned to microporous materials. However, the interparticle connection of zeolite crystals creates different channels and cavities with larger size up to mesopore (2–50 nm) and macropore (>50 nm) ranges [48]. Zeolites are sometimes called small-pore (≤8-ring), medium-pore (10-ring), large-pore (12-ring), and extra-large-pore (≥12-ring) according to the number of PBUs that form the largest pore window (i.e., ring) [49] as shown in Figure 1.7.

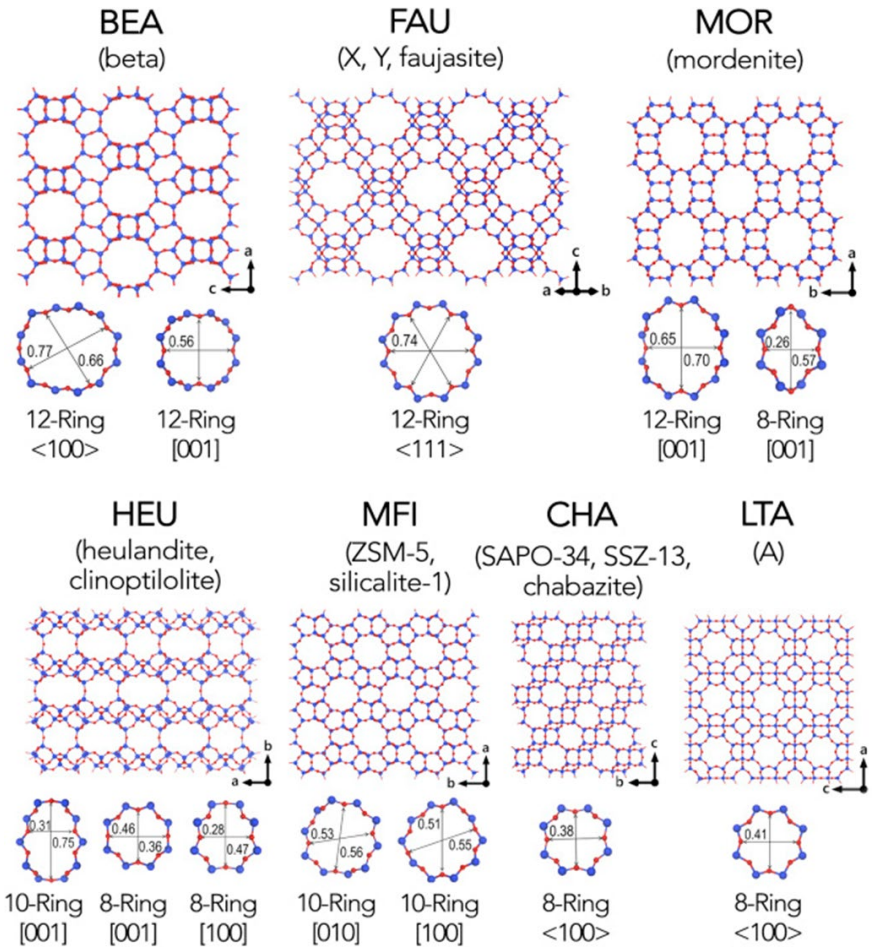

Figure 1.7 Structures of some common zeolites showing their pore sizes based on PBU number-ring [49]. Reprinted from Chem, 3, Yi Li, Lin Li, Jihong Yu, Applications of zeolites in sustainable chemistry, 928–949, Copyright (2017), with permission from Elsevier.

Based on the Si/Al ratio, zeolites can be categorized as low-silica or Al-rich, medium-silica, high-silica or Si-rich, and pure silica (Si/Al = ∞) zeolite. The definite ranges of Si/Al for a particular Al-rich or Si-rich zeolites vary depending on the framework types. For example, FAU-type becomes high-silica when the Si/Al > 3 while BEA-type is Si-rich when the Si/Al > 10 [50]. When the Si/Al changes, the amount of negative charge due to $[AlO_2]^-$ alters the hydrophobicity of zeolites, namely, the lower Al content, the higher hydrophobicity. Some other properties of zeolites are also strongly Si/Al ratio-dependent such as acidity, thermal stability, and catalytic properties [51]. These tunable Si/Al ratios with various pore sizes and unique properties of zeolites make them very useful in broad applications as catalysts in industries, biomass conversion, fuel cells, thermal energy storage [49,50], and adsorbents or ion exchangers in environmental treatment [50]. Zeolites are additionally approved as safe substances by the United States Food and Drug Administration, the European Food Safety Authority, the International Agency for Research on Cancer, and the Codex Alimentarius Commission, they are thus also applied in food productions as antimicrobial materials, fillers for food packaging and so on [52].

In spite of the fact that zeolites have wide range of applications, the scope of this dissertation will focus on environmental applications. Small-pore zeolites exhibit molecular sieve properties that are selective to specific molecules or ions, known as molecular sieve effect. Therefore, pore diffusion depends on size of the target molecules. This property is applied as zeolite membranes in gas separation to purify natural gases [53] or to capture toxic gases released from industrial productions [54]. Furthermore, owing to the optimizable hydrophobicity or ion exchange capacity, zeolites are utilized as adsorbents in removal of many organic and inorganic species from water during wastewater treatment. The application ranges from adsorption of inorganic species i.e., hardness-causing cations (Ca^{2+}, Mg^{2+}), heavy metals (Pb(II), Cd(II), Cr(III), Ni(II), Cu(II), etc.) to organic pollutants such as cationic organic dyes (methylene blue, rhodamine B, crystal violet, etc.), organic solvents (benzene, toluene), phenolic compounds, pesticides [55], and micro-organic pollutants (pharmaceuticals, personal care products, etc.) [56]. According to the literature survey, removal efficiency above 90% can be accomplished using zeolites. However,

sometimes adsorption performance of zeolites can be enhanced by modifying the surface or compositing with other materials such as minerals, metal oxides, magnetic particles, activated carbon, reduced graphene oxide, polymers, biopolymers [9], and photocatalysts [57]. One outstanding features among them is magnetic zeolite composites in which the magnetic content allows for easy collection of the adsorbents after adsorption process by means of external magnetic field. This advantage point is very useful in practical applications.

1.3 Magnetic adsorbents

Magnetic adsorbents are referred to adsorbents that show magnetic response to external magnetic field, which basically contains magnetic elements such as Fe, Co, and Ni. Some examples of magnetic adsorbents are iron oxides and ferrites (MFe_2O_4, where M can be Co, Ni, Mn, Zn, Mg, etc.) [58]. When these paramagnetic materials are placed in a magnetic field (*H*), their randomly aligned atomic magnetic moments rearrange in the same direction which results in a small net magnetic moment. These materials are also called ferromagnetic materials. Then, their magnetic strength (*M*) increases to saturation point, called saturation magnetization (M_s).

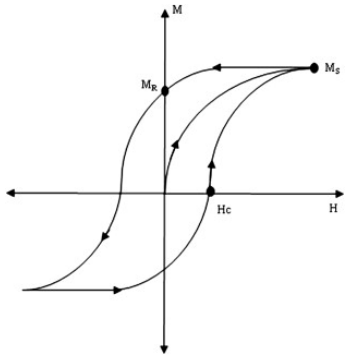

Figure 1.8 Hysteresis loop of magnetization when magnetic field is applied to ferromagnetic materials [59]. Reprinted from Progress in Crystal Growth and Characterization of Materials, 55, Amyn S. Teja, Pei-Yoong Koh, Synthesis, properties, and applications of magnetic iron oxide nanoparticles, 22–45, Copyright (2008), with permission from Elsevier.

When H is removed and reduces to zero, M values decreases but remains to some extent at remanence point (M_R). In order to completely return M values to zero, coercive field (H_C) must be applied in an opposite direction. Ferromagnetic materials typically create the hysteresis loop as shown in Figure 1.8 [59]. Magnetite (Fe_3O_4) is the most widely used magnetic particles among other magnetic iron oxides, i.e., maghemite (γ-Fe_2O_3) and hematite (α-Fe_2O_3), due to its superior magnetism, biocompatibility and environmentally friendliness [59,60]. Fe_3O_4 shows relatively high chemical reactivity and easily oxidizes, which degrades its magnetic properties. This drawback limits its direct use as adsorbents although it possesses adsorption ability to some extent owing to the abundancy of hydroxy groups on the surface upon exposure in aqueous environment [61]. However, the magnetic properties are widely implemented by integrating magnetic particles with diverse adsorbents such as clays (including zeolites), carbon-based materials, polymers, metal organic frameworks, covalent organic frameworks [62], and biosorbents [63]. In this manner, the collection of adsorbents is much easier than the conventional filtration or sedimentation of non-magnetic adsorbents. The used magnetically collected adsorbents can be regenerated and subsequently reused for another several cycles. The manipulation of magnetic separation at laboratory-scale can be simply done by decantation as presented in Figure 1.9 [64]. In practical larger scale, separation and collection of magnetic adsorbents could be carried out using gradient magnetic separators with various design as depicted in Figure 1.10 [65]. As seen, the separator can be operated in cyclic or continuous mode. Highly effective separation of magnetic adsorbents that have very small particle sizes can be accomplished using the separator design that equipped with magnetic flux density above 1 T [65].

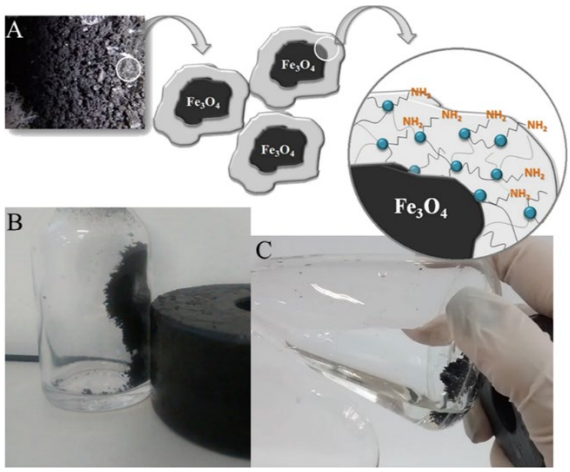

Figure 1.9 Magnetic separation of magnetic adsorbents in laboratory scale [64]. Reprinted with permission from "Mariana de Rezende Bonesio and Fábio Luiz Pissetti, Magnetite particles covered by amino-functionalized poly(dimethylsiloxane) network for copper(II) adsorption from aqueous solution, Journal of Sol-Gel Science and Technology, 94, 154–164, 2020, Springer Nature".

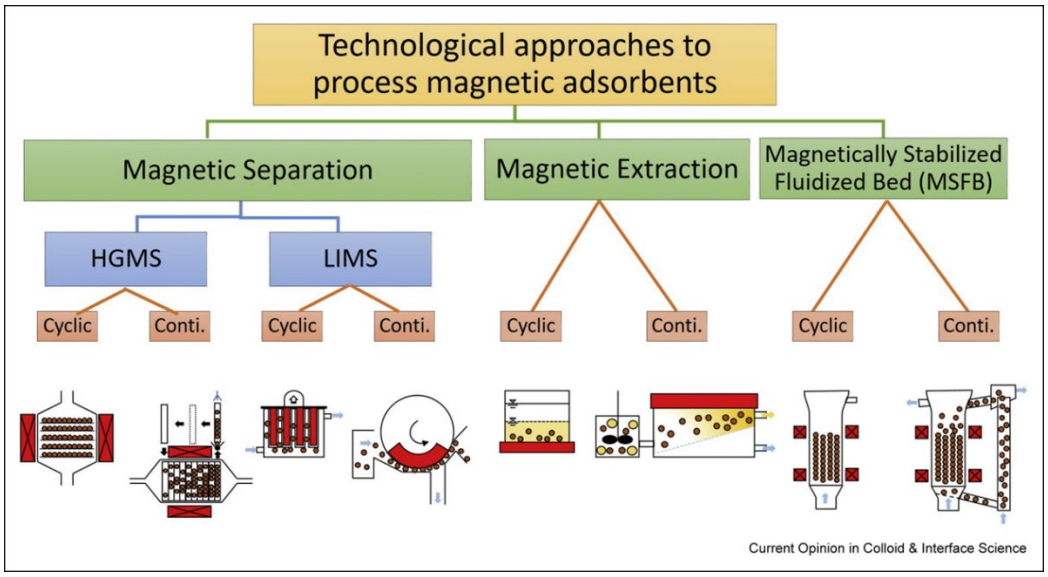

Figure 1.10 Magnetic separation technologies in larger scales using gradient-magnetic separators [65]. Reprinted from Current Opinion in Colloid & Interface Science, 46, Matthias Franzreb, New classes of selective separations exploiting magnetic adsorbents, 65–76, Copyright (2020), with permission from Elsevier.

Considering the unique adsorption abilities of zeolites and the advantage of using magnetic particles, composite of these two materials is of interest in this dissertation. Magnetic zeolite is therefore evaluated as a good candidate that shall improve effectiveness and efficiency in removal of various types of pollutants from wastewater. Development of a synthesis method that provides magnetic zeolite with well-incorporation of magnetic particles and high productivity is still challenging.

1.4 Synthesis of magnetic zeolite composites

1.4.1 Conventional methods

So far, magnetic zeolite composites can be conventionally prepared by few routes (Figure 1.11). According to the literatures, attaching zeolites and magnetic particles (see route (i) in Figure 1.11), i.e., iron oxides, using adhesives is found to be the simplest way. Organic adhesive such as urethane in combination with a thinner [66] and polyvinyl alcohol [67] are used to bind pre-synthesized or commercial zeolite and magnetic particles together. The attachment can be easily carried out even at low temperature, i.e., 60 °C [66]. However, the physical binding between zeolites and magnetic particles could shorten the stability of the composites and the presence of adhesive shall affect the adsorption properties [68]. Another synthesis route is synthesizing magnetic particles in the presence of pre-synthesized or commercial zeolites using co-precipitation of iron salts [69] or pyrolysis of Fe(III)-impregnated zeolite under carboxylic acid vapor [70] (see route (ii) in Figure 1.11). In these ways, magnetic iron oxides are formed and precipitated on the surface of zeolites. As a result of the above two synthesis routes, the magnetic particles are not well protected which is prone to be easily oxidized when expose to aqueous solutions [71].

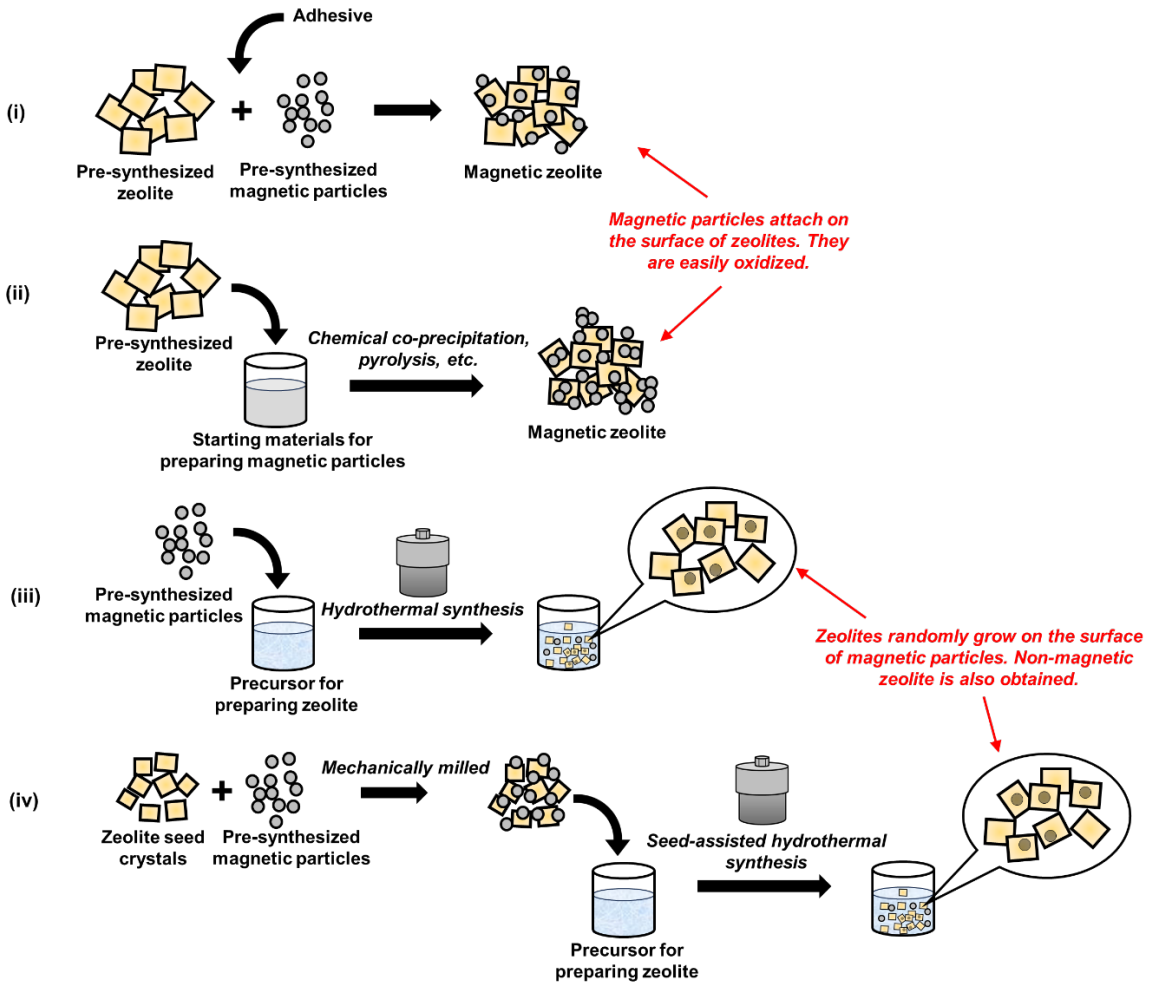

Figure 1.11 Conventional routes for synthesis of magnetic zeolite composites.

One more approach is crystallizing zeolites using conventional hydrothermal synthesis in the presence of pre-synthesized or commercial magnetic particles (see route (iii) in Figure 1.11). By this manner, crystallization of zeolite randomly takes place around magnetic particles which allows incorporation of some magnetic particles to be fixed inside zeolite crystals. However, the magnetic zeolite yield is relatively low since the crystallization relies on probability. To increase yield, the magnetic particles can be pre-mixed with zeolite seed crystals by methods such as mechanical milling in order to promote the nucleation right near the magnetic particles. Additionally, this method can also shorten the hydrothermal synthesis time by providing the nucleation points [72] (see route (iv) in Figure 1.11). The pre-milled additives create larger number of nuclei due to vast seed

embedment, resulting in smaller particle sizes in the final product. However, these methods are carried out in large solution volumes and require washing solutions to obtain clean products. A method that permits more crystallization of zeolite around the magnetic particles in a lower solution volume is necessary to reduce waste generation.

1.4.2 Dry-gel conversion method

In 1990, Xu et al. discovered that large excess amount of water is not necessary for crystallizing MFI zeolite during hydrothermal synthesis. In their experiments, a mixture of water, organic solvent and volatile organic template was separately placed at the bottom of the closed vessel, while the amorphous gel was placed on a porous sieve plate without direct contact with the solvents, as shown in Figure 1.12 [73]. This vapor-phase method allowed for reusing the solvents which reduced consumption of organic solvents. However, this method is not suitable when non-volatile organic templates are used.

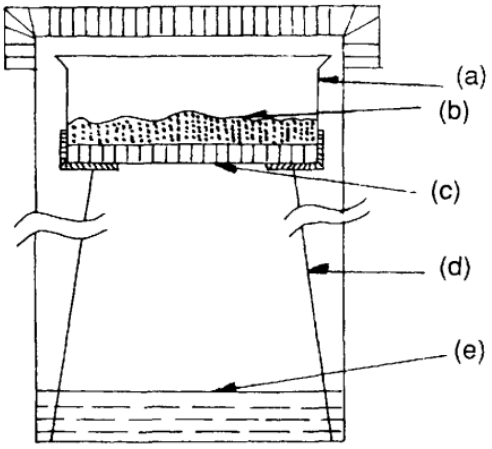

Figure 1.12 The reaction vessel used in vapor-phase method consists of container (a), amorphous gel (b), porous sieve plate (c), stainless steel supporter (d), and solution phase (e) [73]. Used with permission of Royal Society of Chemistry, from Journal of the Chemical Society, Chemical Communications, A novel method for the preparation of Zeolite ZSM-5, Xu et al., issue 10, 1990; permission conveyed through Copyright Clearance Center, Inc.

In 1993, Sano et al. attempted to monitored the crystal growth of MFI from dry amorphous gel under steaming conditions. This work succeeded in using an amorphous gel that was prepared by direct mixing the organic template with other precursor ingredients, and only water was required in the vapor supplier phase [74]. Three years later, Hari Prasad Rao and Matsukata succeeded in using a similar method to prepare high-silica BEA zeolite by converting a dried amorphous gel including tetraethyl ammonium hydroxide as a template to crystalline BEA zeolite under steam conditions. This method allowed for complete conversion of dry gel to zeolite crystals with a uniform particle size. The authors therefore called this method as dry-gel conversion (DGC) for the first time [75]. These developed methods indicate that large solution volume is not necessary for crystallization of zeolites–that means the crystallization can take place in a denser gel (Figure 1.13a). Hence, the synthesis of magnetic zeolite composite could become possible if magnetic particles are added during the amorphous gel preparation. The dense precursor gel shall be formed around each magnetic particle, resulting in well-incorporated magnetic particles inside the zeolite, as depicted in Figure 1.13b.

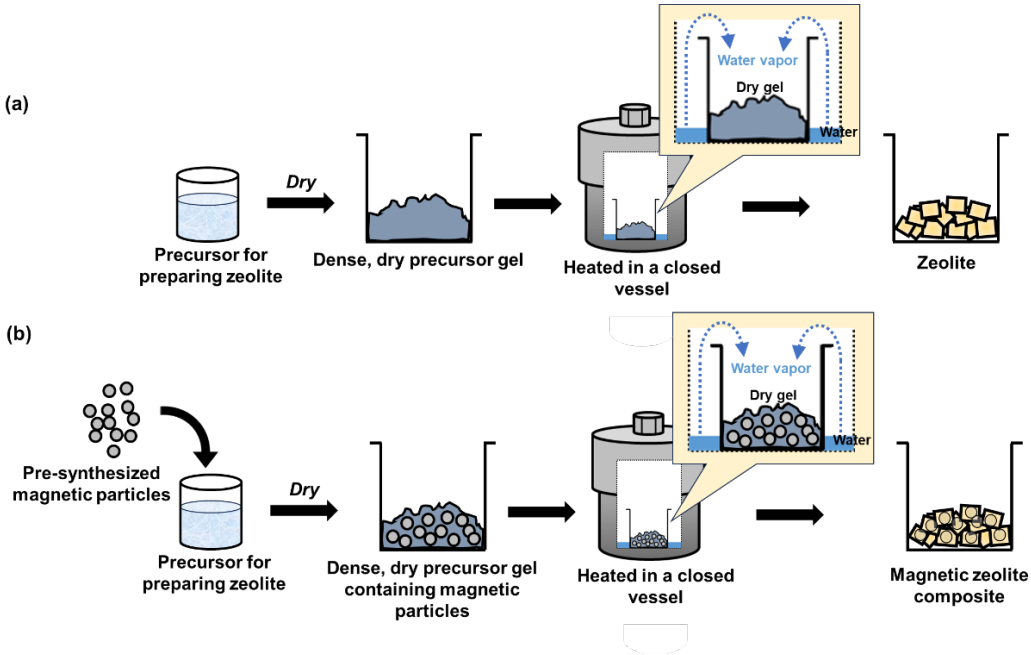

Figure 1.13 Dry-gel conversion synthesis of (a) non-magnetic zeolite, and (b) magnetic zeolite composite.

This anticipation has been proved by our laboratory in the preparation of magnetic high-silica BEA zeolite for the first time. Magnetic particle-contained dry precursor gel can be completely converted to BEA zeolite without any severe effect on the surface morphologies from the included magnetic particles. The inclusion of magnetic particles also did not disturb the adsorption of cationic dye in aqueous solutions [14]. This work revealed that using DGC method is possible to prepare composites. However, the DGC conditions for obtaining the magnetic zeolite composite with optimal crystallinity and surface morphologies have not been studied in detail yet. Also, given that lower reactor volume is used and no solvent is required for washing the solid product, DGC method is thus considered as an environmentally friendly method. Moreover, utilizing recycled waste as a source of starting materials in DGC is a good choice to provide more sustainable and eco-friendly synthesis method of magnetic zeolite composites. Due to the global abundance of agriculture wastes, this dissertation utilized such waste-derived material as stating material to demonstrate the hypothesis.

1.5 Agricultural wastes and their environmental utilizations

Agriculture is a main resource that greatly enhances global living standard and reduce malnutrition issues. Modern technologies that have been developed vastly increase agricultural production over the last 50 years to sufficiently supply food to the big growth in global population [76]. Along with the main agricultural products (i.e., crops, vegetables, fruits, etc.), waste and pollution are also generated simultaneously. However, agricultural wastes are found to be a good source of biomass, i.e., cellulose, hemicellulose, lignin, etc., that is utilized for bioenergy production [77] such as heat and electricity to replace the consumption of fossil fuels. Material circulation in production and consumption is one agenda included in the SDGs [78].

Plant-based agricultural wastes such as husk, straws, shell are abundant source of biopolymers, i.e., polysaccharides, which takes up more than 50% of the whole compositions [79]. Given that biopolymers have dominant functional groups, these materials can be thus used in environmental applications as raw or surface-modified biosorbents [2], or be converted to carbonaceous materials, i.e., biochar [80]. Numerous

raw and modified biosorbents have been utilized in removal of wide range of pollutants from water such as heavy metals [30], dyes [81], starting materials for producing plastics, i.e., bisphenol A [82], and CECs (i.e., pharmaceuticals, hormones, pesticides) [83]. Apart from organic contents, agricultural wastes also contain significant amount of inorganic matter, i.e., mineral ash, which can be traditionally reused as fertilizers [84]. Rice husk is an abundant agricultural waste that is generated from the massive global rice production, which is reused to produce bioenergy via burning. Approximately one fourth of the total mass of rice husk becomes ash after incineration [85]. Rice husk ash greatly contains amorphous SiO_2 up to 97% [13]. It is therefore a prospective alternative source for preparing zeolites [86–90]. The enormous availability of rice husk and its high SiO_2 content attracts this doctoral research in utilizing it to develop a low-cost, sustainable, and environmentally friendly synthesis method of magnetic zeolite composites.

1.6 Objective of this dissertation

Aim of this dissertation is to demonstrate the sustainable circulation of materials in agricultural activities. This work challenges to utilize agricultural waste-derived materials, rice husk ash-derived SiO_2, as a low-cost and alternative source of SiO_2 in DGC method for developing a sustainable and environmentally friendly synthesis method of magnetic BEA zeolite composite. Here, BEA zeolite was chosen since it has large pore sizes and can be prepared with various Si/Al ratios that could be adjustable for targeted pollutants. The magnetic BEA zeolite composite was evaluated as adsorbent for removal of pollutants from water that were potentially released from using agrochemicals, i.e., antibiotics, herbicides, and heavy metals, during agricultural activities. The overall objectives were achieved by carrying out the following experimental contents,

(i) studying the optimal synthesis conditions of DGC method for preparing magnetic BEA zeolite that was used for adsorption of antibiotics, and

(ii) synthesizing magnetic BEA zeolite using rice husk ash-derived SiO_2 in the optimal conditions of DGC, and evaluating it as adsorbent for removal of herbicide and heavy metals from water.

1.7 Structure overview of this dissertation

This dissertation consists of five chapters as follows,

(i) **Introduction.** This chapter introduces the overview on background of this doctoral research.

(ii) **Dry-gel conversion synthesis of magnetic BEA zeolite: optimization of synthesis conditions and assessment of antibiotic adsorption.** In this chapter, the optimal DGC conditions were studied for preparation of magnetic BEA zeolite that was tested for removal of antibiotics, i.e., sulfadiazine, from water.

(iii) **Using rice husk ash–SiO_2 in dry-gel conversion synthesis of magnetic BEA zeolite: assessment of herbicide removal.** This chapter presents the feasibility study of directly using solid-state rice husk ash–SiO_2 to prepare a magnetic contained dry gel that is converted to magnetic BEA zeolite via DGC method. The optimal conditions that were studied in Chapter 2 were applied. The composite was evaluated the adsorption performance on removal of herbicides, paraquat, from water.

(iv) **Removal of heavy metals from water using magnetic BEA zeolite prepared using rice husk ash-SiO_2 via DGC method.** This chapter presents the extension of using the rice husk ash–SiO_2 derived magnetic BEA zeolite that was prepared as lower Si/Al for adsorption of toxic heavy metals, i.e., Pb(II), Cu(II), and Zn(II).

(v) **Conclusion.** This chapter summarizes the research findings obtained from Chapter 2–4 and concludes the results in accordance to the main objectives.

References

[1] R.K. Sharma, K. Solanki, R. Dixit, S. Sharma, S. Dutta, Nanoengineered iron oxide-based sorbents for separation of various water pollutants: Current status, opportunities and future outlook, Environ. Sci. (Camb). 7 (2021) 818–860. https://doi.org/10.1039/d1ew00108f.

[2] N. Karić, A.S. Maia, A. Teodorović, N. Atanasova, G. Langergraber, G. Crini, A.R.L. Ribeiro, M. Đolić, Bio-waste valorisation: Agricultural wastes as biosorbents for removal of (in)organic pollutants in wastewater treatment, Chem. Eng. J. Adv. 9 (2022). https://doi.org/10.1016/j.ceja.2021.100239.

[3] A.E. Evans, J. Mateo-Sagasta, M. Qadir, E. Boelee, A. Ippolito, Agricultural water pollution: key knowledge gaps and research needs, Curr. Opin. Environ. Sustain. 36 (2019) 20–27. https://doi.org/10.1016/j.cosust.2018.10.003.

[4] M.N.E. Alam, M.M. Hosen, A.K.M.A. Ullah, M.A. Maksud, S.R. Khan, L.N. Lutfa, T.R. Choudhury, S.B. Quraishi, Pollution characteristics, source identification, and health risk of heavy metals in the soil-vegetable system in two districts of Bangladesh, Biol. Trace Elem. Res. 201 (2023) 4985–4999. https://doi.org/10.1007/s12011-023-03558-7.

[5] A. Aguilar-Aguilar, L.D. de León-Martínez, A. Forgionny, N.Y. Acelas Soto, S.R. Mendoza, A.I. Zárate-Guzmán, A systematic review on the current situation of emerging pollutants in Mexico: A perspective on policies, regulation, detection, and elimination in water and wastewater, Sci. Total Environ. 905 (2023) 167426. https://doi.org/https://doi.org/10.1016/j.scitotenv.2023.167426.

[6] I.A. Saleh, N. Zouari, M.A. Al-Ghouti, Removal of pesticides from water and wastewater: Chemical, physical and biological treatment approaches, Environ. Technol. Innov. 19 (2020). https://doi.org/10.1016/j.eti.2020.101026.

[7] D. Marcu, S. Keyser, L. Petrik, S. Fuhrimann, L. Maree, Contaminants of emerging concern (CECs) and male reproductive health: Challenging the future with a double-edged sword, Toxics. 11 (2023). https://doi.org/10.3390/toxics11040330.

[8] R. Rashid, I. Shafiq, P. Akhter, M.J. Iqbal, M. Hussain, A state-of-the-art review on wastewater treatment techniques: the effectiveness of adsorption method, Environ. Sci. Pollut. Res. 28 (2021) 9050–9066. https://doi.org/10.1007/s11356-021-12395-x.

[9] L. Roshanfekr Rad, M. Anbia, Zeolite-based composites for the adsorption of toxic matters from water: A review, J. Environ. Chem. Eng. 9 (2021). https://doi.org/10.1016/j.jece.2021.106088.

[10] T.M. Jackson, J. Newby, K. Phouyyavong, S. Vorlason, P. Simali, V. Sihathep, K. Zeleke, P. Sengxua, D. Harnpichitvitaya, L.J. Wade, Performance and adoption of submergence-tolerant TDK1-Sub1 rice in southern Lao PDR, Crop Environ. 1 (2022) 108–114. https://doi.org/https://doi.org/10.1016/j.crope.2022.04.001.

[11] B. Vongvisith, Z. Wudi, Y. Fang, W. Kai, L. Ming, J. Xiyan, W. Changmei, Z. Xingling, L. Jing, Y. Hong, Agricultural waste resources and biogas energy potential in rural areas of Lao PDR, Energy Sources A: Recovery Util. Environ. Eff. 40 (2018) 2334–2341. https://doi.org/10.1080/15567036.2018.1488017.

[12] M. Poupaud, V. Putthana, A. Patriarchi, D. Caro, A. Agunos, N. Tansakul, F.L. Goutard, Understanding the veterinary antibiotics supply chain to address antimicrobial resistance in Lao PDR: Roles and interactions of involved stakeholders, Acta Trop. 220 (2021) 105943. https://doi.org/https://doi.org/10.1016/j.actatropica.2021.105943.

[13] K. Kordatos, A. Ntziouni, L. Iliadis, V. Kasselouri-Rigopoulou, Utilization of amorphous rice husk ash for the synthesis of ZSM-5 zeolite under low temperature, J. Mater. Cycles Waste Manag. 15 (2013) 571–580. https://doi.org/10.1007/s10163-013-0141-x.

[14] V. Phouthavong, M. Hiraiwa, T. Hagio, S. Nijpanich, V. Chounlamany, T. Nishihama, Y. Kamimoto, R. Ichino, Magnetic BEA-type zeolites: preparation by dry-gel conversion method and assessment of dye removal performance, J. Mater. Cycles Waste Manag. 22 (2020) 375–382. https://doi.org/10.1007/s10163-020-00994-8.

[15] R. Yousef, H. Qiblawey, M.H. El-Naas, Adsorption as a process for produced water treatment: A review, Processes. 8 (2020) 1–22. https://doi.org/10.3390/pr8121657.

[16] V.J. Inglezakis, A.A. Zorpas, Heat of adsorption, adsorption energy and activation energy in adsorption and ion exchange systems, Desalination Water Treat. 39 (2012) 149–157. https://doi.org/10.1080/19443994.2012.669169.

[17] R.A. Sims, S.L. Harmer, J.S. Quinton, The role of physisorption and chemisorption in the oscillatory adsorption of organosilanes on aluminium oxide, Polymers (Basel). 11 (2019). https://doi.org/10.3390/polym11030410.

[18] A.N. Doyo, R. Kumar, M.A. Barakat, Recent advances in cellulose, chitosan, and alginate based biopolymeric composites for adsorption of heavy metals from wastewater, J. Taiwan Inst. Chem. Eng. 151 (2023) 105095. https://doi.org/https://doi.org/10.1016/j.jtice.2023.105095.

[19] J. Wang, X. Guo, Adsorption kinetic models: Physical meanings, applications, and solving methods, J. Hazard. Mater. 390 (2020) 122156. https://doi.org/https://doi.org/10.1016/j.jhazmat.2020.122156.

[20] K.L. Tan, B.H. Hameed, Insight into the adsorption kinetics models for the removal of contaminants from aqueous solutions, J. Taiwan Inst. Chem. Eng. 74 (2017) 25–48. https://doi.org/10.1016/j.jtice.2017.01.024.

[21] M.O. Usman, G. Aturagaba, M. Ntale, G.W. Nyakairu, A review of adsorption techniques for removal of phosphates from wastewater, Water Sci. Technol. 86 (2022) 3113–3132. https://doi.org/10.2166/wst.2022.382.

[22] G. Crini, E. Lichtfouse, L.D. Wilson, N. Morin-Crini, Adsorption-oriented processes using conventional and non-conventional adsorbents for wastewater treatment, in: G. Crini, E. Lichtfouse (Eds.), Green Adsorbents for Pollutant Removal: Fundamentals and Design, Springer International Publishing, Cham, 2018: pp. 23–71. https://doi.org/10.1007/978-3-319-92111-2_2.

[23] E. Pérez-Botella, S. Valencia, F. Rey, Zeolites in adsorption processes: State of the art and future prospects, Chem. Rev. 122 (2022) 17647–17695. https://doi.org/10.1021/acs.chemrev.2c00140.

[24] S. Bose, P. Senthil Kumar, G. Rangasamy, G. Prasannamedha, S. Kanmani, A review on the applicability of adsorption techniques for remediation of recalcitrant pesticides, Chemosphere. 313 (2023) 137481. https://doi.org/https://doi.org/10.1016/j.chemosphere.2022.137481.

[25] R.H. Krishna, M.N. Chandraprabha, K. Samrat, T.P. Krishna Murthy, C. Manjunatha, S.G. Kumar, Carbon nanotubes and graphene-based materials for adsorptive removal of metal ions – A review on surface functionalization and related adsorption mechanism, Appl. Surf. Sci. Adv. 16 (2023) 100431. https://doi.org/https://doi.org/10.1016/j.apsadv.2023.100431.

[26] B.K. Biswal, R. Balasubramanian, Use of biochar as a low-cost adsorbent for removal of heavy metals from water and wastewater: A review, J. Environ. Chem. Eng. 11 (2023) 110986. https://doi.org/https://doi.org/10.1016/j.jece.2023.110986.

[27] G. Lin, B. Zeng, J. Li, Z. Wang, S. Wang, T. Hu, L. Zhang, A systematic review of metal organic frameworks materials for heavy metal removal: Synthesis, applications and mechanism, Chem. Eng. J. 460 (2023) 141710. https://doi.org/https://doi.org/10.1016/j.cej.2023.141710.

[28] E.A. Gendy, J. Ifthikar, J. Ali, D.T. Oyekunle, Z. Elkhlifia, I.I. Shahib, A.I. Khodair, Z. Chen, Removal of heavy metals by covalent organic frameworks (COFs): A review on its mechanism and adsorption properties, J. Environ. Chem. Eng. 9 (2021) 105687. https://doi.org/https://doi.org/10.1016/j.jece.2021.105687.

[29] T. He, Q. Li, T. Lin, J. Li, S. Bai, S. An, X. Kong, Y.-F. Song, Recent progress on highly efficient removal of heavy metals by layered double hydroxides, Chem. Eng. J. 462 (2023) 142041. https://doi.org/https://doi.org/10.1016/j.cej.2023.142041.

[30] A. Alsulaili, K. Elsayed, A. Refaie, Utilization of agriculture waste materials as sustainable adsorbents for heavy metal removal: A comprehensive review, J. Eng. Res. (2023). https://doi.org/https://doi.org/10.1016/j.jer.2023.09.018.

[31] M.J. Zamzow, B.R. Eichbaum, K.R. Sandgren, D.E. Shanks, Removal of heavy metals and other cations from wastewater using zeolites, Sep. Sci. Technol. 25 (1990) 1555–1569. https://doi.org/10.1080/01496399008050409.

[32] S. Gu, X. Kang, L. Wang, E. Lichtfouse, C. Wang, Clay mineral adsorbents for heavy metal removal from wastewater: a review, Environ. Chem. Lett. 17 (2019) 629–654. https://doi.org/10.1007/s10311-018-0813-9.

[33] M.H. Salmani, M.H. Ehrampoush, H. Eslami, B. Eftekhar, Synthesis, characterization and application of mesoporous silica in removal of cobalt ions from contaminated water, Groundw. Sustain. Dev. 11 (2020) 100425. https://doi.org/https://doi.org/10.1016/j.gsd.2020.100425.

[34] J. Georgin, D.S.P. Franco, C.G. Ramos, D.G.A. Piccilli, E.C. Lima, F. Sher, A review of the antibiotic ofloxacin: Current status of ecotoxicology and scientific advances in its removal from aqueous systems by adsorption technology, Chem. Eng. Res. Des. 193 (2023) 99–120. https://doi.org/https://doi.org/10.1016/j.cherd.2023.03.025.

[35] A. Martucci, M.A. Cremonini, S. Blasioli, L. Gigli, G. Gatti, L. Marchese, I. Braschi, Adsorption and reaction of sulfachloropyridazine sulfonamide antibiotic on a high silica mordenite: A structural and spectroscopic combined study, Microporous Mesoporous Mater. 170 (2013) 274–286. https://doi.org/10.1016/j.micromeso.2012.11.031.

[36] Y. Zhou, J. Wang, Detection and removal technologies for ammonium and antibiotics in agricultural wastewater: Recent advances and prospective, Chemosphere. 334 (2023) 139027. https://doi.org/https://doi.org/10.1016/j.chemosphere.2023.139027.

[37] M. Parlapiano, Ç. Akyol, A. Foglia, M. Pisani, P. Astolfi, A.L. Eusebi, F. Fatone, Selective removal of contaminants of emerging concern (CECs) from urban water cycle via Molecularly Imprinted Polymers (MIPs): Potential of upscaling and enabling reclaimed water reuse, J. Environ. Chem. Eng. 9 (2021) 105051. https://doi.org/https://doi.org/10.1016/j.jece.2021.105051.

[38] M.N. Alnajrani, O.A. Alsager, Removal of antibiotics from water by polymer of intrinsic microporosity: isotherms, kinetics, thermodynamics, and adsorption mechanism, Sci. Rep. 10 (2020) 794. https://doi.org/10.1038/s41598-020-57616-4.

[39] B. Almazrouei, D. Islayem, F. Alskafi, M.K. Catacutan, R. Amna, S. Nasrat, B. Sizirici, I. Yildiz, Steroid hormones in wastewater: Sources, treatments, environmental risks, and regulations, Emerg. Contam. 9 (2023) 100210. https://doi.org/https://doi.org/10.1016/j.emcon.2023.100210.

[40] A. Pérez-González, V. Pinos-Vélez, I. Cipriani-Avila, M. Capparelli, E. Jara-Negrete, A. Alvarado, J.F. Cisneros, P. Tripaldi, Adsorption of estradiol by natural clays and daphnia magna as biological filter in an aqueous mixture with emerging contaminants, Eng. 2 (2021) 312–324. https://doi.org/10.3390/eng2030020.

[41] M. Moshoeshoe, M. Silas Nadiye-Tabbiruka, V. Obuseng, A Review of the chemistry, structure, properties and applications of zeolites, Am. J. Mater. Sci. 2017 (2017) 196–221. https://doi.org/10.5923/j.materials.20170705.12.

[42] A. Khaleque, M.M. Alam, M. Hoque, S. Mondal, J. Bin Haider, B. Xu, M.A.H. Johir, A.K. Karmakar, J.L. Zhou, M.B. Ahmed, M.A. Moni, Zeolite synthesis from low-cost materials and environmental applications: A review, Environ. Adv. 2 (2020) 100019. https://doi.org/https://doi.org/10.1016/j.envadv.2020.100019.

[43] M.O. Daramola, E.F. Aransiola, T. V. Ojumu, Potential applications of Zeolite membranes in reaction coupling separation processes, Materials. 6 (2013) 1432–1433. https://doi.org/10.3390/ma6041432.

[44] C. Li, M. Moliner, A. Corma, Synthese von Zeolithen aus vorkristallisierten Baustei-nen: Architektur im Nanomaßstab, Adv. Mater. 130 (2018) 15554–15578. https://doi.org/10.1002/ANGE.201711422.

[45] M.M. Zagho, M.K. Hassan, M. Khraisheh, M.A.A. Al-Maadeed, S. Nazarenko, A review on recent advances in CO_2 separation using zeolite and zeolite-like materials as adsorbents and fillers in mixed matrix membranes (MMMs), Chem. Eng. J. Adv. 6 (2021) 100091. https://doi.org/https://doi.org/10.1016/j.ceja.2021.100091.

[46] A.J. Schwanke, R. Balzer, S. Pergher, Microporous and Mesoporous Materials from Natural and Inexpensive Sources, in: L.M.T. Martínez, O.V. Kharissova, B.I. Kharisov (Eds.), Handbook of Ecomaterials, Springer International Publishing, Cham, 2019: pp. 3379–3399. https://doi.org/10.1007/978-3-319-68255-6_43.

[47] H. de S. Claire-Deville, Reproduction de la levyne, Comptes Rendus. 54 (1862) 324–327.

[48] N. Salahudeen, A Review on zeolite: application, synthesis and effect of synthesis parameters on product properties, Chem. Afr. 5 (2022) 1889–1906. https://doi.org/10.1007/s42250-022-00471-9.

[49] Y. Li, L. Li, J. Yu, Applications of zeolites in sustainable chemistry, Chem. 3 (2017) 928–949. https://doi.org/https://doi.org/10.1016/j.chempr.2017.10.009.

[50] J. Li, M. Gao, W. Yan, J. Yu, Regulation of the Si/Al ratios and Al distributions of zeolites and their impact on properties, Chem. Sci. 14 (2022) 1935–1959. https://doi.org/10.1039/d2sc06010h.

[51] M. Sadrara, M. Khanmohammadi Khorrami, J. Towfighi Darian, A. Bagheri Garmarudi, Rapid determination and classification of zeolites based on Si/Al ratio using FTIR spectroscopy and chemometrics, Infrared Phys. Technol. 116 (2021) 103797. https://doi.org/https://doi.org/10.1016/j.infrared.2021.103797.

[52] C.C. Villa, G.A. Valencia, A. López Córdoba, R. Ortega-Toro, S. Ahmed, T.J. Gutiérrez, Zeolites for food applications: A review, Food Biosci. 46 (2022) 101577. https://doi.org/https://doi.org/10.1016/j.fbio.2022.101577.

[53] Z. Cao, N.D. Anjikar, S. Yang, Small-pore zeolite membranes: a review of gas separation applications and membrane preparation, Separations. 9 (2022). https://doi.org/10.3390/separations9020047.

[54] T. Yu, Z. Chen, Z. Liu, J. Xu, Y. Wang, Review of hydrogen sulfide removal from various industrial gases by zeolites, Separations. 9 (2022). https://doi.org/10.3390/separations9090229.

[55] L.F. de Magalhães, G.R. da Silva, A.E.C. Peres, Zeolite application in wastewater treatment, Adsorpt. Sci. Technol. 2022 (2022) 4544104. https://doi.org/10.1155/2022/4544104.

[56] N. Jiang, R. Shang, S.G.J. Heijman, L.C. Rietveld, High-silica zeolites for adsorption of organic micro-pollutants in water treatment: A review, Water. Res. 144 (2018) 145–161. https://doi.org/10.1016/j.watres.2018.07.017.

[57] G. Hu, J. Yang, X. Duan, R. Farnood, C. Yang, J. Yang, W. Liu, Q. Liu, Recent developments and challenges in zeolite-based composite photocatalysts for environmental applications, Chem. Eng. J. 417 (2021) 129209. https://doi.org/https://doi.org/10.1016/j.cej.2021.129209.

[58] T. Tatarchuk, L. Soltys, W. Macyk, Magnetic adsorbents for removal of pharmaceuticals: A review of adsorption properties, J. Mol. Liq. 384 (2023) 122174. https://doi.org/https://doi.org/10.1016/j.molliq.2023.122174.

[59] A.S. Teja, P.-Y. Koh, Synthesis, properties, and applications of magnetic iron oxide nanoparticles, Prog. Cryst. Growth Charact. Mater. 55 (2009) 22–45. https://doi.org/https://doi.org/10.1016/j.pcrysgrow.2008.08.003.

[60] M.D. Nguyen, H.V. Tran, S. Xu, T.R. Lee, Fe_3O_4 nanoparticles: Structures, synthesis, magnetic properties, surface functionalization, and emerging applications, Appl. Sci. (Switzerland). 11 (2021). https://doi.org/10.3390/app112311301.

[61] M.K. Shahid, Y. Kim, Y.-G. Choi, Magnetite synthesis using iron oxide waste and its application for phosphate adsorption with column and batch reactors, Chem. Eng. Res. Design 148 (2019) 169–179. https://doi.org/https://doi.org/10.1016/j.cherd.2019.06.001.

[62] Z. Shen, Y. Kuang, S. Zhou, J. Zheng, G. Ouyang, Preparation of magnetic adsorbent and its adsorption removal of pollutants: An overview, TrAC Trends Anal. Chemi. 167 (2023) 117241. https://doi.org/https://doi.org/10.1016/j.trac.2023.117241.

[63] A.I. Osman, E.M.A. El-Monaem, A.M. Elgarahy, C.O. Aniagor, M. Hosny, M. Farghali, E. Rashad, M.I. Ejimofor, E.A. López-Maldonado, I. Ihara, P.-S. Yap, D.W. Rooney, A.S. Eltaweil, Methods to prepare biosorbents and magnetic sorbents for water treatment: a review, Environ. Chem. Lett. 21 (2023) 2337–2398. https://doi.org/10.1007/s10311-023-01603-4.

[64] M. de Rezende Bonesio, F.L. Pissetti, Magnetite particles covered by amino-functionalized poly(dimethylsiloxane) network for copper(II) adsorption from aqueous solution, J. Sol-gel Sci. Technol. 94 (2020) 154–164. https://doi.org/10.1007/s10971-019-05154-5.

[65] M. Franzreb, New classes of selective separations exploiting magnetic adsorbents, Curr. Opin. Colloid Interface Sci. 46 (2020) 65–76. https://doi.org/https://doi.org/10.1016/j.cocis.2020.03.012.

[66] I.W. Nah, K.-Y. Hwang, Y.-G. Shul, A simple synthesis of magnetically modified zeolite, Powder Technol. 177 (2007) 99–101. https://doi.org/https://doi.org/10.1016/j.powtec.2007.02.044.

[67] S. Buzukashvili, W. Hu, R. Sommerville, O. Brooks, O. Kökkılıç, N.A. Rowson, P. Ouzilleau, K.E. Waters, Magnetic zeolite: synthesis and copper adsorption followed

by magnetic separation from treated water, Crystals (Basel). 13 (2023) 1369. https://doi.org/10.3390/cryst13091369.

[68] V. Phouthavong, R. Yan, S. Nijpanich, T. Hagio, R. Ichino, L. Kong, L. Li, Magnetic adsorbents for wastewater treatment: advancements in their synthesis methods, Materials. 15 (2022). https://doi.org/10.3390/ma15031053.

[69] L.C.A. Oliveira, D.I. Petkowicz, A. Smaniotto, S.B.C. Pergher, Magnetic zeolites: a new adsorbent for removal of metallic contaminants from water, Water Res. 38 (2004) 3699–3704. https://doi.org/https://doi.org/10.1016/j.watres.2004.06.008.

[70] A.B. Bourlinos, R. Zboril, D. Petridis, A simple route towards magnetically modified zeolites, Microporous and Mesoporous Materials. 58 (2003) 155–162. https://doi.org/https://doi.org/10.1016/S1387-1811(02)00613-3.

[71] A.R. Loiola, R.A. Bessa, C.P. Oliveira, A.D.L. Freitas, S.A. Soares, F. Bohn, S.B.C. Pergher, Magnetic zeolite composites: classification, synthesis routes, and technological applications, J. Magn. Magn. Mater. 560 (2022). https://doi.org/10.1016/j.jmmm.2022.169651.

[72] T. Hagio, S. Nijpanich, H. Kunishi, K. Yamaoka, V. Phouthavong, Y. Kamimoto, R. Ichino, K. Iwai, Synthesis of MOR zeolite/magnetite composite via seed assisted method, J. Nanosci. Nanotechnol. 19 (2019) 6841–6848. https://doi.org/10.1166/jnn.2019.17123.

[73] W. Xu, J. Dong, J. Li, J. Li, F. Wu, A novel method for the preparation of zeolite ZSM-5, J. Chem. Soc. Chem. Commun. (1990) 755–756. https://doi.org/10.1039/C39900000755.

[74] T. Sano, Y. Kiyozumi, F. Mizukami, A. Iwasaki, M. Ito, M. Watanabe, In-situ observation of crystal growth of zeolite ZSM-5 under steaming conditions by optical microscopy, Microporous Materials. 1 (1993) 353–357. https://doi.org/https://doi.org/10.1016/0927-6513(93)80051-U.

[75] P.R. Hari Prasad Rao, M. Matsukata, Dry-gel conversion technique for synthesis of zeolite BEA, Chem. Commun. (1996) 1441–1442.

[76] M. Duque-Acevedo, L.J. Belmonte-Ureña, F.J. Cortés-García, F. Camacho-Ferre, Agricultural waste: Review of the evolution, approaches and perspectives on alternative uses, Glob. Ecol. Conserv. 22 (2020) e00902. https://doi.org/https://doi.org/10.1016/j.gecco.2020.e00902.

[77] J.A. Kumar, S. Sathish, D. Prabu, A.A. Renita, A. Saravanan, V.C. Deivayanai, M. Anish, J. Jayaprabakar, O. Baigenzhenov, A. Hosseini-Bandegharaei, Agricultural waste biomass for sustainable bioenergy production: feedstock, characterization and pre-treatment methodologies, Chemosphere. 331 (2023) 138680. https://doi.org/https://doi.org/10.1016/j.chemosphere.2023.138680.

[78] M. Duque-Acevedo, I. Lancellotti, F. Andreola, L. Barbieri, L.J. Belmonte-Ureña, F. Camacho-Ferre, Management of agricultural waste biomass as raw material for the construction sector: an analysis of sustainable and circular alternatives, Environ. Sci. Eur. 34 (2022) 70. https://doi.org/10.1186/s12302-022-00655-7.

[79] A.H. Nordin, A.S. Norfarhana, S.F.M. Noor, S.H. Paiman, M.L. Nordin, S.M.N. Husna, R.A. Ilyas, N. Ngadi, A.A. Bakar, Z. Ahmad, M.S. Azami, W.I. Nawawi, W. Nabgan, Recent advances in using adsorbent derived from agricultural waste for antibiotics and non-steroidal anti-inflammatory wastewater treatment: a review, Separations. 10 (2023). https://doi.org/10.3390/separations10050300.

[80] D.M. Juela, Promising adsorptive materials derived from agricultural and industrial wastes for antibiotic removal: a comprehensive review, Sep. Purif. Technol. 284 (2022) 120286. https://doi.org/https://doi.org/10.1016/j.seppur.2021.120286.

[81] J.O. Paul Nayagam, K. Prasanna, Utilization of shell-based agricultural waste adsorbents for removing dyes: A review, Chemosphere. 291 (2022) 132737. https://doi.org/https://doi.org/10.1016/j.chemosphere.2021.132737.

[82] F.M. Mpatani, R. Han, A.A. Aryee, A.N. Kani, Z. Li, L. Qu, Adsorption performance of modified agricultural waste materials for removal of emerging

micro-contaminant bisphenol A: a comprehensive review, Sci. Total Environ. 780 (2021) 146629. https://doi.org/https://doi.org/10.1016/j.scitotenv.2021.146629.

[83] M. Varsha, P. Senthil Kumar, B. Senthil Rathi, A review on recent trends in the removal of emerging contaminants from aquatic environment using low-cost adsorbents, Chemosphere. 287 (2022) 132270. https://doi.org/https://doi.org/10.1016/j.chemosphere.2021.132270.

[84] F. Akhter, S.A. Soomro, A.R. Jamali, Z.A. Chandio, M. Siddique, M. Ahmed, Rice husk ash as green and sustainable biomass waste for construction and renewable energy applications: a review, Biomass Convers. Biorefin. 13 (2023) 4639–4649. https://doi.org/10.1007/s13399-021-01527-5.

[85] S. Kumar Das, A. Adediran, C. Rodrigue Kaze, S. Mohammed Mustakim, N. Leklou, Production, characteristics, and utilization of rice husk ash in alkali activated materials: An overview of fresh and hardened state properties, Constr. Build. Mater. 345 (2022) 128341. https://doi.org/https://doi.org/10.1016/j.conbuildmat.2022.128341.

[86] S. Sivalingam, S. Sen, Rice husk ash derived nanocrystalline ZSM-5 for highly efficient removal of a toxic textile dye, J. Mater. Res. Technol. 9 (2020) 14853–14864. https://doi.org/10.1016/j.jmrt.2020.10.074.

[87] W. Rongchapo, O. Sophiphun, K. Rintramee, S. Prayoonpokarach, J. Wittayakun, Paraquat adsorption on porous materials synthesized from rice husk silica, Water Sci. Technol. 68 (2013) 863–869. https://doi.org/10.2166/wst.2013.311.

[88] Y. Wang, T. Du, H. Jia, Z. Qiu, Y. Song, Synthesis, characterization and CO_2 adsorption of NaA, NaX and NaZSM-5 from rice husk ash, Solid State Sci. 86 (2018) 24–33. https://doi.org/10.1016/j.solidstatesciences.2018.10.003.

[89] C.G. Flores, H. Schneider, J.S. Dornelles, L.B. Gomes, N.R. Marcilio, P.J. Melo, Synthesis of potassium zeolite from rice husk ash as a silicon source, Clean. Eng. Technol. 4 (2021). https://doi.org/10.1016/j.clet.2021.100201.

[90] D. Prasetyoko, Z. Ramli, S. Endud, H. Hamdan, B. Sulikowski, Conversion of rice husk ash to zeolite beta, Waste Manag. 26 (2006) 1173–1179. https://doi.org/10.1016/j.wasman.2005.09.009.

CHAPTER 2

Dry-gel conversion synthesis of magnetic BEA zeolite: optimization of synthesis conditions and assessment of antibiotic adsorption

2.1 Background

2.1.1 Antibiotics in environments: sources and effects

The discovery of antibiotics in the 20th century has greatly increased human lifespan and plays important roles in modern medical treatments [1]. The main functions of antibiotics are treating and preventing infections in humans and animals [2]. Antibiotics can be classified into natural, semisynthetic, and synthetic ones based on their origin and production manner. More than thirty thousand of natural products found in bacteria and fungi are said to behave antibiotic properties, and the synthetic antibiotics are derived from the natural ones, e.g., the well-known penicillin [3]. Not only preventing human from disease, antibiotics are also used in the production of livestock and poultry. In agricultural production, there are several classes of antibiotics that were mostly used such as ionophores, arsenicals, tetracycline, penicillin, sulfonamides, aminoglycosides, and fluoroquinolones [4]. Chemical structures of some antibiotics belong to these classes are depicted in Figure 2.1.

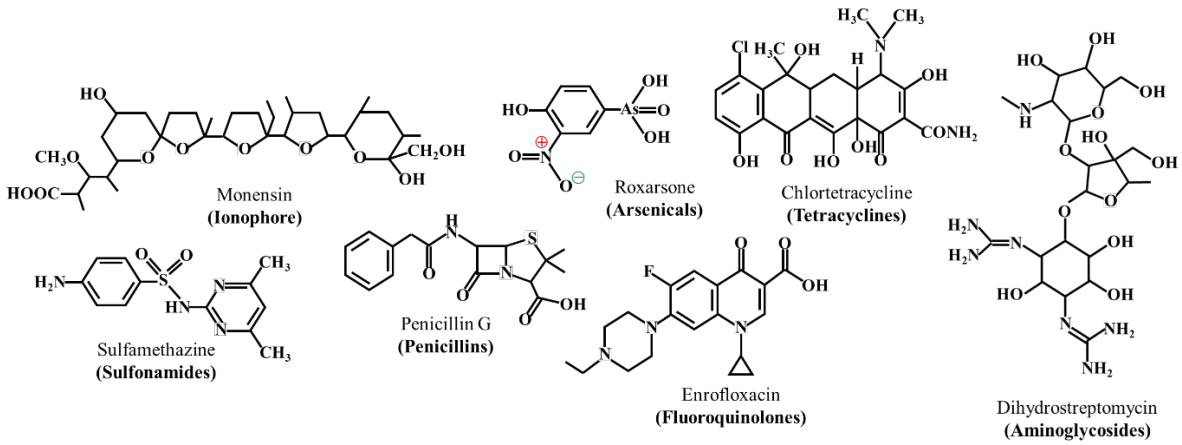

Figure 2.1 Chemical structures of some antibiotics belong to the most widely used groups.

The global consumption of antibiotics in livestock and poultry production is estimated to be 104,079 tonnes in 2023 [5]. Using antibiotics can enhance the livestock production efficiency and prevent the spreading of infection between the animals and farmers [6]. However, it was reported that most of the consumed antibiotics are hardly absorbed by the digestion system, therefore they released from the animal bodies through excretion [7]. Generally, livestock manure is further utilized as fertilizers in agricultural fields. Thus, this becomes one of the starting points of antibiotics releasing pathway into environment as shown in Figure 2.2 [8].

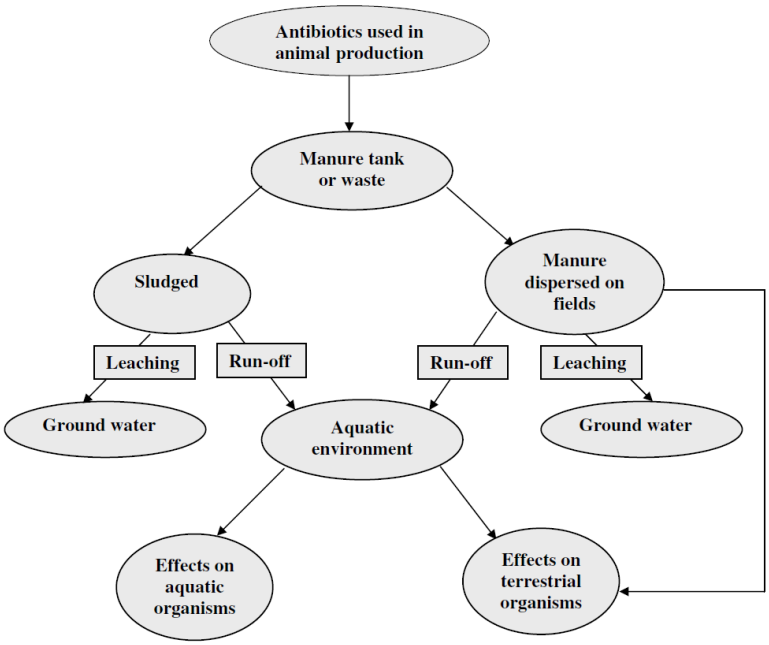

Figure 2.2 Expected releasing pathway of antibiotics from animal production [8]. Reprinted from Chemosphere, 65, A.K. Sarmah, M.T. Meyer, A.B.A. Boxall, A global perspective on the use, sales, exposure pathways, occurrence, fate and effects of veterinary antibiotics (VAs) in the environment, 725–759, Copyright (2006), with permission from Elsevier.

Anh et al. have studied on antibiotic contamination status in surface water in East and Southeast Asian countries which revealed that various classes of antibiotic were detected ranging from few ng/L levels to hundreds μg/L levels [9]. Although the contamination of

antibiotics was found at trace to ultra-trace levels, this level is enough to greatly affect the endocrine system in human [10]. The forms of antibiotics exist in environments, especially in water, are still active. This leads to the accumulating and spreading of their metabolite products in the water and nearby environments. The existing of antibiotics also disturbs the function of bacteria in metabolism of aquatic animal wastes [8]. Antibiotic contamination in water additionally interrupts the growth and reproduction and causes liver toxicity of organisms [11]. Releasing of antibiotics into water therefore becomes global environmental concerns. Awareness of proper treating antibiotic contaminated water has become important in many countries which leads to urgent issuance of regulations for minimizing the problems. The United State Environmental Protection Agency has classified veterinary medicines, i.e., including antibiotics, as a group among contaminants of emerging concern. In this chapter, sulfonamides are selected as a representative pollutant among widely used antibiotics, since they have a broad range of bacterial infections treatment in human and animals [12] and been used for a long time. Typical chemical structures of sulfonamides and some sulfonamide antibiotics are presented in Figure 2.3.

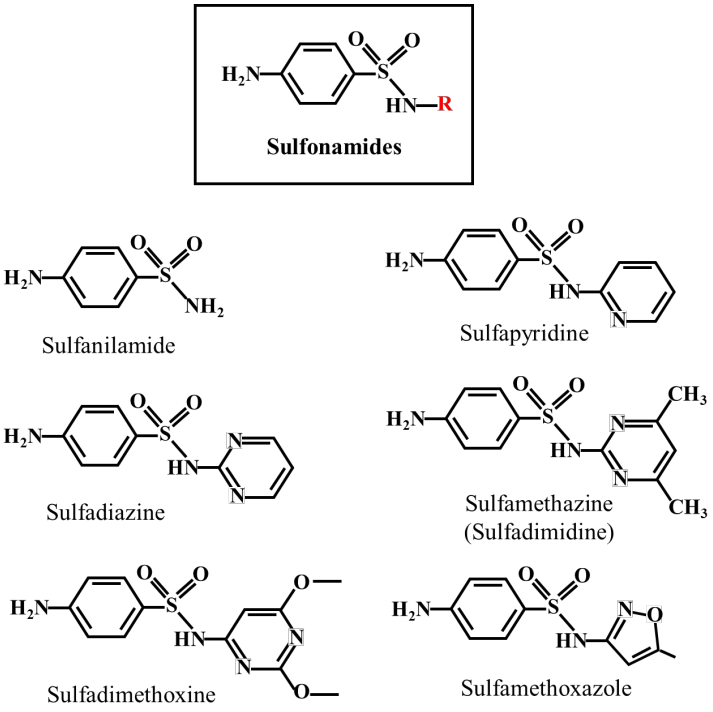

Figure 2.3 Typical structure of sulfonamides and some sulfonamide antibiotics.

2.1.2 Removal of sulfonamide by adsorption using zeolitic adsorbents

There are several types of zeolites ranging from medium to large pore sizes that were previously examined and potentially showed adsorption ability for removal of several sulfonamides from water. In most cases, the adsorption was found more pronounced when large pore zeolites with high Si/Al ratios ranging from 200 to 1000 were used such as MFI, FAU, and MOR [13], compared to medium to small pore ones, i.e., LTA, and hydrophilic HEU zeolites [14,15]. These findings reveal that most sulfonamides were adsorbed via hydrophobic interaction [14,16]. Some other interactions such as hydrogen bond between silanol groups on zeolite and amine groups on sulfonamide, and van de Waals forces were also found [14]. However, sulfonamide antibiotics can be ionized to cationic or anionic forms according to the pH values [15]. The adsorption is promoted when the pH of solutions was in acidic region due to the electrostatic interaction between the cationic site on sulfonamide and the negative charge on $[AlO_2]^-$ of the zeolite framework [17]. In most literatures, Freundlich adsorption isotherm model was found suitable to explain the adsorption behavior of sulfonamide on zeolites. This model reflects the physisorption of sulfonamide through multilayer adsorption on zeolite surface.

In addition to the adsorption performance, the zeolites showed numbers of reusability after regeneration by using solvent extraction or heat treatment [18]. As seen that large-pore and high-SiO_2 zeolites are preferable for sulfonamide adsorption via hydrophobic interaction. BEA zeolite is another large pore zeolites with rather high hydrophobicity, therefore it should be a promising candidate which has not been previously used for removal of sulfonamide antibiotics from wastewater. Moreover, the integration of magnetic moiety of the zeolitic adsorbents is beneficial in practical removal of sulfonamide antibiotics.

2.1.3 BEA zeolite

BEA, a code name for zeolite beta given by the International Zeolite Association, is a large pore 12-membered ring zeolite with a diameter of 0.76 × 0.64 and 0.55 × 0.55 nm [19]. BEA zeolite was first synthesized by Wadlinger et al. in 1967 [20], and was then found in 1988 that it is a highly faulted intergrowth of two different but correlated polymorphs,

i.e., A and B [21]. An example of stacking of polymorphs A and B that forms disordered structure of BEA zeolite is shown in Figure 2.4.

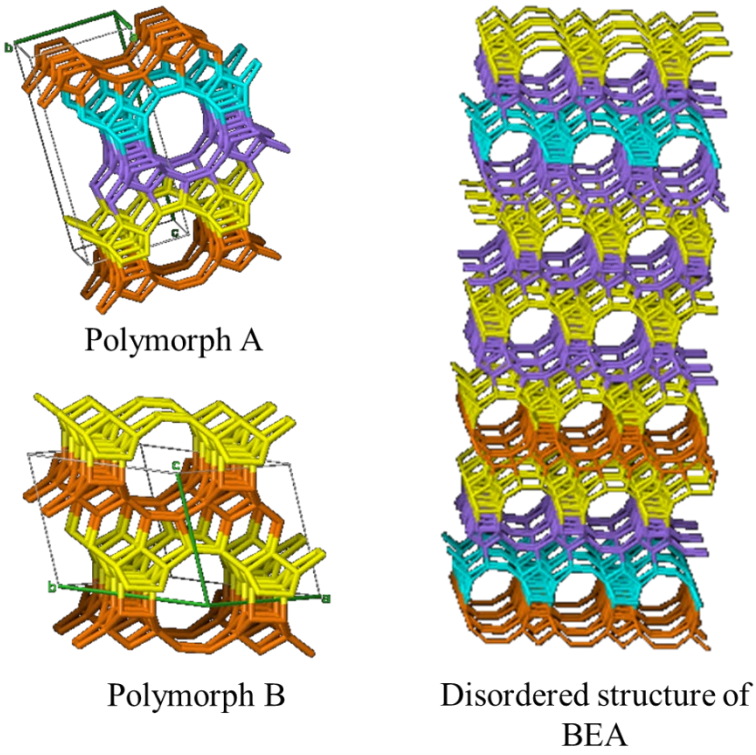

Figure 2.4 Polymorph A and B, and disordered structure of BEA zeolite (from Ch. Baerloche, L.B. McCusker, H. Gies and B. Marle, Database of Disordered Zeolite Structures, http://www.iza-structure.org/databases/)

BEA zeolite is one of the Big Five zeolites, i.e., MFI, BEA, MOR, FAU and FER, that are mostly used as catalyst in petrochemical industry [22]. It is a useful catalyst in many industrial reactions owing to its high Si/Al ratio, hydrothermal stability, and surface acidity [23]. For wastewater treatment purpose, BEA zeolite has been evaluated for adsorption of assorted pollutants such as pesticides [24,25], aromatic compounds (i.e., phenol [26], nitrobenzene [27]), alkaloids (i.e., nicotine [28]), organic dyes [29], and heavy metals [30,31]. These studies indicate that BEA zeolite also potentially shows adsorption performance on the broad range of pollutants.

2.1.4 Synthesis of magnetic BEA zeolite via DGC method

Generally, BEA zeolite is commercially available or can be prepared using the conventional hydrothermal method. Owing to the advantages of using DGC method in preparation of MFI zeolite that were discovered by Xu et al. [32], BEA zeolite was first successfully synthesized under the same method by Hari Prasad Rao and Matsukata in 1996 [33]. By using DGC method, dry precursor gel completely converted to BEA zeolite inside a low-volume reactor and the generation of wastewater barely produced. Approximately 3-time higher Si/Al ratio of BEA zeolite can be obtained within a shorter crystallization time when using DGC method with the assistance of an organic template, i.e., tetraethyl ammonium hydroxide (TEAOH). Furthermore, the crystal size is found uniform and has high crystallinity and thermal stability [34]. These features should be also beneficial for synthesis of zeolitic composites, i.e., magnetic zeolites. In 2020, our research group successfully adopted DGC method in the preparation of BEA zeolite/Fe_3O_4 composite for the first time [35]. The preliminary studies show that the crystallization of BEA zeolite was not hindered by the inclusion of Fe_3O_4. The magnetic Fe_3O_4 particles were well incorporated inside BEA zeolite particles, and the composite had uniform size. Though, this study only proved the idea of using DGC method in the preparation of composites. Further investigation of the influential synthesis parameters in the presence of magnetic particles and evaluation of the potential adsorption performance of the composite are necessary.

2.2 Objective

This chapter aims to investigate the possibility of using DGC method for preparation of magnetic BEA zeolites as an adsorbent for removal of sulfonamide antibiotic from water. The optimal DGC synthesis conditions were investigated and subsequently used for synthesis of magnetic BEA zeolite. Magnetic properties and adsorption performance of the synthesized magnetic composite sample were also investigated for removal of sulfadiazine (SFDZ), a representative sulfonamide antibiotic, from aqueous solutions. This work expects to represent the use of magnetic zeolite prepared by DGC method for remediation of antibiotic contaminated water released from livestock production.

2.3 Materials

Chemicals and equipment used in this work are listed in Table 2.1 and 2.2, respectively.

Table 2.1 Chemicals

Name (Formula, purity)	Manufacturer, country
Colloidal silica (SiO_2, HS-30, 30 wt% in water)	Sigma Aldrich, USA
Aluminum sulfate ($Al_2(SO_4)_3 \cdot 14\sim18H_2O$, 51.0–57.5% as $Al_2(SO_4)_3$)	Nacalai Tesque, Japan
Sodium hydroxide (NaOH, 97.0 wt%)	Nacalai Tesque, Japan
Tetraethylammonium hydroxide (TEAOH, 35 wt% in water)	TCI, Japan
Magnetite (Fe_3O_4, 80.0 wt%)	Kanto Chemical, Japan
Sulfadiazine ($C_{10}H_{10}N_4O_2S$, >99.0%)	TCI, Japan
Hydrochloric acid (HCl, 35.0–37.0wt%)	Nacalai Tesque, Japan
Phosphate buffer pH6.86 ± 0.015 (KH_2PO_4/Na_2HPO_4)	Kanto Chemical, Japan

TCI = Tokyo Chemical Industry

Table 2.2 Equipment

Name	Model	Manufacturer, country
Convection oven	SOFW-300SB	AS ONE Corporation, Japan
Hotplate stirrer	RSH-1DN	AS ONE Corporation, China
Electric furnace	VF-3000	SK Medical, Japan
Field emission-scanning electron microscope (FE-SEM)	JSM-6330F	JEOL, Japan
X-ray diffractometer (XRD, Cu-Kα, α = 1.54056 Å)	RINT 2500TTR	Rigaku Corporation, Japan
Vibrating-sample magnetometer (VSM)	BH-5501	Denshijiki Industry, Japan
pH meter	AS800	AS ONE Corporation, Japan
Orbital shaker	SK-O180-S	DLAB Scientific, China
UV-Visible spectrophotometer	UV-2450	Shimadzu, Japan

2.4 DGC synthesis and characterization of magnetic BEA zeolite

Gel composition and magnetic content in the gel used in our first reported work were adopted in this current work [35]. Brief synthesis procedure, depicted in Figure 2.5, consists of 2 main steps: i) preparation of dry precursor gel and ii) conversion of dry gel to zeolite by heating. To confirm whether the inclusion of Fe_3O_4 particles affects the crystallization of BEA zeolite, the gel without Fe_3O_4 particles was also prepared. The H_2O/gel weight ratio in the PTFE container, crystallization temperature and time were varied in order to investigate the optimal synthesis conditions. This will be discussed in the following sub-sections.

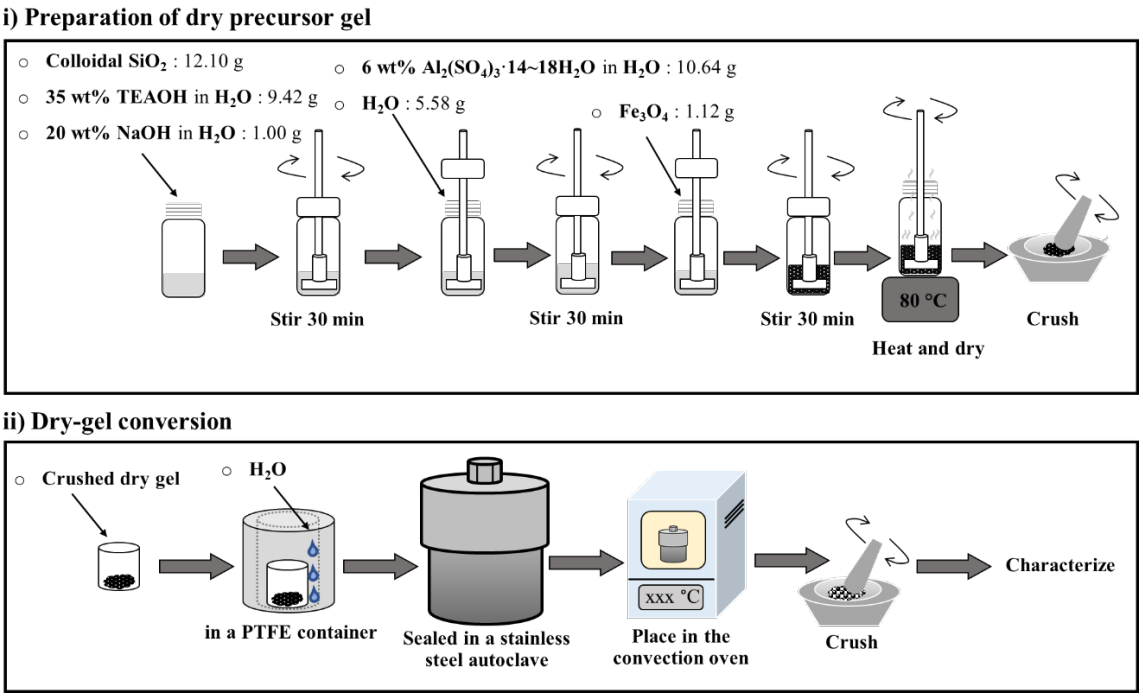

Figure 2.5 Procedure of magnetic BEA zeolite synthesis including i) preparation of dry precursor gel and ii) dry-gel conversion.

2.4.1 Effect of H_2O/gel ratio

In DGC, appropriate amount of water is required to ensure water vapor is maintain to be saturated during the crystallization [34]. Here, the optimal water amount used to generate steam was studied by changing H_2O/gel ratios while the synthesis temperature and time

were fixed (180 °C and 12 h). The results of XRD patterns and comparison of peak intensities are shown in Figure 2.6a. When the ratio was 0.5, amorphous phase with no characteristic peak of BEA-structure was observed by XRD, as well as no evidence of BEA crystallization observed by FE-SEM (Figure 2.7). This may be caused by insufficient amount of water for carrying energy to the precursor for crystallizing BEA zeolite. Using too low H_2O/gel ratio can lead to producing amorphous product as reported in the literature [33]. When the H_2O/gel ratio was increased to 1 and 2, the BEA peak intensity became obviously intense, as represents by the most intense peak at $2\theta = 22.5°$. Also, the FE-SEM images reveal the crystalline appearance of the BEA zeolite. The results were found in the same trend for both non-magnetic and magnetic BEA zeolite and confirm that amount of H_2O became sufficient when the ratios of 1 and 2 were used. In this case, the H_2O/gel ratio of 1 was chosen as it is enough for crystallizing BEA zeolite with the presence of Fe_3O_4.

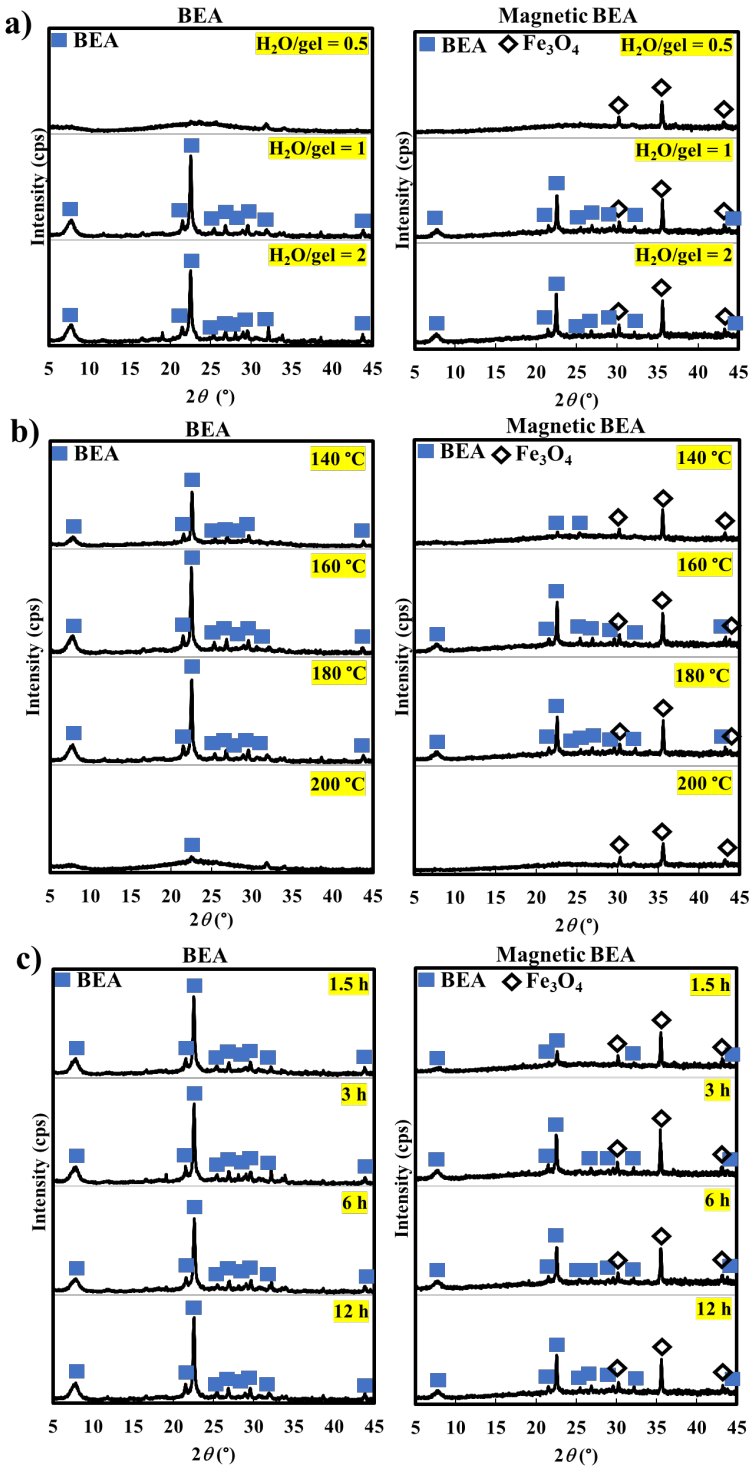

Figure 2.6 XRD patterns of BEA and magnetic BEA zeolite synthesized via DGC using varied a) H_2O/gel ratios, b) crystallization temperatures, and c) crystallization times.

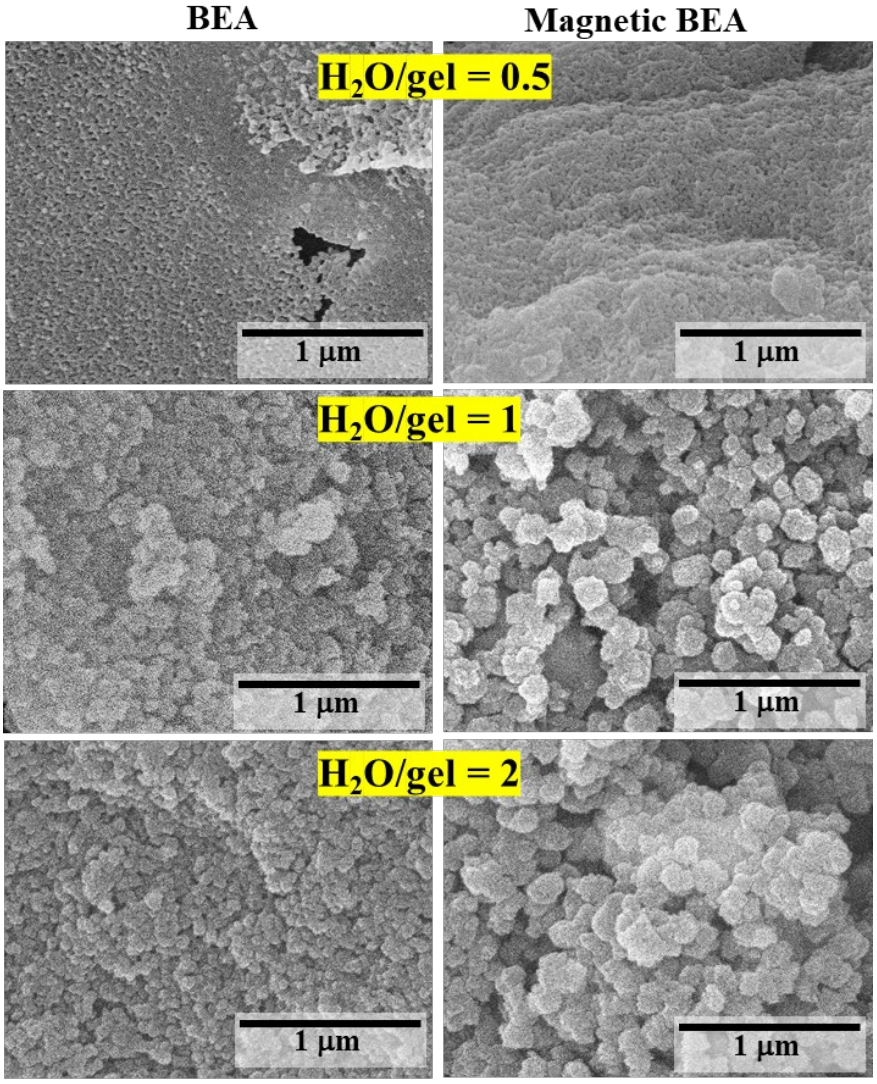

Figure 2.7 FE-SEM observation of BEA and magnetic BEA zeolite synthesized via DGC using varied H_2O/gel ratios.

2.4.2 Effect of crystallization temperature

Temperature plays crucial role in crystallization process and greatly affects the crystallinity of zeolites [36–38]. For DGC of magnetic BEA zeolite, crystallization temperature ranging from 140 to 200 °C was studied. The H_2O/gel ratio and crystallization time were maintained at 1 and 12 h, respectively. The BEA diffraction peaks appeared in Figure 2.6b for non-magnetic sample indicates that BEA was crystallized at 140 °C and became more intense at higher temperature up to 180 °C. On the other hand, the BEA peaks with very low intensity were detected in the magnetic sample at the crystallization temperature of 140 °C which is indicative of low crystallinity of the zeolite phase. The FE-SEM image of the magnetic sample synthesized at 140 °C indicates that the sample was not mainly crystal-like particles (Figure 2.8). When compared to the non-magnetic sample obtained at same synthesis temperature, Fe_3O_4 particles might have decelerated the nucleation and crystal growth. However, at higher temperature up to 180 °C, the crystallinity became higher, as shown in the XRD pattern where BEA peaks were detected along with the Fe_3O_4 peaks. When the temperature increased to 200 °C, all BEA peaks of both samples were hardly observed in their XRD patterns indicating extreme decreasing in the crystallinity. The higher magnification FE-SEM images of the samples synthesized at 200 °C show the small voids on the surface of the samples (Figure 2.9). It was suspected that some component of the gel may have been lost during heating. It was reported in the literature that the TEAOH template started to decompose from 200 °C [23]. Therefore, this can be anticipated that the template partially decomposed at 200 °C, resulting in its inhibition of nucleation and crystal growth. Decreasing in crystallinity of zeolite products when high synthesis temperatures were used was also found in some previous papers [23,38–40]. The results reveal that the crystallization of BEA zeolite with the presence of Fe_3O_4 particles is also a temperature-dependent process. The optimal crystallization temperature was found to fall between 160 and 180 °C. The samples synthesized at 180 °C was selected as the representatives for further studies.

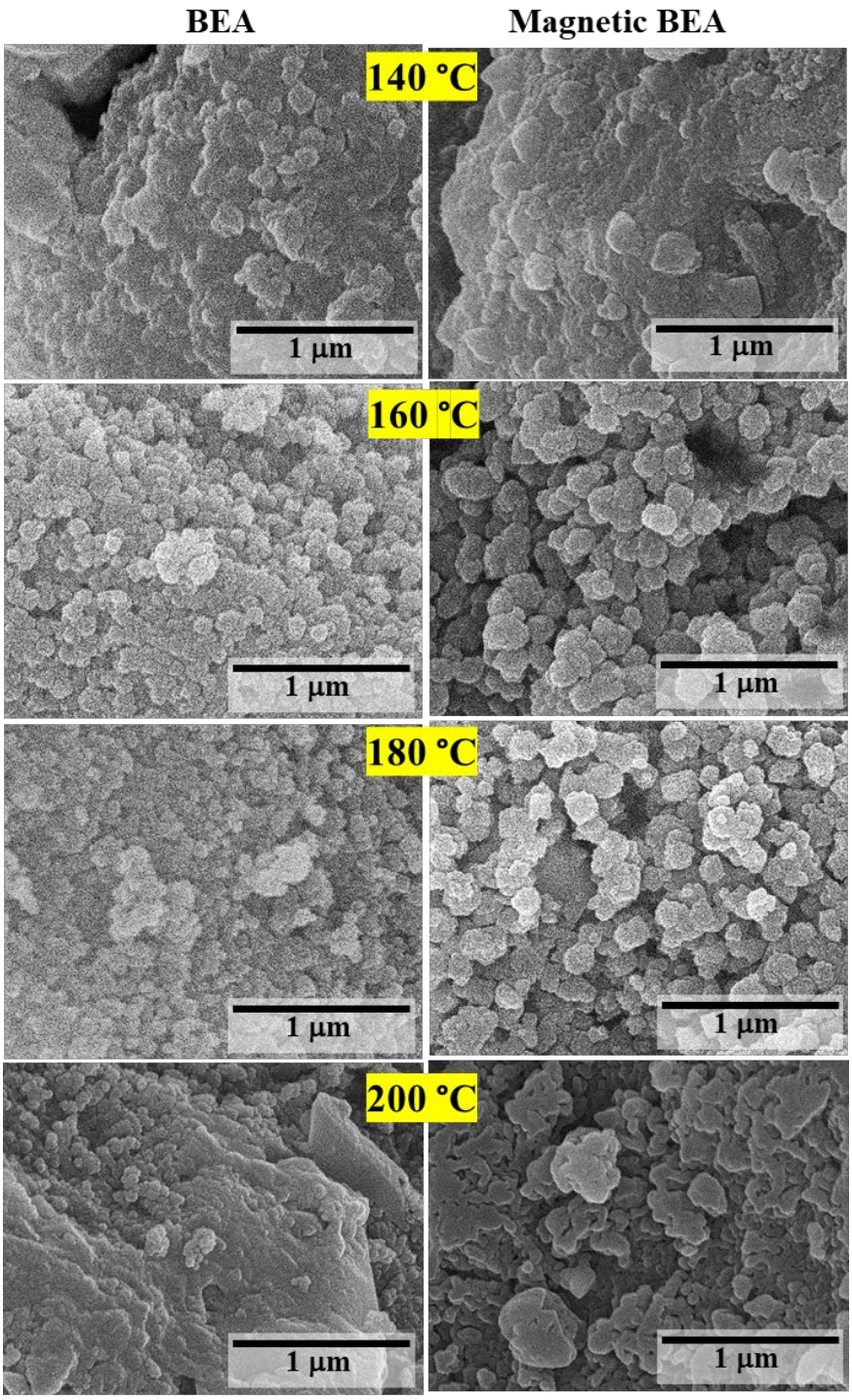

Figure 2.8 FE-SEM observation of BEA and magnetic BEA zeolite synthesized via DGC using different crystallization temperatures.

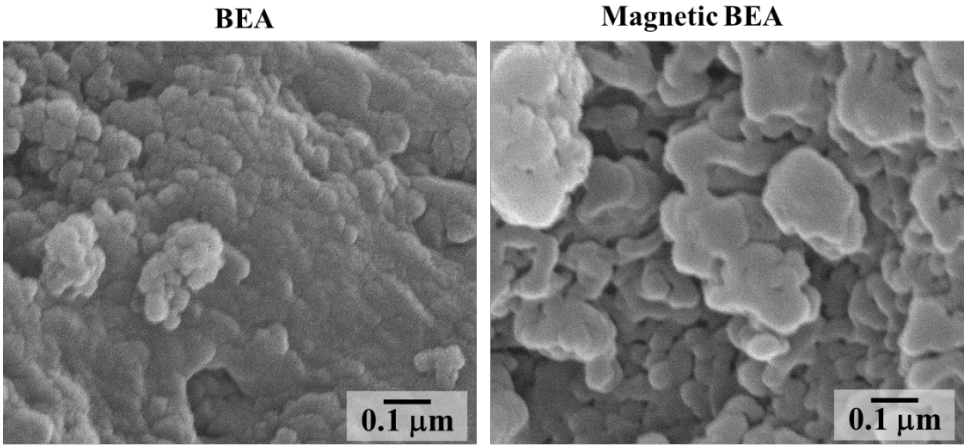

Figure 2.9 Higher magnification (100000×) FE-SEM observation of non-magnetic and magnetic BEA samples synthesized at 200 °C.

2.4.3 Effect of crystallization time

Crystallization time was studied in order to examine the suitable time for BEA zeolite to crystallize with high crystallinity with the presence of Fe_3O_4 particles. The crystallization time ranging from 1.5 to 12 h was examined by using constant H_2O/gel ratio (1) and crystallization temperature (180 °C). BEA zeolite crystallized from 1.5 h with high crystallinity, as indicated by the intense XRD peaks in Figure 2.6c for the non-magnetic sample, but lower crystallinity of BEA zeolite phase was found for the magnetic sample (see Figure 2.6c and FE-SEM images in Figure 2.10). When the crystallization time was extended to 3 h the peaks of the magnetic sample became more intense, indicating more BEA crystallized. The XRD peak intensity seemed to be constant from the crystallization time of 3 h. However, the yield was found to become constant after 6 h. Therefore, the crystallization time of 12 h was subsequently used to obtain the optimal crystallinity.

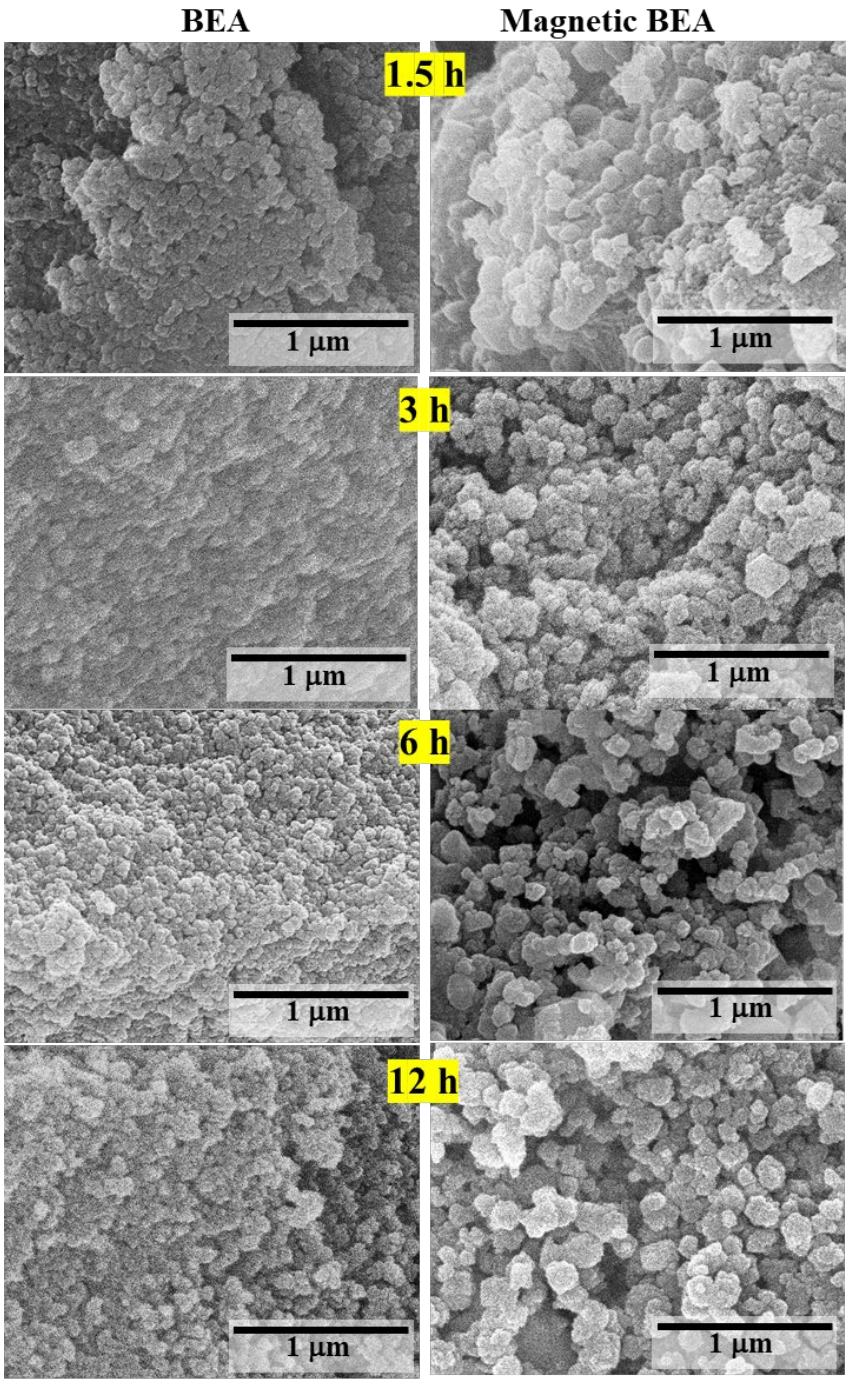

Figure 2.10 FE-SEM observation of BEA and magnetic BEA zeolite synthesized via DGC using different crystallization times.

The results obtained from the optimization studies indicate that the addition of Fe_3O_4 slightly decelerated the crystallization of BEA zeolite but the structure of the product could be maintained by optimizing the condition. The optimal conditions i.e., H_2O/gel ratio of 1, crystallization temperature at 180 °C and crystallization time of 12 h, were used for further studies on the effect of calcination temperature on the magnetic properties of the composite.

2.5 Effect of calcination temperature on magnetic properties

The as-synthesized samples were calcined in order to remove the organic TEAOH template from the zeolite pore, allowing for the adsorption of the target adsorbate. Huang et al. [41] and do Nascimento et al. [23] reported that thermal degradation of TEAOH was mainly found in the temperature range 400–500 °C. On the other hand, high temperature causes oxidation of Fe_3O_4 to different iron oxides [42] which was concerned to the magnetic properties of the magnetic BEA samples. Here, the calcination temperature of 400, 450, 500 °C that cover the reported degradation temperature range were studied. The samples were put in alumina crucibles before being placed in the electric furnace and calcined at 400, 450 or 500 °C for 12 h using a heating rate of 100 °C/h. After calcination, the magnetic properties of the samples were evaluated by measuring the magnetization saturation (*M*s) using VSM at room temperature in comparison to that of non-composited Fe_3O_4 particles.

When the magnetic field (*H*) between ±2 kOe was applied to the calcined magnetic BEA samples, the magnetization hysteresis loops were obtained as shown in Figure 2.11a. It was found that the M_s values decreased when the calcination temperature increased. The M_s values of the magnetic BEA samples calcined at 400, 450, and 500 °C, shown in Table 2.3 were lower than that of the bulk Fe_3O_4 phase. This is obviously due to the presence of the large quantity non-magnetic BEA zeolite phase in the samples. The apparent magnetic content (in wt%) in each sample was estimated using Equation 2.1

$$\text{Apparent magnetic content} = \frac{(M_S)_{MBEA} - (M_S)_{BEA}}{(M_S)_{Fe_3O_4} - (M_S)_{BEA}} \times 100 \quad \text{Equation2.1}$$

where $(M_S)_{MBEA}$ and $(M_S)_{BEA}$ are the saturation magnetization values of calcined magnetic and non-magnetic BEA zeolite at one temperature (emu/g), and $(M_S)_{Fe_3O_4}$ is the saturation magnetization value of bulk Fe_3O_4 (emu/g). The average apparent magnetic content was calculated, as shown in Table 2.3, using the apparent magnetic content from both positive and negative *H* applied.

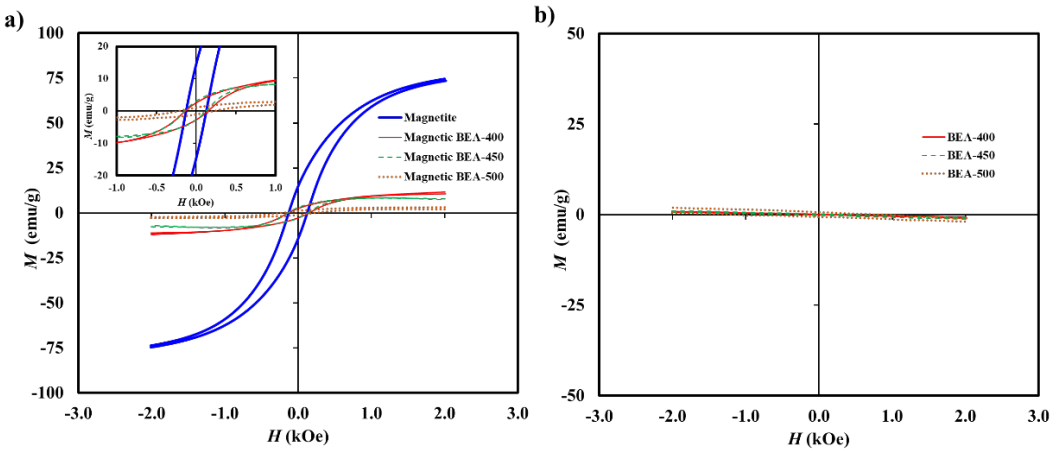

Figure 2.11 Magnetization curves of a) Fe_3O_4 and magnetic BEA, and b) BEA zeolite measured by VSM at room temperature. Numbers shown in the data series name denote the calcination temperatures.

Table 2.3 M_S values and apparent magnetic content of the BEA and magnetic BEA samples measured by VSM at ±2 kOe

Sample	M_S (emu/g)		Apparent magnetic content (wt%)		
	+2 kOe	−2 kOe	+2 kOe	−2 kOe	Average
Fe_3O_4	73.949	−74.221	-	-	-
BEA (400)	−0.860	0.757	16.132	16.754	16.443
Magnetic BEA (400)	11.208	−11.505			
BEA (450)	−0.973	0.853	11.411	11.100	11.256
Magnetic BEA (450)	7.576	−7.261			
BEA (500)	−1.502	1.217	5.330	5.163	5.247
Magnetic BEA (500)	2.520	−2.538			

The number in parentheses after each sample name represents the calcination temperature.

The calculated apparent magnetic contents decreased when the calcination temperatures increased. The XRD studies in the previous report [35] showed that different weakly magnetic iron oxide phase (hematite; α-Fe_2O_3) was observed in the diffraction patterns when magnetic BEA zeolite was calcined at 450 °C, and it became more intense at 500 °C. In this work, the XRD peaks of α-Fe_2O_3 were also detected (Figure 2.12), indicating the oxidation of Fe_3O_4 took place to some extent.

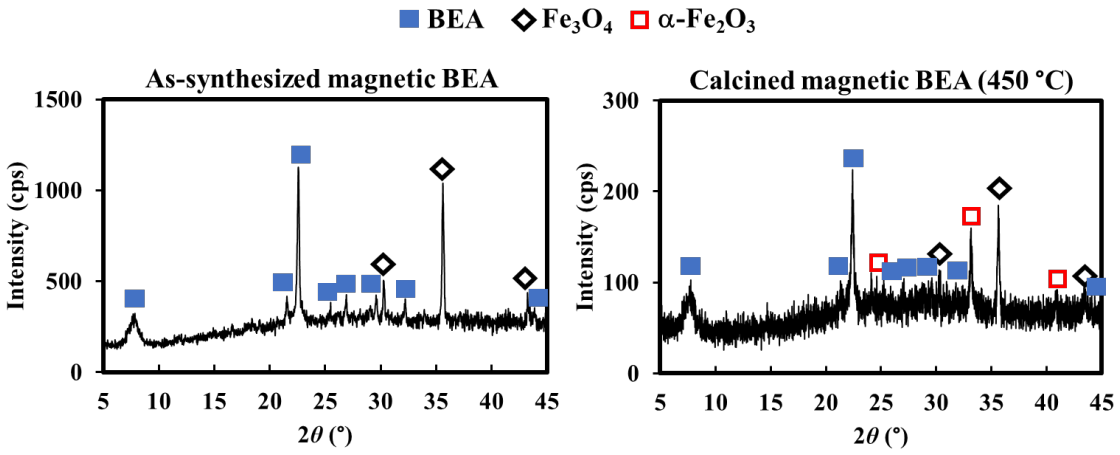

Figure 2.12 XRD patterns of magnetic BEA zeolite obtained before and after calcination at 450 °C (12 h).

In order to find out the degree of oxidation at the calcination temperature at 450 °C, the ideal magnetic content without oxidation was calculated. The average apparent magnetic content in the magnetic BEA sample calcined at 400 °C, where no oxidation was found, was considered as the original magnetic content (16.44 wt%). This magnetic content should ideally be maintained regardless of the oxidation. After calcination at 400 °C, the magnetic weight fraction in the magnetic BEA was 0.1644, therefore the BEA fraction was 1 - 0.1644 = 0.8356. By tracking weight difference between before and after calcination at 400 °C, the decreased weight fraction of the BEA sample was 0.1857 which attributed to the burned off organic SDA content. Thus, the original BEA fraction (including SDA) was 0.8356 / (1 - 0.1857) = 1.026. When the BEA sample was calcined at 450 °C, the burned off organic SDA fraction was 0.2491, therefore the BEA fraction only should be 1.026(1 - 0.2491) = 0.7705. The ideal magnetic content in the magnetic BEA sample calcined at 450 °C should be (0.1644 / (0.7705 + 0.1644)) × 100 = 17.60 wt%. The apparent magnetic content of the magnetic BEA sample calcined at 450 °C was 11.26 wt%, approximately 37% decreased from the ideal value which therefore attributes to the fraction of Fe_3O_4 oxidized to the weaker magnetic iron oxide: α-Fe_2O_3. However, when *H* dropped to zero the magnetization showed slight remanence value of 3.06 emu/g for the magnetic sample calcined at 450 °C (see the inset zoomed-in loops in Figure 2.11a), indicating that

the samples still exhibit ferromagnetism but easily redisperse in aqueous solution when detaching the external magnet [43]. The magnetic sample still practically attracted well to the external magnet, while the non-magnetic BEA sample did not (the inset digital images in Figure 2.11b). The BEA behaved diamagnetic as shown by the small negative *M* values when positive *H* was applied and vice versa. The calcination temperature of 450 °C was found optimal to maintain the magnetic properties of the sample. The magnetic BEA and BEA samples calcined at 450 °C were subsequently used for sulfadiazine adsorption studies.

2.6 Determination of SFDZ adsorption performance

In this section, SFDZ adsorption performance of BEA and magnetic BEA zeolite calcined at 450 °C was tested by studying the adsorption isotherm. Effect of initial pH on the adsorption performance was also investigated. All adsorption tests were performed using fixed adsorbent concentration of 1 g/L and orbital shaking speed of 120 rpm for 24 h at room temperature (26 °C). Aqueous solutions of SFDZ were used throughout the experiments. Quantification of SFDZ in the solutions was performed on the UV-Visible spectrophotometer (λ = 264 nm). Adsorption capacity of the adsorbent was calculated using Equation 2.2.

$$q_e = \frac{(C_0 - C_e)V}{m} \qquad \text{Equation 2.2}$$

where q_e is the adsorption capacity of the adsorbent (mg/g), C_0 and C_e are the initial and equilibrium concentrations of SFDZ, respectively (mg/L), V is the solution volume (L), and m is the mass of the adsorbent (g). In the study on effect of initial pH, percentage of SFDZ adsorbed amount ($\%AA_{SFDZ}$) was used, calculated by Equation 2.3.

$$\%AA_{SFDZ} = \frac{(C_0 - C_e) \times 100}{C_0} \qquad \text{Equation 2.3}$$

where C_0 and C_e are the initial and equilibrium SFDZ concentrations, respectively (mg/L).

2.6.1 Adsorption isotherms

The adsorption isotherms were studied using initial SFDZ concentration in the range 10–50 mg/L. Further concentration was not considered due to the limitation of SFDZ solubility. Figure 2.13a shows the increasing in adsorption capacity when the equilibrium SFDZ concentration increased. The result indicated that SFDZ can be adsorbed onto the BEA and magnetic BEA prepared by DGC method. The linear form of Langmuir and Freundlich adsorption isotherm models were applied to evaluate the adsorption behavior, as shown in Equation 2.4 and 2.5

Langmuir: $$\frac{C_e}{q_e} = \frac{C_e}{q_m} + \frac{1}{bq_m} \qquad \text{Equation 2.4}$$

Freundlich: $$\log q_e = \frac{1}{n}\log C_e + \log K_F \qquad \text{Equation 2.5}$$

where q_m is the maximum adsorption capacity calculated from the Langmuir model (mg/g), b is the Langmuir adsorption constant (L/mg), n = intensity of the Freundlich adsorption, and K_F is the relative adsorption capacity ($mg^{1-(1/n)} L^{1/n} g^{-1}$).

The greater determination coefficient (R^2) values of the linear plot between $\log C_e$ vs. $\log q_e$ (for Freundlich) than that between C_e vs. C_e/q_e (for Langmuir), shown in Figure 2.13b, indicate that the adsorption has a higher tendency to fit with Freundlich model. The trends were similar for both BEA and magnetic BEA adsorbents. Thus, SFDZ was anticipated to be adsorbed onto the BEA and magnetic BEA zeolite *via* multilayered physisorption [44].

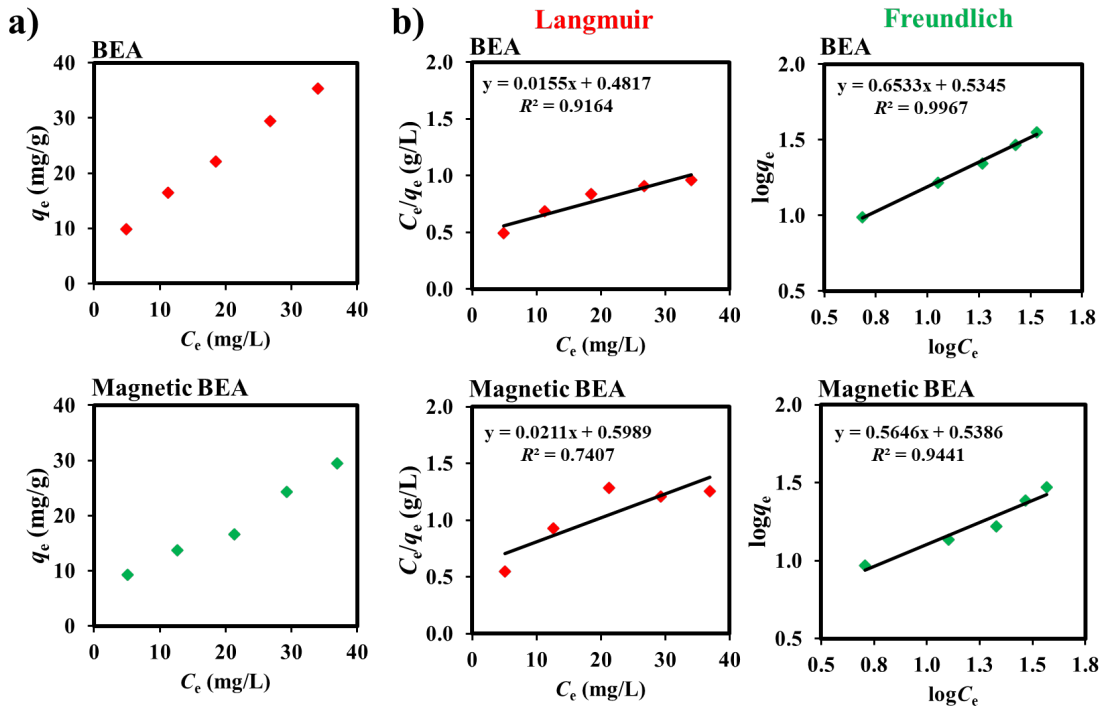

Figure 2.13 a) SFDZ adsorption isotherm studies and b) linear adsorption model plots of BEA and magnetic BEA zeolite calcined at 450 °C (12 h).

This study agrees well with many previous papers that the Freundlich model was better to describe the adsorption of SFDZ [16,45] and other sulfonamides onto zeolites [16,46–49], while Langmuir model was found suitable in some cases [17,50]. The Freundlich isotherm parameter, i.e., n and K_F values obtained in this work were compared with that from previous reported zeolites in Table 2.4. The n values greater than 1 indicate that the adsorption of SFDZ on BEA and magnetic BEA occurred *via* physical process [16]. The K_F values, reflecting the relative adsorption capacity, were comparable to that of other zeolites—that means the BEA and magnetic BEA adsorbents synthesized by DGC method show possibility of using in removal of antibiotics from wastewater.

Table 2.4 Freundlich isotherm parameters for sulfonamide adsorption onto zeolites of this work and previous papers

Zeolite	Si/Al	Sulfonamides	Freundlich parameters		Reference
			K_F	n	
FAU	50	Sulfamethoxazole	8611.5	2.92	[17]
FAU	41.295	Sulfamethoxazole	105.46	0.54	[46]
MFI	250	Sulfamethoxazole	42.66	1.393	[16]
FAU	15.31	Sulfamethoxazole	26.10	0.64	[46]
MFI	250	Sulfamethoxazole	20.97	1.74	[47]
MOR	20	Sulfamethoxazole	9.63	1.00	[49]
MFI	250	Sulfadiazine	5.68	1.21	[47]
Magnetic BEA	22[a]	Sulfadiazine	3.456	1.771	This study
BEA	22[a]	Sulfadiazine	3.424	1.531	This study
MFI	250	Sulfadiazine	2.74	2.134	[16]
HEU	6.25	Sulfamethoxazole	2.65	2.23	[48]
HEU/TiO2	n.r.	Sulfadiazine	0.0811	0.9077	[45]

n.r. = not reported; [a]According to our previous studies [35]

2.6.2 Effect of pH on SFDZ adsorption

Given that SFDZ species are pH-dependent, different ionic states: cationic ($SFDZ^+$), neutral ($SFDZ^0$), and anionic ($SFDZ^-$) with varied percentage mole fraction (%*MF*) are formed (see primary *y*-axis in Figure 2.14a), potentially affecting the adsorption behavior of SFDZ onto zeolite surface. The pH of SFDZ solution (20 mg/L, initial pH ≈6) was adjusted to 2, 4, and 7 before performing the adsorption test. After adsorption, aliquots of SFDZ solutions were diluted in phosphate buffer solution (pH 6.86) before UV adsorption measurement in order to suppress the variation due to the change of analytical wavelength caused by distinct pH (Figure 2.14b). As shown in the secondary *y*-axis in Figure 2.14a, adsorption of SFDZ on zeolite surface was pH-influenced. The percentage of SFDZ adsorbed amount (%AA_{SFDZ}) for non-magnetic BEA increased by similar order to that of

the increased $\%MF_{SFDZ}{}^{0}$ (i.e., ≈12%) when the pH decreased from 6 to 4. More pronounced $\%AA_{SFDZ}$ was found, by ≈30%, when the pH decreased from 4 to more acidic medium, i.e., pH 2. At this point, $\%MF_{SFDZ}{}^{0}$ decreased to 50% whereas $\%MF_{SFDZ}{}^{+}$ conversely increased by the same extent. On the other hand, increasing the pH from 6 to pH 7 lowered $\%AA_{SFDZ}$ to half, where ≈80% of SFDZ mainly existed as $SFDZ^{-}$ and the rest 20% was $SFDZ^{0}$. The results obtained from magnetic BEA were found in the same trend for all cases. It is seen that adsorption of SDZ was promoted at lower pH and suppressed at higher pH which is likely to be caused by the interaction of $[AlO_{4/2}]^{-}$ on the zeolite through ion exchange between $SFDZ^{+}$ and the counter cations (i.e., Na^{+}), and through repulsion by $SFDZ^{-}$, respectively. $SFDZ^{0}$ showed potential adsorbed amount at pH 4, indicates that hydrophobic interaction also occurred, and was believed to mainly take place in wide pH region between the aromatic rings of sulfadiazine and abundant siloxane network in the zeolite [16,17,47,51].

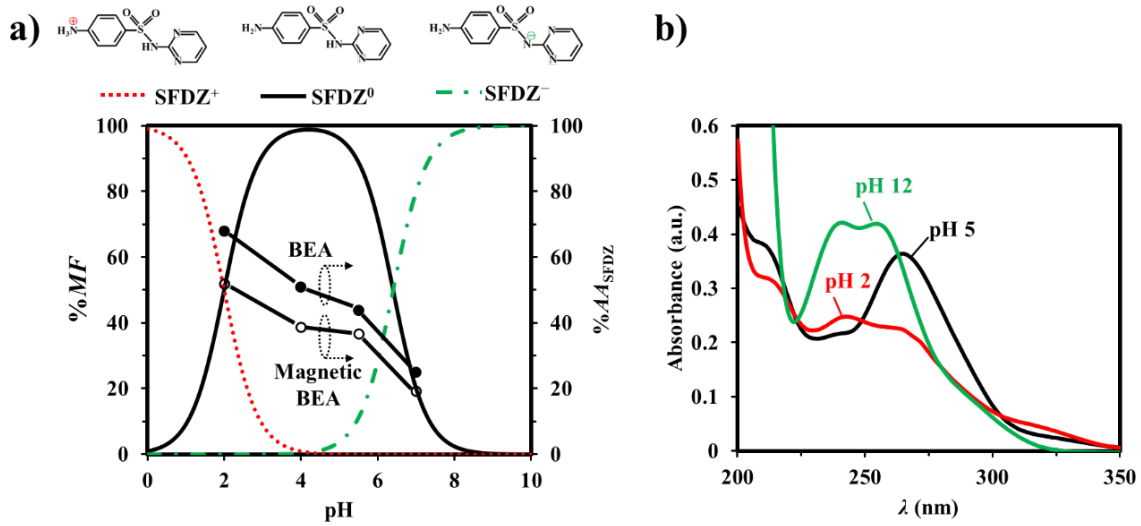

Figure 2.14 a) Percentage mole fraction of SFDZ species and percentage adsorbed amount of SFDZ at various initial pH values, b) UV absorption spectra of 5 mg/L-SFDZ solutions in different pH values.

2.7 Reusability of the adsorbents and evaluation for practical application

Reuse of adsorbents is necessary to make them economically possible in practical water treatments [52]. Regeneration of adsorbents should not only recover the adsorption properties but the structure of the adsorbents. To remove adsorbed sulfonamide from zeolitic adsorbents, use of mixed organic solvents [18], alkali solutions [14], or heat treatment at 400 °C [14] and 500 °C [18] have been reported. Owing to the fact that organic compounds are thermal degradable. Therefore, thermal regeneration of the used BEA and magnetic BEA zeolite was used. After adsorption, the spent adsorbents were collected and calcined at 400 °C for 12 h. Higher temperature was not considered in order to maintain the magnetic properties of the adsorbent. The thermal regenerated adsorbents were used in subsequent adsorption cycles which were found to be reusable for at least another 2 cycles, as shown in Figure 2.15. 20 mg/L of SFDZ solutions were used in each adsorption cycle.

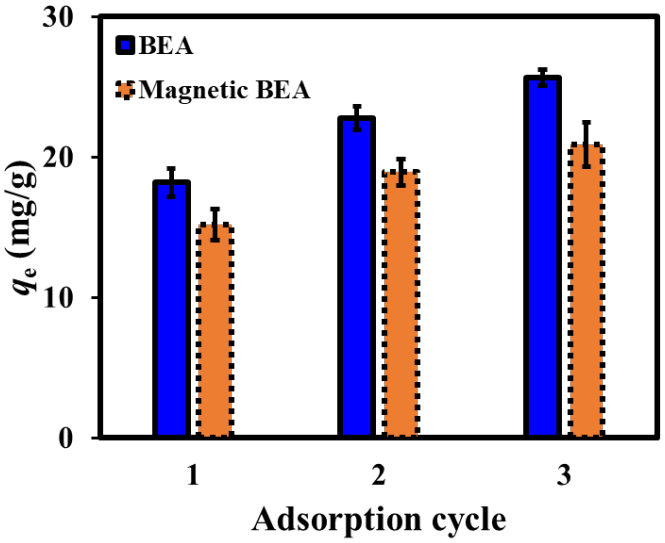

Figure 2.15 Reusability of BEA and magnetic BEA after thermal regeneration.

Interestingly, the q_e values were found to increase after each thermal regeneration for BEA and magnetic BEA zeolite. Proton, i.e., H^+, that has a smaller ionic size might have replaced larger ionic size Na^+ at the $[AlO_2]^-$ sites during the thermal degradation of the adsorbed SFDZ, which increases pore accessibility during the adsorption. Moreover, the residual SDA might have been burned off more to some extent during the thermal regeneration. These reasons may be the cause of larger amount of SFDZ molecules at higher cycles. The surprising results reflect the hidden advantages of BEA and magnetic BEA zeolites in removal of antibiotics and further study is necessary to understand this phenomenon.

The typical concentrations of antibiotics fall in ppb level (e.g., 0.01–1.0 μg/L) in surface water and sewage treatment plants were reported [53]. It was found in this work that lower initial concentrations of SFDZ resulted in higher removal efficiency. Approximately 74 and 72% removal efficiencies were obtained for the initial 1 and 5 mg/L-SFDZ, respectively, tested using 1 g of magnetic BEA zeolite per 1 L solution. In that the detection limit of the measurement, adsorption amount at lower SFDZ concentration could not be accurately quantified. However, it can be assumed in possible practical application using the removal efficiency of 74%. If 100 L wastewater assumably containing antibiotics in the reported typical range, e.g., 0.3 μg/L was treated using 500 g magnetic BEA zeolite, then approximately 0.08 μg/L-SFDZ would remain in the water which shall comply with the recommended discharge limit, i.e., 0.1 μg/L, set by the United States Food and Drug Administration [53]. To separated and collect the spent magnetic adsorbents in large scale treatment plants, a continuous flow system shown in Figure 2.16 could be possibly implemented [54]. The wastewater is mixed with magnetic adsorbents to reach adsorption equilibrium before transferring to the magnetic separation unit. The magnetic adsorbents are separated from the treated water by attracting to the rotating magnet and transported by the conveyor belt, and finally collected for regeneration and further reuse.

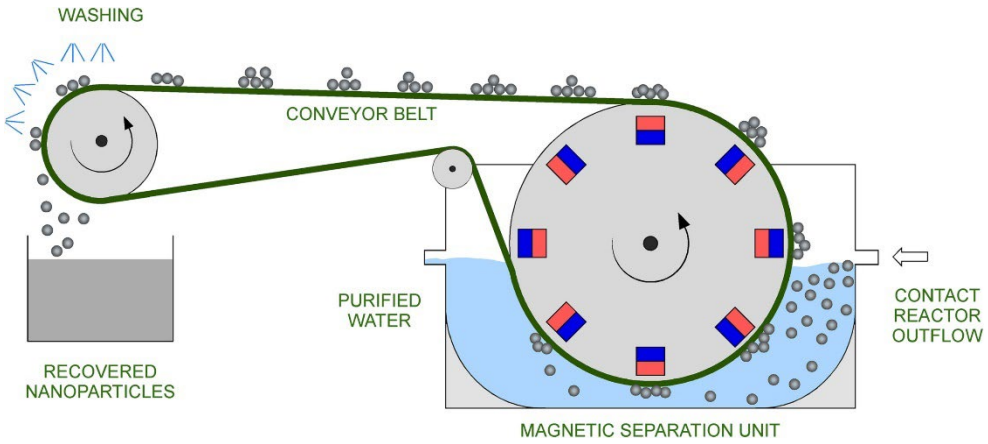

Figure 2.16 Rotary magnetic separator in a continuous flow system [54]. Reprinted from Journal of Water Process Engineering, 53, N. Maniotis, K. Kalaitzidou, E. Asimoulas, K. Simeonidis, A rotary magnetic separator integrating nanoparticle-assisted water purification: Simulation and laboratory validation, 103825, Copyright (2023), with permission from Elsevier.

2.8 Conclusion

In this chapter, optimization of synthesis conditions in DGC method were studied for preparation of magnetic BEA zeolite. Environmentally friendly magnetic particles (Fe_3O_4) were mixed with the zeolite precursor to obtain homogeneous dry precursor gel before converting to magnetic BEA zeolite upon heating. The optimal synthesis conditions were found to be H_2O/gel ratio of 1, crystallization temperature in the range 160–180 °C, and crystallization time of at least 6 h. Magnetic properties of the magnetic BEA calcined at different temperature were investigated and 450 °C was found to preserve magnetic properties with minimum co-existing of weaker magnetic iron oxide phase. Adsorption performance of the synthesized magnetic BEA zeolite was investigated for removal of SFDZ, a typical antibiotic, from aqueous solutions. The antibiotic can be adsorbed on the magnetic BEA adsorbent which follows the linear Freundlich adsorption isotherm. This research reveals that magnetic BEA zeolite can be prepared using the optimal DGC synthesis conditions and potentially applied for removal of antibiotics from agricultural wastewater (livestock farm).

The studies in this chapter provides optimal DGC synthesis conditions that will be applying in the synthesis of magnetic BEA zeolite using rich husk ash-derived SiO_2 in the next chapter.

Acknowledgement

Material from: 'VANPASEUTH PHOUTHAVONG, TAKESHI HAGIO, SUPINYA NIJPANICH, JAE-HYEOK PARK, MASATAKE HIRAIWA, TEERANUN SRIHIRUNTHANON, NUTCHANAN CHANTANURAK, RATANA RUJIRAVANIT, YUKI KAMIMOTO, XINLING LI, LONG KONG, LIANG LI, RYOICHI ICHINO, DRY-GEL CONVERSION SYNTHESIS OF MAGNETIC BEA-TYPE ZEOLITES FOR ANTIBIOTICS ADSORPTION, JOURNAL OF SOL-GEL SCIENCE AND TECHNOLOGY, published [2023], [Springer Nature]'. *Reproduced with permission from Springer Nature*.

References

[1] M.I. Hutchings, A.W. Truman, B. Wilkinson, Antibiotics: past, present and future, Curr. Opin. Microbiol. 51 (2019) 72–80. https://doi.org/https://doi.org/10.1016/j.mib.2019.10.008.

[2] Y. Mehdi, M.-P. Létourneau-Montminy, M.-L. Gaucher, Y. Chorfi, G. Suresh, T. Rouissi, S.K. Brar, C. Côté, A.A. Ramirez, S. Godbout, Use of antibiotics in broiler production: global impacts and alternatives, Anim. Nutr. 4 (2018) 170–178. https://doi.org/https://doi.org/10.1016/j.aninu.2018.03.002.

[3] M. Ferrer, C. Méndez-García, D. Rojo, C. Barbas, A. Moya, Antibiotic use and microbiome function, Biochem. Pharmacol. 134 (2017) 114–126. https://doi.org/https://doi.org/10.1016/j.bcp.2016.09.007.

[4] T.F. Landers, B. Cohen, T.E. Wittum, E.L. Larson, A Review of antibiotic use in food animals: perspective, policy, and potential, Public Health Rep. 127 (2012) 4–22. https://doi.org/10.1177/003335491212700103.

[5] K. Tiseo, L. Huber, M. Gilbert, T.P. Robinson, T.P. Van Boeckel, Global trends in antimicrobial use in food animals from 2017 to 2030, Antibiotics. 9 (2020) 1–14. https://doi.org/10.3390/antibiotics9120918.

[6] V. Kasimanickam, M. Kasimanickam, R. Kasimanickam, Antibiotics use in food animal production: escalation of antimicrobial resistance: where are we now in combating AMR?, Med. Sci. (Basel). 9 (2021). https://doi.org/10.3390/medsci9010014.

[7] M.S. Cheong, K.H. Seo, H. Chohra, Y.E. Yoon, H. Choe, V. Kantharaj, Y.B. Lee, Influence of sulfonamide contamination derived from veterinary antibiotics on plant growth and development, Antibiotics. 9 (2020) 1–18. https://doi.org/10.3390/antibiotics9080456.

[8] A.K. Sarmah, M.T. Meyer, A.B.A. Boxall, A global perspective on the use, sales, exposure pathways, occurrence, fate and effects of veterinary antibiotics (VAs) in

the environment, Chemosphere. 65 (2006) 725–759. https://doi.org/https://doi.org/10.1016/j.chemosphere.2006.03.026.

[9] H.Q. Anh, T.P.Q. Le, N. Da Le, X.X. Lu, T.T. Duong, J. Garnier, E. Rochelle-Newall, S. Zhang, N.-H. Oh, C. Oeurng, C. Ekkawatpanit, T.D. Nguyen, Q.T. Nguyen, T.D. Nguyen, T.N. Nguyen, T.L. Tran, T. Kunisue, R. Tanoue, S. Takahashi, T.B. Minh, H.T. Le, T.N.M. Pham, T.A.H. Nguyen, Antibiotics in surface water of East and Southeast Asian countries: A focused review on contamination status, pollution sources, potential risks, and future perspectives, Sci. Total Environ. 764 (2021) 142865. https://doi.org/https://doi.org/10.1016/j.scitotenv.2020.142865.

[10] J. Muhammad, S. Khan, J.Q. Su, A.E.-L. Hesham, A. Ditta, J. Nawab, A. Ali, Antibiotics in poultry manure and their associated health issues: a systematic review, J. Soils Sediments. 20 (2020) 486–497. https://doi.org/10.1007/s11368-019-02360-0.

[11] Z. Maghsodian, A.M. Sanati, T. Mashifana, M. Sillanpää, S. Feng, T. Nhat, B. Ramavandi, Occurrence and distribution of nntibiotics in the water, sediment, and biota of freshwater and marine environments: a review, Antibiotics. 11 (2022). https://doi.org/10.3390/antibiotics11111461.

[12] A. Ovung, J. Bhattacharyya, Sulfonamide drugs: structure, antibacterial property, toxicity, and biophysical interactions, Biophys. Rev. 13 (2021) 259–272. https://doi.org/10.1007/s12551-021-00795-9.

[13] N. Jiang, R. Shang, S.G.J. Heijman, L.C. Rietveld, High-silica zeolites for adsorption of organic micro-pollutants in water treatment: A review, Water. Res. 144 (2018) 145–161. https://doi.org/10.1016/j.watres.2018.07.017.

[14] F. Sannino, M. Pansini, A. Marocco, A. Cinquegrana, S. Esposito, O. Tammaro, G. Barrera, P. Tiberto, P. Allia, D. Pirozzi, Removal of sulfanilamide by tailor-made magnetic metal-ceramic nanocomposite adsorbents, J. Environ. Manage. 310 (2022). https://doi.org/10.1016/j.jenvman.2022.114701.

[15] Z. Li, C. Stockwell, J. Niles, S. Minegar, H. Hong, Uptake of sulfadiazine sulfonamide from water by clinoptilolite, Appl. Environ. Soil Sci. 2013 (2013). https://doi.org/10.1155/2013/648697.

[16] X. Zuo, C. Qian, S. Ma, J. Xiong, J. He, Z. Chen, Removal of sulfonamide antibiotics from water by high-silica ZSM-5, Water Sci. Technol. 80 (2019) 507–516. https://doi.org/10.2166/wst.2019.294.

[17] S. Fukahori, T. Fujiwara, R. Ito, N. Funamizu, PH-Dependent adsorption of sulfa drugs on high silica zeolite: Modeling and kinetic study, Desalination. 275 (2011) 237–242. https://doi.org/10.1016/j.desal.2011.03.006.

[18] I. Braschi, S. Blasioli, E. Buscaroli, D. Montecchio, A. Martucci, Physicochemical regeneration of high silica zeolite Y used to clean-up water polluted with sulfonamide antibiotics, J. Environ. Sci. (China). 43 (2016) 302–312. https://doi.org/10.1016/j.jes.2015.07.017.

[19] T.O. Bok, E.P. Andriako, E.E. Knyazeva, I.I. Ivanova, Engineering of zeolite BEA crystal size and morphology: via seed-directed steam assisted conversion, RSC Adv. 10 (2020) 38505–38514. https://doi.org/10.1039/d0ra07610d.

[20] R.L. Wadlinger, G.T. Kerr, E.J. Rosinski, A crystalline zeolite with improved adsorption and catalytic properties, Pat. USA. 3308069 (1967).

[21] M.M.J. Treacy, J.M. Newsam, Two new three-dimensional twelve-ring zeolite frameworks of which zeolite beta is a disordered intergrowth, Nature. 332 (1988) 249–251. https://doi.org/10.1038/332249a0.

[22] S. Narayanan, P. Tamizhdurai, V.L. Mangesh, C. Ragupathi, P. Santhana krishnan, A. Ramesh, Recent advances in the synthesis and applications of mordenite zeolite – review, RSC Adv. 11 (2021) 250–267. https://doi.org/10.1039/D0RA09434J.

[23] A.R. do Nascimento, G.P. De Figueredo, E.M.F. Silva, M.A.F. Melo, D.M.A. Melo, M.J.B. De Souza, Synthesis, optimization and characterization of Zeolite Beta

(BEA): Production of ZSM-5 and $NaAlSiO_4$ as secondary phases, Rev. Virtual Quim. 9 (2017) 1570–1582. https://doi.org/10.21577/1984-6835.20170092.

[24] C. De Smedt, F. Ferrer, K. Leus, P. Spanoghe, Removal of pesticides from aqueous solutions by adsorption on zeolites as solid adsorbents, Adsorpt. Sci. Technol. 33 (2015) 457–485. https://doi.org/10.1260/0263-6174.33.5.457.

[25] W. Rongchapo, O. Sophiphun, K. Rintramee, S. Prayoonpokarach, J. Wittayakun, Paraquat adsorption on porous materials synthesized from rice husk silica, Water Sci. Technol. 68 (2013) 863–869. https://doi.org/10.2166/wst.2013.311.

[26] B. Bayati, A. Ghorbani, H. Kazemian, Phenol removal from aqueous media using BEA zeolite: A molecular simulation study on the effect of zeolite mobile cations, Microporous and Mesoporous Materials. 364 (2024) 112854. https://doi.org/https://doi.org/10.1016/j.micromeso.2023.112854.

[27] J. Reungoat, J.S. Pic, M.H. Manéro, H. Debellefontaine, Adsorption of nitrobenzene from water onto high silica zeolites and regeneration by ozone, Sep. Sci. Technol. 42 (2007) 1447–1463. https://doi.org/10.1080/01496390701289948.

[28] V. Rakić, L. Damjanović, V. Rac, D. Stošić, V. Dondur, A. Auroux, The adsorption of nicotine from aqueous solutions on different zeolite structures, Water Res. 44 (2010) 2047–2057. https://doi.org/https://doi.org/10.1016/j.watres.2009.12.019.

[29] M. Rakanović, A. Vukojević, M.M. Savanović, S. Armaković, S. Pelemiš, F. Živić, S. Sladojević, S.J. Armaković, Zeolites as adsorbents and photocatalysts for removal of dyes from the aqueous environment, Molecules. 27 (2022). https://doi.org/10.3390/molecules27196582.

[30] L.M. Pratti, G.M. Reis, F.S. dos Santos, G.R. Gonçalves, J.C.C. Freitas, M.K. de Pietre, Effects of textural and chemical properties of β-zeolites on their performance as adsorbents for heavy metals removal, Environ. Earth Sci. 78 (2019). https://doi.org/10.1007/s12665-019-8568-6.

[31] S. Motlagh Bahadory Esfahani, H. Faghihian, Modification of synthesized β-zeolite by ethylenediamine and monoethanolamine for adsorption of Pb^{2+}, J. Water Process Eng. 3 (2014) 62–66. https://doi.org/https://doi.org/10.1016/j.jwpe.2014.05.007.

[32] W. Xu, J. Dong, J. Li, J. Li, F. Wu, A novel method for the preparation of zeolite ZSM-5, J. Chem. Soc. Chem. Commun. (1990) 755–756. https://doi.org/10.1039/C39900000755.

[33] P.R. Hari Prasad Rao, M. Matsukata, Dry-gel conversion technique for synthesis of zeolite BEA, Chem. Commun. (1996) 1441–1442.

[34] M. Matsukata, M. Ogura, T. Osaki, P.R. Hari Prasad Rao, M. Nomura, E. Kikuchi, Conversion of dry gel to microporous crystals in gas phase, Top. Catal. 9 (1999) 77–92. https://doi.org/10.1023/A:1019106421183.

[35] V. Phouthavong, M. Hiraiwa, T. Hagio, S. Nijpanich, V. Chounlamany, T. Nishihama, Y. Kamimoto, R. Ichino, Magnetic BEA-type zeolites: preparation by dry-gel conversion method and assessment of dye removal performance, J. Mater. Cycles Waste Manag. 22 (2020) 375–382. https://doi.org/10.1007/s10163-020-00994-8.

[36] H. Liu, S. Peng, L. Shu, T. Chen, T. Bao, R.L. Frost, Magnetic zeolite NaA: Synthesis, characterization based on metakaolin and its application for the removal of Cu^{2+}, Pb^{2+}, Chemosphere. 91 (2013) 1539–1546. https://doi.org/10.1016/j.chemosphere.2012.12.038.

[37] F. Mohammadparast, R. Halladj, S. Askari, The synthesis of nano-sized zsm-5 zeolite by dry gel conversion method and investigating the effects of experimental parameters by Taguchi experimental design, J. Exp. Nanosci. 13 (2018) 160–173. https://doi.org/10.1080/17458080.2018.1453172.

[38] S.M. Alipour, R. Halladj, S. Askari, Effects of the different synthetic parameters on the crystallinity and crystal size of nanosized ZSM-5 zeolite, Rev. Chem. Eng. 30 (2014) 289–322. https://doi.org/10.1515/revce-2014-0008.

[39] R. Karimi, B. Bayati, N. Charchi Aghdam, M. Ejtemaee, A.A. Babaluo, Studies of the effect of synthesis parameters on ZSM-5 nanocrystalline material during template-hydrothermal synthesis in the presence of chelating agent, Powder Technol. 229 (2012) 229–236. https://doi.org/10.1016/j.powtec.2012.06.037.

[40] M. Nakai, K. Miyake, R. Inoue, K. Ono, H. Al Jabri, Y. Hirota, Y. Uchida, M. Miyamoto, N. Nishiyama, Synthesis of high silica *BEA type ferrisilicate (Fe-Beta) by dry gel conversion method using dealuminated zeolites and its catalytic performance on acetone to olefins (ATO) reaction, Microporous Mesoporous Mater. 273 (2019) 189–195. https://doi.org/10.1016/j.micromeso.2018.06.008.

[41] Z. Huang, J.-F. Su, Y.-H. Guo, X.-Q. Su, L.-J. Teng, Synthesis of well-crystallized zeolite beta at large scale and its incorporation into polysulfone matrix for gas separation, Chem. Eng. Commun. 196 (2009) 969–986. https://doi.org/10.1080/00986440902797824.

[42] Y.-S. Li, J.S. Church, A.L. Woodhead, Infrared and Raman spectroscopic studies on iron oxide magnetic nano-particles and their surface modifications, J. Magn. Magn. Mater. 324 (2012) 1543–1550. https://doi.org/10.1016/j.jmmm.2011.11.065.

[43] Y. Yang, P. Zhang, J. Jiang, Y. Dai, M. Wu, Y. Pan, L. Ni, Synthesis and properties of magnetic zeolite with good magnetic stability from fly ash, J. Sol-gel Sci Technol. 87 (2018) 408–418. https://doi.org/10.1007/s10971-018-4733-8.

[44] M.N. Alnajrani, O.A. Alsager, Removal of antibiotics from water by polymer of intrinsic microporosity: isotherms, kinetics, thermodynamics, and adsorption mechanism, Sci. Rep. 10 (2020). https://doi.org/10.1038/s41598-020-57616-4.

[45] X. Liu, Y. Liu, S. Lu, W. Guo, B. Xi, Performance and mechanism into TiO_2/Zeolite composites for sulfadiazine adsorption and photodegradation, Chem. Eng. J. 350 (2018) 131–147. https://doi.org/10.1016/j.cej.2018.05.141.

[46] D.N.R. de Sousa, S. Insa, A.A. Mozeto, M. Petrovic, T.F. Chaves, P.S. Fadini, Equilibrium and kinetic studies of the adsorption of antibiotics from aqueous

solutions onto powdered zeolites, Chemosphere. 205 (2018) 137–146. https://doi.org/10.1016/j.chemosphere.2018.04.085.

[47] X. Zuo, C. Qian, S. Ma, J. Xiong, Sulfonamide antibiotics sorption by high silica ZSM-5: Effect of pH and humic monomers (vanillin and caffeic acid), Chemosphere. 248 (2020). https://doi.org/10.1016/j.chemosphere.2020.126061.

[48] Y. Liu, X. Liu, S. Lu, B. Zhao, Z. Wang, B. Xi, W. Guo, Adsorption and biodegradation of sulfamethoxazole and ofloxacin on zeolite: Influence of particle diameter and redox potential, Chem. Eng. J. 384 (2020). https://doi.org/10.1016/j.cej.2019.123346.

[49] Y. Doekhi-Bennani, N.M. Leilabady, M. Fu, L.C. Rietveld, J.P. van der Hoek, S.G.J. Heijman, Simultaneous removal of ammonium ions and sulfamethoxazole by ozone regenerated high silica zeolites, Water Res. 188 (2021). https://doi.org/10.1016/j.watres.2020.116472.

[50] S. Fukahori, T. Fujiwara, Modeling of sulfonamide antibiotic removal by TiO_2/high-silica zeolite HSZ-385 composite, J. Hazard. Mater. 272 (2014) 1–9. https://doi.org/10.1016/j.jhazmat.2014.02.028.

[51] S. Fukahori, T. Fujiwara, N. Funamizu, K. Matsukawa, R. Ito, Adsorptive removal of sulfonamide antibiotics in livestock urine using the high-silica zeolite HSZ-385, Water Sci. Technol. 67 (2013) 319–325. https://doi.org/10.2166/wst.2012.513.

[52] D.A. Gkika, A.C. Mitropoulos, G.Z. Kyzas, Why reuse spent adsorbents? The latest challenges and limitations, Sci. Total Environ. 822 (2022) 153612. https://doi.org/https://doi.org/10.1016/j.scitotenv.2022.153612.

[53] G. Le Page, L. Gunnarsson, J. Snape, C.R. Tyler, Integrating human and environmental health in antibiotic risk assessment: a critical analysis of protection goals, species sensitivity and antimicrobial resistance, Environ. Int. 109 (2017) 155–169. https://doi.org/10.1016/j.envint.2017.09.013.

[54] N. Maniotis, K. Kalaitzidou, E. Asimoulas, K. Simeonidis, A rotary magnetic separator integrating nanoparticle-assisted water purification: Simulation and laboratory validation, J. Water Process Eng. 53 (2023) 103825. https://doi.org/https://doi.org/10.1016/j.jwpe.2023.103825.

CHAPTER 3

Using rice husk ash–SiO_2 in dry-gel conversion synthesis of magnetic BEA zeolite: assessment of herbicide removal

3.1 Background

3.1.1 Environmental impact of using herbicides

Herbicides are commonly used to kill weeds or inhibit the growth of undesired plants in modern plant production to ensure a sufficient food chain for the increasing global population [1]. Paraquat, one of several commercial names for 1,1′-dimethyl-4,4′-bipyridinium dichloride, is a well-known and widely used bipyridyl herbicide because of its non-selectivity and cost-effectiveness. Figure 3.1 presents the structure of paraquat dichloride.

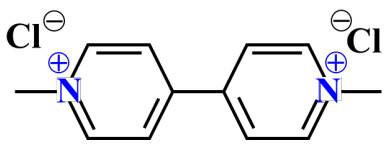

Figure 3.1 Chemical structure of paraquat dichloride.

Paraquat is a cost-effective herbicide; however, it becomes toxic if it is released into the natural environment [2]. The extensive use of paraquat with long-term exposure seriously affects human and mammalian health, causing kidney, liver, and neurological diseases (Parkinson's disease); many types of cancers (skin, brain, breast, etc.); and death in severe cases owing to inflammation and respiratory failure [3,4]. Paraquat has been banned in several countries, but its residue from excessive use in agricultural areas accumulates in the soil and migrates to groundwater and surface water due to its high solubility in water, which harms animal and human health [5]. To address these environmental and health concerns, the removal of paraquat contamination from water is therefore necessary.

3.1.2 Removal of paraquat from water by adsorption

Adsorption is an effective physical approach for the treatment of water contaminated with pesticides (including herbicides) and other organic pollutants. So far, diverse adsorbents with different structures, properties, and pore sizes have been developed for selectively removal of the target pollutants [6]. Removal of paraquat from aqueous solutions has been studied using clays (including zeolites), mesoporous SiO_2, graphene oxide, activated carbon, and biopolymers, etc., which were summarized in a review article [7]. These adsorbents have shown potential adsorption performance from a few milligrams to hundreds of milligrams of paraquat per gram of adsorbent. However, a sustainable and environmentally friendly adsorbent for herbicide removal is still necessary. Utilizing zeolitic adsorbents might be a good choice owing to the various microporous structures of zeolites with high stability and low toxicity. In 2013, Rongchapo et al. found that paraquat was effectively adsorbed on a large pore BEA zeolite that was prepared using rice husk ash-SiO_2 in the conventional hydrothermal route [8]. The paper shows the advantage of using a low-cost SiO_2 source derived from agricultural waste in the preparation of adsorbent. However, sustainability of the method should be improved by developing a more environmentally friendly protocol, which is to overcome the drawback of the hydrothermal method. Additionally, incorporating BEA zeolite with magnetic properties is more attractive to enhance the practicality of the adsorbent.

3.1.3 Rice husk: a potential source of SiO_2

Agricultural solid wastes from crop and livestock productions are a result of a huge global demand due to the increasing population. Disposal of agricultural wastes greatly contribute to production of greenhouse gases [9]. Therefore, converting these solid wastes into energy or useful resources is an essential approach to meet the 3-R principle, i.e., reduce, reuse, recycle, and SDGs [10]. According to the database reported by Food and Agriculture Organization of the United Nations, over 80 to 1.5 of billion tons of paddy and milled rice have been produced in Asian countries such as China, India, Indonesia, Bangladesh, Vietnam, Thailand, Myanmar, the Philippines, and Japan in the 2010s [11], which accounts for approximately 90% of the global rice product share. A huge amount of

rice husk (RH) is therefore generated as waste. Due to its high heating value, RH can be used as biomass to generate green energy [12] but still its ash is left behind as a secondary waste. Protuberances and hairs on the outer epidermis of RH contain the most concentrated SiO_2, in which Si bonds with carbohydrate [13]. Generally, calcination of RH at temperatures up to 700 °C yields amorphous SiO_2, as shown in Figure 3.2, with 95% purity whereas higher purity up to 99% can achieved using chemical methods [14]. Amorphous SiO_2 is very reactive due to its high surface area with ultrafine particle sizes. The temperature above 700 °C leads to formation of crystalline SiO_2 polymorphs such as α-cristobalite, α-quartz, and α-tridymite [13].

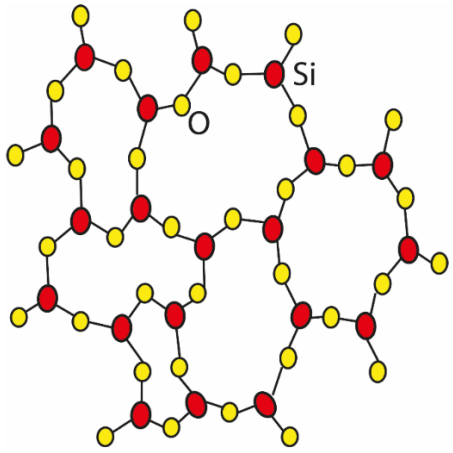

Figure 3.2 Chemical structure of amorphous SiO_2. Reprinted from Khouchaf et al. [15], MDPI, under the terms and conditions of the Creative Commons Attribution (CC BY) license.

Burning of RH greatly removes the organic impurity before subsequent use of chemical method. Washing RH ash (RHA) with acid solution can further remove metallic impurities prior to dissolution of SiO_2 using alkali solution. Finally, amorphous SiO_2 particles are precipitated using acid solution [14]. Highly reactive form of RHA-SiO_2 is a sustainable and inexpensive alternative SiO_2 source for synthesizing SiO_2-based materials for using in broad applications such as concrete [16], catalysis/catalyst supports, drug carriers, and environmental remediation [17]. For synthesis of zeolites, using RHAS is successful for MFI [18,19], FAU [8,19,20], LTA [19], CHA [21], ANA [22], and BEA

[8,23]. These works contribute to value addition of agricultural wastes. However, the reported zeolites were mainly prepared using conventional hydrothermal method. If solid-state RHA-SiO_2 can be applied to a more effective and environmentally friendly method, i.e., DGC, a more sustainable and environmentally friendly synthesis protocol for zeolitic adsorbents will be obtained.

3.2 Objective

This chapter aims to develop a sustainable, environmentally friendly and cost-effective synthesis method of magnetic BEA zeolite by utilizing agricultural waste derived materials, solid rice husk ash–SiO_2, in the replacement of the commercial colloidal SiO_2 in DGC method. The synthesized magnetic zeolite composite was investigated as a sustainable adsorbent for removal of paraquat, a type of herbicide, from water. This work realizes a sustainable material circulation in agricultural activities since agricultural waste is utilized in preparation of a remediation tool of water affected by the use of agrochemicals.

3.3 Materials

Chemicals and equipment used in this work are listed in Table 3.1 and 3.2, respectively. RHA-SiO_2 was prepared at The Petroleum and Petrochemical College and Center of Excellence on Petrochemical and Materials Technology, Chulalongkorn University, Bangkok, Thailand, using an alkali treatment of rice husk ash (CP All Public Co., Ltd., Thailand) followed by acid precipitation.

Table 3.1 Chemicals

Name (Formula, purity)	Manufacturer, country
Aluminum sulfate ($Al_2(SO_4)_3 \cdot 14\sim18H_2O$, 51.0–57.5% as $Al_2(SO_4)_3$)	Nacalai Tesque, Japan
Sodium hydroxide (NaOH, 97.0 wt%)	Nacalai Tesque, Japan
Tetraethylammonium hydroxide (TEAOH, 35 wt% in water)	TCI, Japan
Magnetite (Fe_3O_4, 80.0 wt%)	Kanto Chemical, Japan
Paraquat dichloride ($C_{12}H_{14}Cl_2N_2$, >98.0%)	TCI, Japan
Diquat dibromide monohydrate ($C_{12}H_{12}Br_2N_2 \cdot H_2O$, 100.0%)	Fujifilm Wako Pure Chemical Corp., Japan
Cibacron blue 3G-A ($C_{29}H_{20}ClN_7O_{11}S_3$, ≥55%)	Sigma Aldrich, USA
Sodium chloride (NaCl, 99.5%)	Fujifilm Wako Pure Chemical Corp., Japan
Hydrochloric acid (HCl, 35.0–37.0wt%)	Nacalai Tesque, Japan
Silicon standard solution (Si, 1.00 mgSi/mL)	Nacalai Tesque, Japan
Aluminum standard solution (Al, 1002 mgAl/L)	Fujifilm Wako Pure Chemical Corp., Japan
Iron standard solution (Fe, 1001 mgFe/L)	Fujifilm Wako Pure Chemical Corp., Japan

TCI = Tokyo Chemical Industry, Corp. = Corporation

Table 3.2 Equipment

Name	Model	Manufacturer, country
Convection oven	SOFW-300SB	AS ONE Corporation, Japan
Hotplate stirrer	RSH-1DN	AS ONE Corporation, China
Electric furnace	VF-3000	SK Medical, Japan
Field emission-scanning electron microscope (FE-SEM)	JSM-6330F	JEOL, Japan
Ultra-high-resolution FE-SEM-energy dispersive X-ray spectroscopy (FE-SEM-EDS)	S-4800	HITACHI, Japan
X-ray diffractometer (XRD, Cu-Kα, α = 1.54056 Å)	RINT 2500TTR	Rigaku Corporation, Japan
pH meter	AS800	AS ONE Corporation, Japan
Turbidimeter	HI93703	Hanna Instruments, USA
Orbital shaker	SK-O180-S	DLAB Scientific, China
UV-Visible spectrophotometer	UV-2450	Shimadzu, Japan
Inductively coupled plasma-atomic emission spectrometer (ICP-AES)	SK-II	Seiko Instrument, Japan

3.4 DGC synthesis of magnetic BEA zeolite using RHA-SiO_2

3.4.1 Characterization of RHA-SiO_2

Solid RHA-SiO_2 particles used in this work had white powdery appearance and was characterized prior to use in gel preparation (see inset in Figure 3.3a). As shown in the XRD patter (Figure 3.3a), the pattern was broad and no crystalline phase was detected, indicating that the RHA-SiO_2 was highly amorphous. Amorphous SiO_2 is said to be highly active, it is therefore preferrable for synthesizing advanced materials [12,24]. The FE-SEM image in

Figure 3.3b reveals that the RHA-SiO_2 particles were ultrafine, i.e., the sizes were below 100 nm.

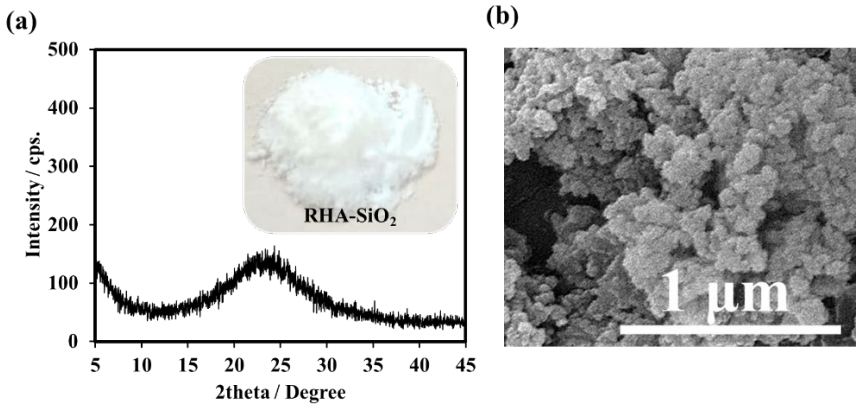

Figure 3.3 XRD pattern with the inset of the photograph (a) and FE-SEM image (b) of the RHA-SiO_2 particles [25].

3.4.2 Preparation of dry precursor gel using solid RHA-SiO_2

Crystallization of BEA zeolite via DGC method by direct use of solid RHA-SiO_2 was confirmed before the inclusion of the magnetic particles. Initially, the procedure described in Chapter 2, Section 2.4 was applied, i.e., room temperature (26 °C) and simple mechanical stirring, but replacing the commercial colloidal SiO_2 with the solid RHA-SiO_2. Amount of each ingredient is as follows: 3.63 g of solid RHA-SiO_2, 0.50 g of a 20 wt% NaOH solution, 16.52 g of a 10 wt% TEAOH solution, and 0.30 g of solid $Al_2(SO_4)_3 \cdot 14{\sim}18H_2O$. After DGC using the optimal synthesis conditions obtained from the studies in Chapter 2, the product was found mainly in amorphous state with minor crystalline phase at 32.0 ° and 34.0 ° in the XRD pattern with inset of FE-SEM image (Figure 3.4a). These peaks could be assigned to chabazite [26,27]. The results might indicate the insufficient dissolution of the RHA-SiO_2 to generate $SiO_{4/2}$ tetrahedra for the formation of a dense aluminosilicate gel. Consequently, double amount of 20 wt% NaOH (1.00 g), increased aging time to 16 h, and elevated aging temperature to 80 °C (kept for 8 h) were used in order to cause more SiO_2 dissolution. The product showed intense BEA characteristic XRD peaks at 7.6 and 22.4 ° (JCPDS 48–0074) [28] and had crystals with clear morphology and grain boundaries as

indicated in Figure 3.4b. Therefore, proper dissolution of RHA-SiO_2 seemed to be an important factor to obtain the crystalline products. The dissolution was then increased by mixing the ingredients using ultrasonic waves in addition to simple mechanical stirring. The XRD pattern and inset FE-SEM image shown in Figure 3.4c clearly indicated that crystalline BEA zeolite was successfully obtained. Several characteristic XRD peaks with higher intensities were detected and the crystals with particle sizes below 1 µm were observed.

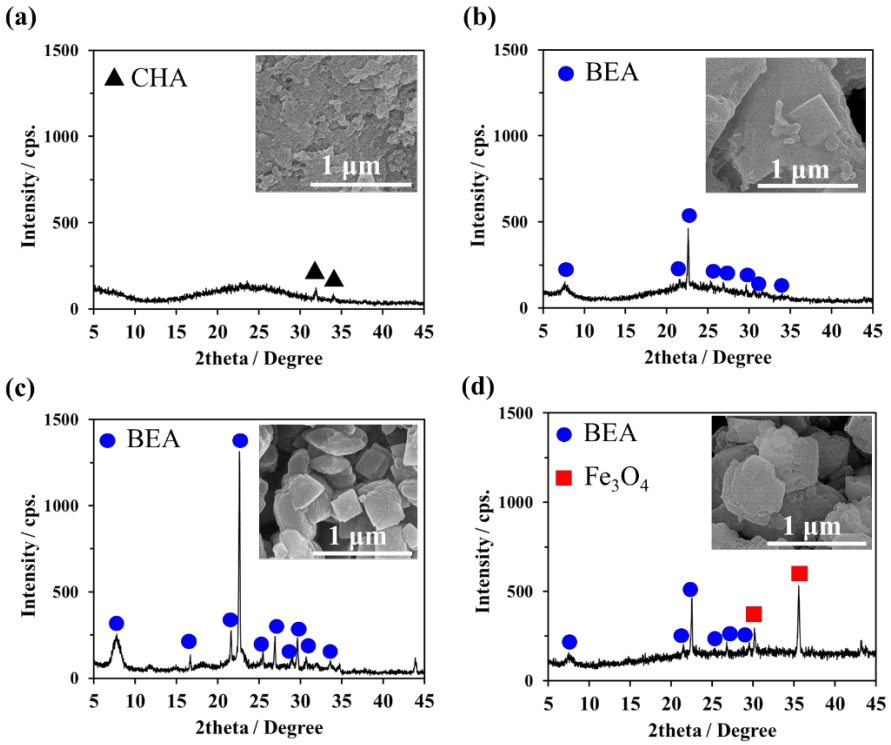

Figure 3.x XRD patterns with the inset FE-SEM images of the DGC products prepared by using RHA-SiO_2 particles at room temperature (a), double amount of NaOH, increased aging time to 16 h, and elevated temperature to 80 °C (kept for 8 h) (b) and additional ultrasonic waves (c), and included Fe_3O_4 particles (d) [25].

Finally, a gel with Fe_3O_4 particles were prepared by adding 1.12 g of Fe_3O_4 just before starting the drying step to confirm the crystallization of BEA with the presence of magnetic particles. As depicted in Figure 3.4d, the BEA zeolite characteristic peaks still appeared in

the XRD pattern along with those of Fe_3O_4 i.e., 30–40 ° (JCPDS 19–0629, [29]) and the crystal shapes and size did not differ from those without Fe_3O_4. This means no severe effect from the included Fe_3O_4 particles to the crystallization of BEA zeolite. Thus, ultrasonic waves greatly assisted the preparation of magnetic precursor gel which allowed synthesis of magnetic BEA zeolite using solid RHA-SiO_2 via DGC method. The synthesis procedure including gel preparation, DGC, and calcination was shown in Figure 3.5. Non-magnetic BEA sample was also synthesized for comparison by excluding the addition of Fe_3O_4 particles during gel preparation. The non-magnetic and magnetic BEA zeolite samples synthesized using RHA-SiO_2 are called RHAS-BEA and magnetic RHAS-BEA hereafter, respectively.

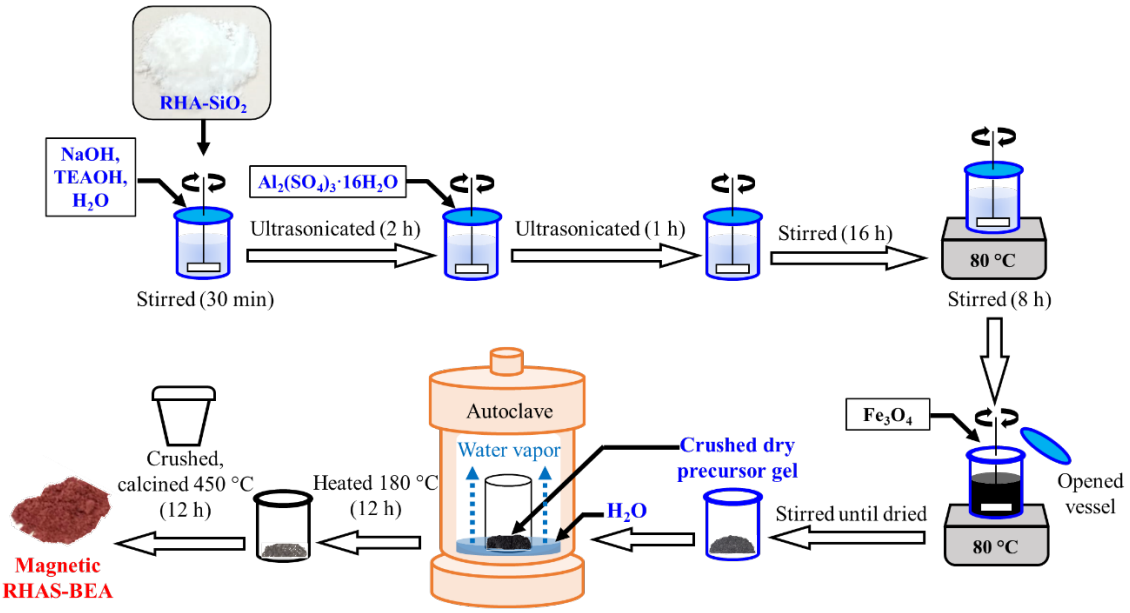

Figure 3.5 The DGC synthesis procedure of magnetic BEA zeolite using RHA-SiO_2 [25].

3.4.3 Characterization of the calcined samples

The as-synthesized samples were calcined at 450 °C for 12 h in order to remove the organic template (TEAOH) from the pore of zeolite. Figure 3.6a shows the XRD peaks of BEA zeolite present in both calcined non-magnetic and magnetic RHAS-BEA samples. This means that BEA zeolite phase was still preserved after calcination. Meanwhile, the

appearance of magnetic RHAS-BEA became reddish (inset photography in Figure 3.6a), and its XRD pattern shows a peak for a weaker magnetic phase, i.e., α-Fe_2O_3 (JCPDS 01–1053, [29]). This indicates the oxidation of Fe_3O_4 during calcination, similar to our study in the previous chapter.

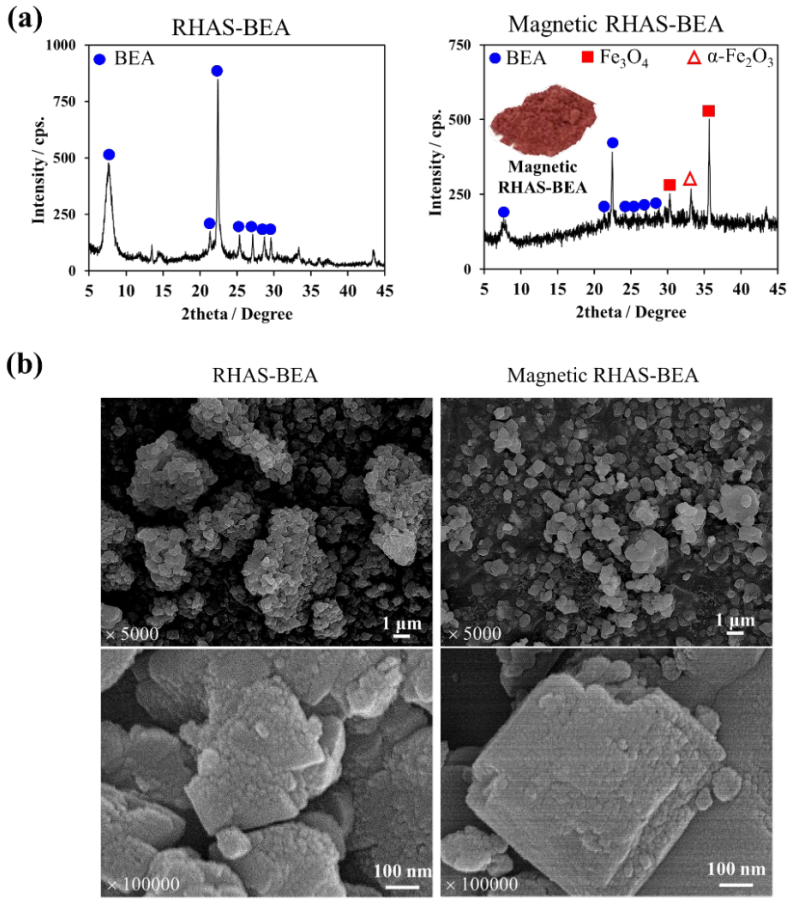

Figure 3.6 (a) XRD patterns of RHAS-BEA and magnetic RHAS-BEA (with inset of the powder photography), (b) FE-SEM images of the samples obtained after calcination at 450 °C for 12 h [25].

Figure 3.6b shows the FE-SEM images of the calcined samples observed at two different magnifications. The morphologies of both RHAS-BEA and magnetic RHAS-BEA were hardly different. The lower magnification images (× 5000) show the aggregates with sizes below 1 µm for both RHAS-BEA and its magnetic composite. The aggregate sizes of magnetic RHAS-BEA were found smaller than those of RHAS-BEA. This might be caused

by the large number of nuclei created between the Fe_3O_4 particles in the precursor gel [30,31]. At higher magnification (× 100000), rectangle-like faces of the crystals with rough surfaces were obviously seen for both samples, indicating aggregated nanoparticles of BEA which was also previously found in the literatures when DGC method was used [32,33].

The elemental analysis using FE-SEM-EDS at several spots reveals that the average Si/Al ratios of RHAS-BEA and magnetic RHAS-BEA were 48.8 ± 9.5 and 45.0 ± 14.8, respectively (Figure 3.7a), which fall in the range of high-SiO_2 zeolites [34]. Figure 3.7b shows the elemental Si and Fe mapping of magnetic RHAS-BEA using FE-SEM-EDS. It is seen that Fe distributed mostly along with Si in the entire analysis area. This implies that all BEA zeolites contained Fe_3O_4 particles. The results clearly indicate that utilizing solid RHA-SiO_2 in synthesis of magnetic BEA zeolite via DGC method is possible. Also, effect of the inclusion of magnetic particles to the morphologies of the composite was hardly seen.

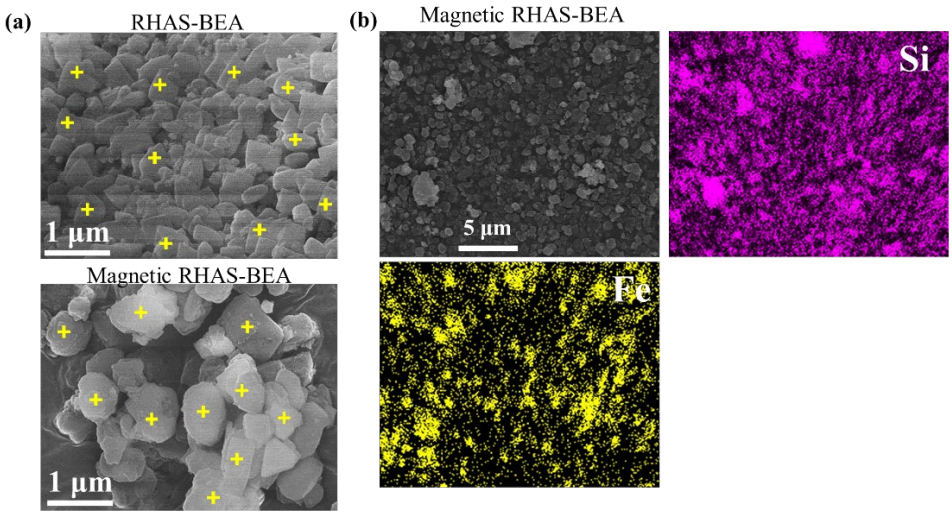

Figure 3.7 (a) FE-SEM-EDS results of the Si/Al ratio analysis of RHAS-BEA and magnetic RHAS-BEA and (b) Si and Fe elemental mapping of magnetic RHAS-BEA [25].

3.4.4 DGC synthesis of lower Si/Al using RHA-SiO_2

This experiment aimed for investigating the effect of Si/Al to adsorption of cationic pollutants, i.e., herbicides (paraquat). In addition, the effect of Si/Al against the morphology

of magnetic RHAS-BEA prepared using RHA-SiO_2 was examined. The Si/Al ratios of RHAS-BEA and magnetic RHAS-BEA were decreased by decreasing amount of RHA-SiO_2 to half of the recipe used in Section 3.4.2. Amount of each ingredient is as follows: 1.82 g of solid RHA-SiO_2, 1.00 g of a 20 wt% NaOH solution, 8.26 g of a 10 wt% TEAOH solution, 0.30 g of solid $Al_2(SO_4)_3 \cdot 14\sim18H_2O$, 4.08 g of distilled water, and 1.12 g of Fe_3O_4. The optimal DGC conditions and procedure shown in Figure 3.5 were also applied.

The XRD patterns in Figure 3.8 indicate that BEA zeolite was able to crystallize regardless of Fe_3O_4 particles addition when RHA-SiO_2 amount in the gel was decreased to half. The calcined magnetic RHAS-BEA still showed a minor mixed phased of α-Fe_2O_3, similar to previous experiments.

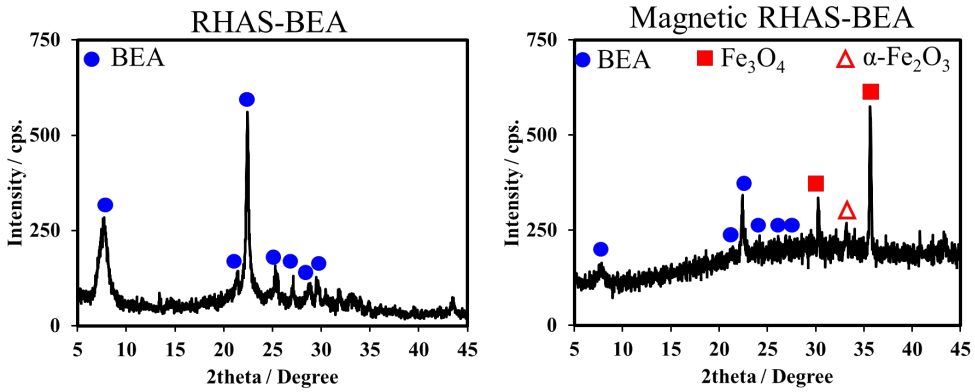

Figure 3.8 XRD patterns of RHAS-BEA and magnetic RHAS-BEA prepared using lower amount of RHA-SiO_2 via DGC method. The samples obtained after calcination at 450 °C for 12 h.

The FE-SEM images in Figure 3.9 indicate that lowering Si content in the gel reduced particle sizes, in comparison to ones with higher Si. This could be assumably explained that lowering RHA-SiO_2 resulted in higher OH^-/Si ratio during gel preparation [35]. This means RHA-SiO_2 could be dissolved more easier which shall have promoted nucleation. More rapid formation of aluminosilicate species results in shorter induction periods, larger number of nuclei and, finally, smaller crystal sizes [36]. However, the high magnification

FE-SEM images show similar rectangle-like faces of aggregated nanoparticles of BEA zeolite to those obtained with higher Si.

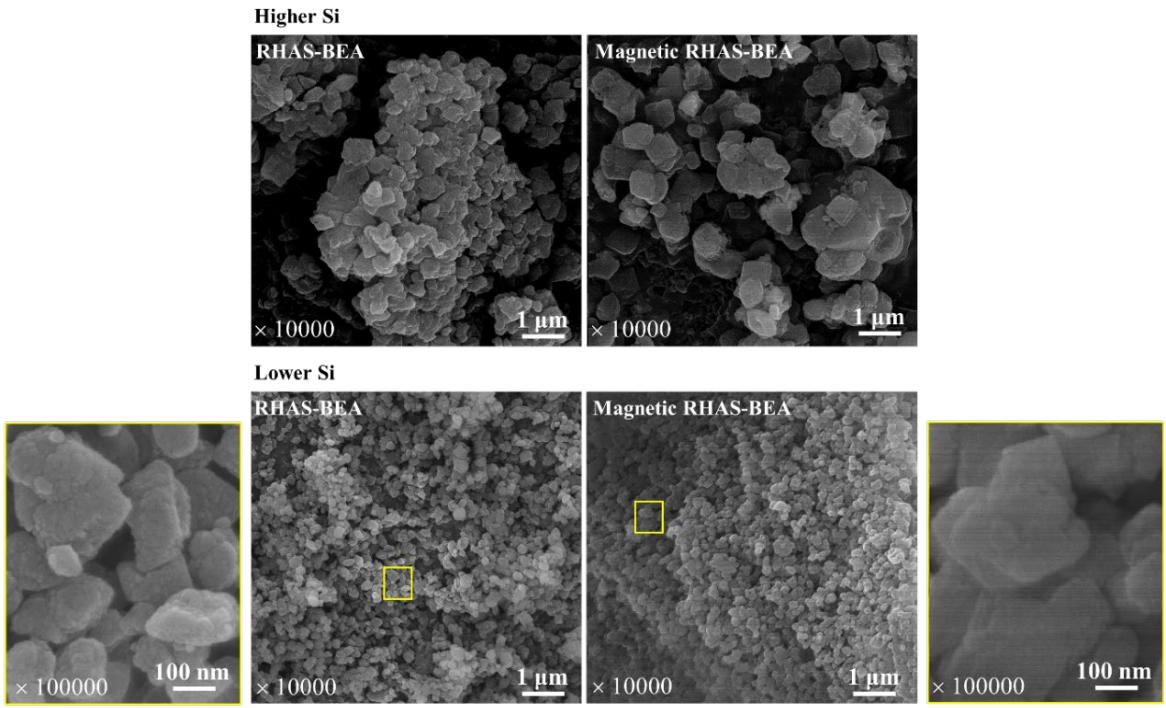

Figure 3.9 Comparison of morphologies observed by using FE-SEM of the calcined samples prepared via DGC method using different amount of RHA-SiO_2.

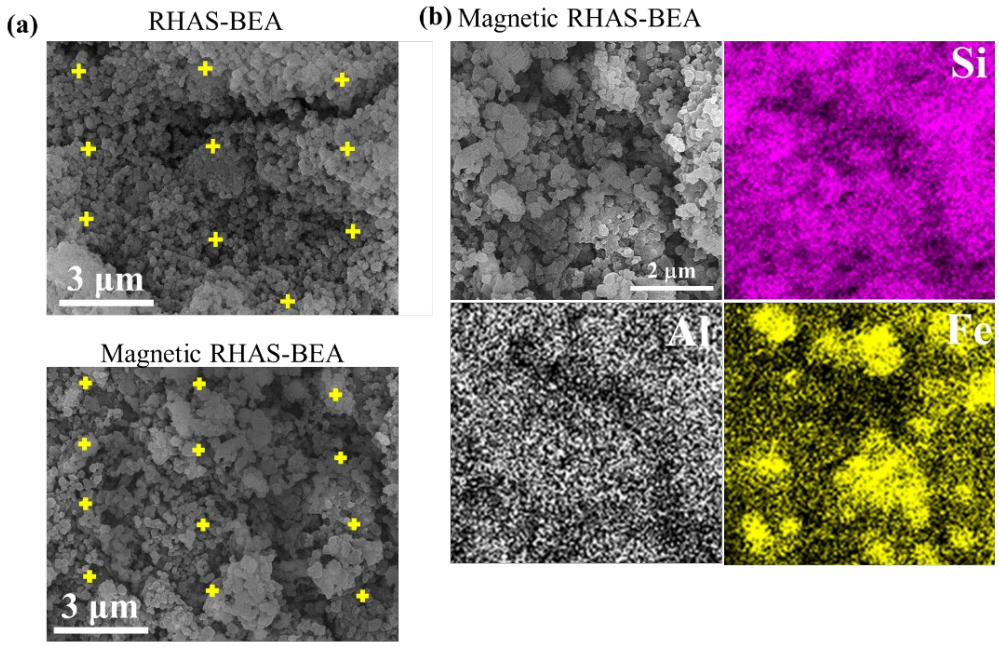

Figure 3.10 FE-SEM-EDS analyses of RHAS-BEA and magnetic RHAS-BEA prepared using lower amount of RHA-SiO_2: (a) Spot analysis, (b) Si, Al, and Fe elemental mapping of magnetic RHAS-BEA.

The Si/Al ratios analyzed by FE-SEM-EDS spot analysis were 23.3 ± 4.0 and 19.8 ± 3.8 for RHAS-BEA and magnetic RHAS-BEA, respectively (Figure 3.10a). The Si/Al ratios are less than half of that of the samples synthesized using higher amount of RHA-SiO_2. The elemental mapping of the magnetic RHAS-BEA shows the distribution of Fe, representing the magnetic particles, along with that of Si and Al of the BEA zeolite phase (Figure 3.10b), considering the surface morphology well resembles that of BEA zeolite, the magnetic particles seem to have been incorporated inside the BEA zeolite particles.

3.5 Determination of paraquat adsorption performance

In this section, paraquat adsorption performance of BEA and magnetic BEA zeolite synthesized via DGC method using higher amount of RHA-SiO_2 was tested by studying the adsorption kinetics and isotherms. Effect of initial pH on the adsorption performance was also investigated. All adsorption tests were performed using fixed adsorbent concentration of 1 g/L and orbital shaking speed of 120 rpm for 24 h at room temperature (26 °C).

Aqueous solutions of paraquat were used throughout the experiments. Quantification of paraquat in the solutions was performed on the UV-Visible spectrophotometer ($\lambda = 257$ nm). Adsorption capacity of the adsorbent was calculated using Equation 2.2 (Chapter 2).

3.5.1 Adsorption kinetics

The adsorption kinetics were studied in order to examine the effect of contact time on paraquat adsorption. The testes were carried out by shaking the adsorbents in a paraquat solution (75 mg/L) for a varied contact time between 1 and 1440 min. The initial pH of the paraquat solution was not adjusted (≈ 5.8). The adsorption capacity for each contact time (q_t) was calculated using the same equation for q_e. The results were shown in Figure 3.11. Within 1 min, a significant amount of paraquat was rapidly adsorbed on RHAS-BEA and magnetic RHAS-BEA. The adsorbed amount continued to sharply increased until 10 min, indicating high adsorption rates of the synthesized adsorbents. Then the adsorption rate became slower and reached saturation at 60 min. In the previous studies that found in literatures, different types of zeolites such as FAU [37], modified FAU [38], and MFI [39] also showed fast adsorption rate of paraquat. Similar adsorption kinetic trends were found for RHAS-BEA and magnetic RHAS-BEA but the non-magnetic one showed higher saturated adsorbed amount. This could be due to the higher fraction of BEA zeolite (i.e., lower fraction of Fe_3O_4) in the non-magnetic one.

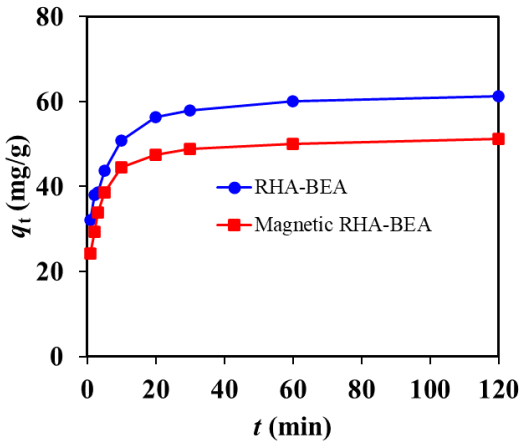

Figure 3.11 Change in amount of paraquat adsorbed on RHAS-BEA and magnetic RHAS-BEA over time [25].

Three most common linearized adsorption kinetic models namely pseudo-first-order (PFO), pseudo-second-order (PSO), and intraparticle diffusion (IPD) [40] were applied to the adsorption kinetic data. The linearized forms of PFO, PSO, and IPD models are shown in Equation 3.1–3.3.

PFO: $$\ln(q_e - q_t) = \ln q_e - k_1 t$$ Equation 3.1

PSO: $$\frac{t}{q_t} = \frac{q}{k_2 q_e^2} + \frac{t}{q_e}$$ Equation 3.2

IPD: $$q_t = k_{ipd}\sqrt{t} + C$$ Equation 3.3

where q_e and q_t are the adsorption capacities of paraquat at equilibrium time (mg/g) and time t (mg/g), respectively; t is the adsorption time (min); k_1, k_2, and k_{ipd} are the adsorption kinetic constants of PFO (1/min), PSO (g/mg min), and IPD (mg/(g $min^{1/2}$)), respectively; C is the intercept of IPD model which represents the thickness of the boundary layer [41]. Considering the highest R^2 value, paraquat adsorption kinetics for RHAS-BEA and magnetic RHAS-BEA PSO model was found to best fit the PSO model, as shown in Figure 3.12. The PSO fitting indicates that the surface adsorption, i.e., chemisorption, took place via electrostatic interaction between paraquat and the adsorbents [42].

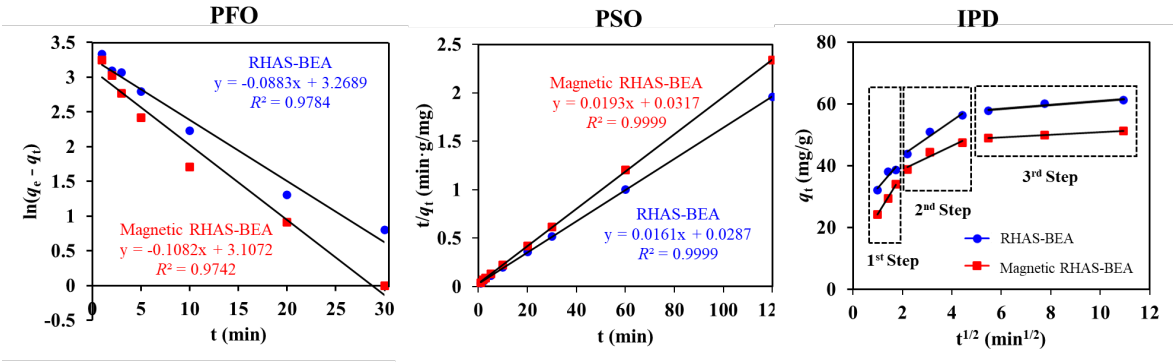

Figure 3.12 PFO, PSO, and IPD adsorption kinetic model plots for paraquat adsorption on RHAS-BEA and magnetic RHAS-BEA [25].

k_2 values calculated from the PSO linear equations of RHAS-BEA (i.e., 0.0087 g/mg) and magnetic RHAS-BEA (i.e., 0.0078 g/mg) were similar, which means the negligible

effect from the inclusion of Fe_3O_4 particles in the BEA zeolite to the adsorption rate of paraquat. The IPD plots show linear trends in three steps which means multiple-step adsorption occurred [43]. However, the trend lines of the first step did not pass through the origin. Intraparticle diffusion was therefore not considered as the primary mechanism in this study. These results reveal that the overall adsorption of paraquat adsorption might be controlled by a surface reaction through a chemisorption mechanism, rather than intraparticle diffusion.

3.5.2 Adsorption isotherms

The adsorption isotherms were studied in order to estimate the adsorption behavior. The tests were carried out by shaking the adsorbents in paraquat solutions prepared at a concentration range 10–750 mg/L for a fixed contact time of 24 h (26 °C). The experiments were carried out in duplicates. The initial pH values of the paraquat solutions were not adjusted (≈ 5.8). The results in Figure 3.13 show an increase in the q_e values with the increasing C_e which saturated at ≈ 70 and 50 mg/g for RHAS-BEA and magnetic RHAS-BEA, respectively.

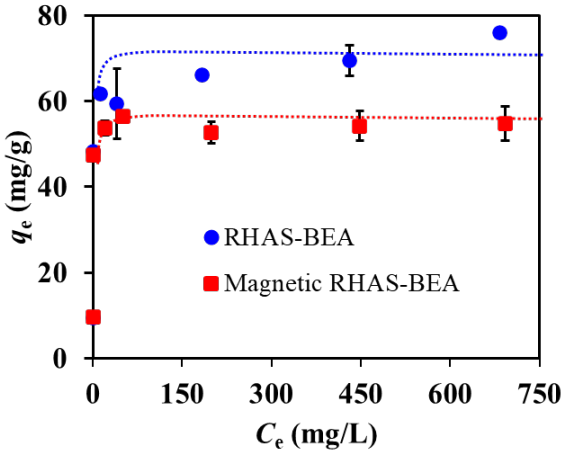

Figure 3.13 Adsorption isotherm of paraquat on RHAS-BEA and magnetic RHAS-BEA (error bars indicate the standard deviation) [25].

Linearized Langmuir and Freundlich adsorption models, as shown in Equation 2.4 and 2.5 in Chapter 2, were used to evaluate the maximum adsorption capacity of paraquat.

The linear plots shown in Figure 3.14 indicate that Langmuir model is more suitable to describe the adsorption behavior of paraquat on RHAS-BEA and magnetic RHAS-BEA, according to the R^2 values.

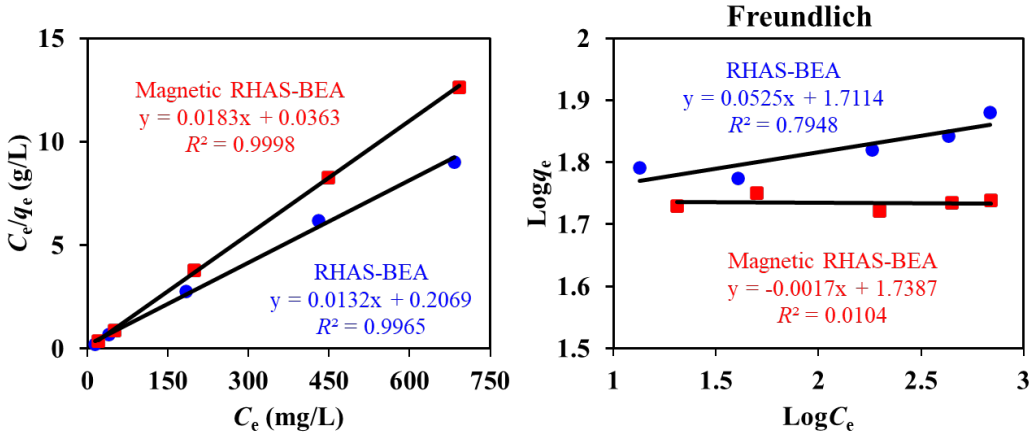

Figure 3.14 Langmuir and Freundlich adsorption model plots for paraquat adsorption on RHAS-BEA and magnetic RHAS-BEA [25].

Langmuir model indicates a monolayer adsorption type on homogeneous sites on the adsorbent surface [44]. This model was found fitted to adsorption of paraquat on zeolites [8,45–48], and various adsorbents such ash mesoporous SiO_2 [8,44,47,48], zeolite/mesoporous SiO_2 composites [47], graphene oxide/mesoporous SiO_2 composites [49], clays [50], and modified biopolymers [5,51,52]. From the Langmuir equations, q_m values for RHAS-BEA and magnetic RHAS-BEA were calculated to be 75.64 ± 1.09 and 54.71 ± 4.19 mg/g, respectively. As seen that q_e value for magnetic RHAS-BEA is approximately 72.3% of the q_e value for the non-magnetic one. The fraction of magnetic content in the as-synthesized magnetic RHAS-BEA was calculated to be 20.9 wt% using weight of the obtained dry gel, the amount of gel used for DGC, and weight of the as-synthesized product. The amount of oxidized phase was small, and therefore the magnetic content should be almost maintained. Meanwhile, weight decrease after calcination of the non-magnetic RHAS-BEA revealed the amount of organic SDA in the samples–that means the total fraction of RHAS-BEA phase after calcination was known, i.e., cal. 71.8 wt%. This RHAS-BEA fraction is believed to be the same as that in the as-synthesized magnetic

RHAS-BEA. For example, when 0.2008 g of as-synthesized magnetic RHAS-BEA was calcined, the amount of RHAS-BEA was 0.718 × (0.2008 g – (0.209 × 0.2008 g)) = 0.1140 g. The experimental data showed that the remaining weight of 0.2008 g sample after calcination was 0.1570 g. This amount might include RHAS-BEA and Fe_3O_4. Therefore, weight percentage of RHAS-BEA in the calcined magnetic RHAS-BEA sample is (0.1140 g/0.1570 g) × 100 = 72.6 wt%. This amount is very similar to 72.3%. This is believed to be the reason of the lower q_m value for magnetic RHAS-BEA sample.

3.5.3 Effect of initial pH on paraquat adsorption

The tests were carried out by shaking the adsorbents in a paraquat solution (100 mg/L), but the initial pH values were pre-adjusted between ≈ 3 to 9 using 0.1 mol/L HCl or 0.1 mol/L NaOH solutions, for 24 h (26 °C). pH values outside this range were not considered since dealumination and dissolution of SiO_2 of the adsorbents can be induced at very acidic region and highly alkali conditions, respectively. Also, most natural water is generally neutral. After 24-h shaking, the supernatants were taken to evaluate the effect of the initial pH to q_e values.

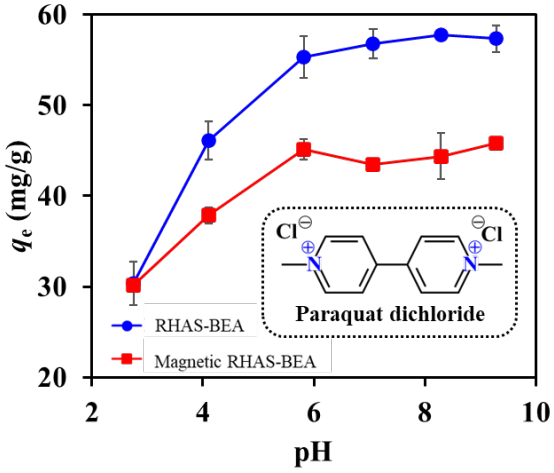

Figure 3.15 Effect of initial pH on paraquat q_e values for RHAS-BEA and magnetic RHAS-BEA with inset of paraquat dichloride structure (error bars represent the standard deviation, n = 2) [25].

As shown in Figure 3.15, the adsorption of paraquat on RHAS-BEA and magnetic RHAS-BEA was pH-dependent in aqueous solutions. The q_e values became lower when the pH decreased from ≈ 6 (the non-adjusted pH value of the paraquat solution) to 3, but tended to slightly increase at higher pH values. The q_e values seemed to be constant above pH 7. This trend was observed for both RHAS-BEA and magnetic RHAS-BEA. The paraquat structure, inset in Figure 3.15, has no protons left at the two positively charged quaternary amine groups to be further protonated or deprotonated. This cationic form therefore might have existed over a wide pH range, which means the change in initial pH values did not change the ionic form of paraquat. The pH values at the point of zero charge on the adsorbent surfaces (pH_{pzc}) was determined by shaking the adsorbents (0.5 g/L) in 0.01 mol/L NaCl solutions that had initial pH values (pH_i) in the range ≈ 3–10 for 24 h at 26 °C. After filtration, the final pH values (pH_f) of the solutions were measured. The differences between pH_i and pH_f were plotted against their pH_i values. The connecting lines that pass $pH_i - pH_f = 0$ is the pH_{pzc} of the adsorbents, as depicted in Figure 3.16.

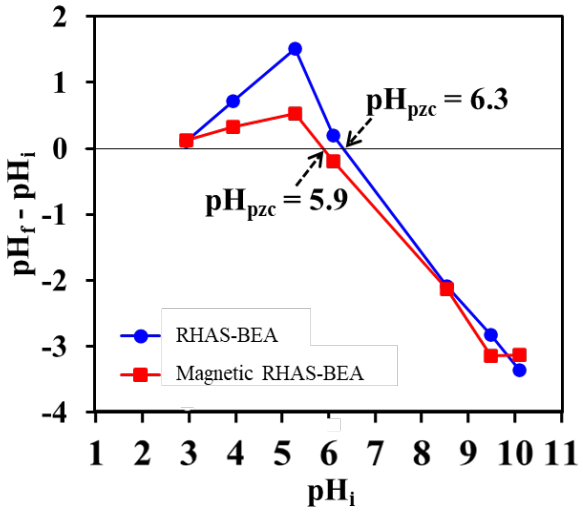

Figure 3.16 pH_{pzc} values of RHAS-BEA and magnetic RHAS-BEA [25].

It was found that the initial pH values affected the surface charges on the adsorbents. Similarly, the pH_{pzc} values for RHAS-BEA and magnetic RHAS-BEA were 6.3 and 5.9, respectively. At pH values below the pH_{pzc} the surface charges tended to be positive due to the protonation of the hydroxy groups [53], i.e., $–OH + H^+ \rightarrow –OH_2^+$, on the surface,

whereas the deprotonation might occur at higher pH region above pH_{pzc}, i.e., –OH + OH^- → $–O^-$ + H_2O, which results in negatively charged on the surface. This might reflect the lower q_e values at lower initial pH due to the electrostatic repulsion between cationic paraquat and the positively charged surface of the adsorbent. In contrast, the negatively charged surface of the adsorbent at higher pH shall attract the cationic paraquat which yielded higher q_e values. However, the q_m values in this study were calculated from the adsorption isotherm studies carried out using the original pH value ≈ 5.8, which is sufficient for the typical pH range in most natural waters [37].

3.5.4 Possible interactions between paraquat and the synthesized adsorbents

It is noteworthy that the surface charge approaches neutral at pH ≈ pH_{pzc} but paraquat was still adsorbed on the adsorbents, as shown by the q_e values at the initial pH ≈ 6. Thus, interactions other than the aforementioned electrostatic forces may be contributing to the adsorption. Ion exchange between Na^+ ions at the $[AlO_{4/2}]^-$ sites and cationic paraquat was reported to happen during adsorption [47,54]. The adsorbents prepared using less RHA-SiO_2 (lower Si/Al ratios), namely with larger ion exchange capacity due to larger amount of $[AlO_{4/2}]^-$ sites, were used to investigate the possible ion exchange.

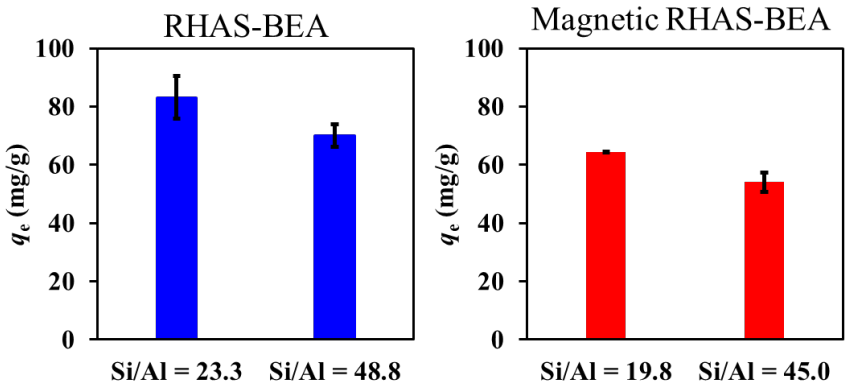

Figure 3.17 Comparison of q_e values for paraquat adsorption on RHAS-BEA and magnetic RHAS-BEA that have different Si/Al ratios (error bars represent the standard deviation, n=2).

As shown in Figure 3.17, significant increase in q_e values was found, approximately 19%, when the adsorbents that had lower Si/Al ratios were used. This means more paraquat was adsorbed on the adsorbents when amount of $[AlO_{4/2}]^-$ sites in BEA zeolite increased. The larger amount of Na^+ available for ion exchange with cationic paraquat may have caused this change. Whereas the smaller crystal sizes might have also resulted higher q_e due to higher surface area. However, the implied the contribution of ion exchange in the adsorption of paraquat on RHAS-BEA and magnetic RHAS-BEA adsorbents. The molecular size of paraquat is 0.64 × 0.34 × 1.34 nm [8,55], which is smaller than Na^+-BEA zeolite cavity. That means the adsorption could take place via pore diffusion. Several studies have previously reported other mechanisms than ion exchange. Rasaie et al. explained that hydrogen bonding also took place during paraquat adsorption on mesoporous SiO_2-modified bentonite [44], while Keawkumay et al. said that hydrogen bond was found between the H atom of paraquat and the O atom centered around Al in FAU zeolite [46]. Osakoo et al. utilized X-ray photoelectron spectroscopy to analyze surface of paraquat-adsorbed FAU zeolite/mesoporous SiO_2 composite, which found binding energy between the C and N atoms of paraquat and the centered O atom in the composite [47]. According to the analysis results obtained from Fourier-transform infrared spectroscopy, Rongchapo et al. found evidence of interaction between the aromatic rings and methyl groups of paraquat and FAU framework [54]. A similar phenomenon may have occurred in this study.

3.6 Magnetic separability of the adsorbents from aqueous solutions

Figure 3.18a presents a simple magnetic separation of the adsorbents. In the absence of Nd magnet, both non-magnetic and magnetic RHAS-BEA slowly settled to the bottom of the bottles, and most of the them remained in the liquid phase. When the Nd magnet was attached to the wall of the bottle the magnetic RHAS-BEA quickly attracted the magnetic field and the solution became much clearer within 1 min, while the non-magnetic one did not attract. This proves that the magnetic adsorbent was effective for quick collection using a magnet.

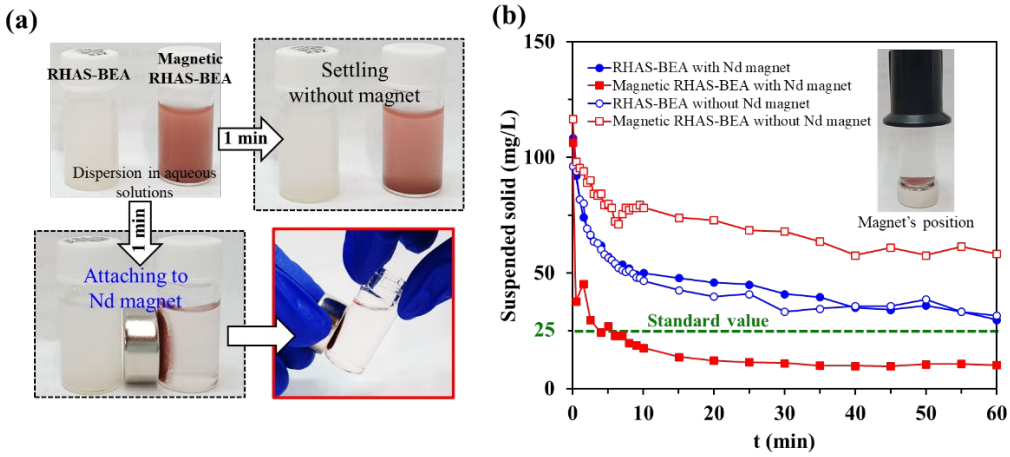

Figure 3.18 (a) Settling of RHAS-BEA and magnetic RHAS-BEA with and without Nd magnet for 1 min, (b) magnetic separability of RHAS-BEA and magnetic RHAS-BEA evaluated by monitoring the change in suspended solid concentrations over time, and inset of magnet's position during the measurement [25].

Ability of the adsorbents to be separated from aqueous solution under magnetic field was evaluated by monitoring the sedimentation behavior of adsorbents suspended in an aqueous media. RHAS-BEA and magnetic RHAS-BEA particles at a concentration of 100 mg/L in distilled water were shaken for 2 h. The suspensions were allowed to stand in the absence or presence of a neodymium magnet (Nd, surface flux density of 0.45 T) for 0.5–60 min at room temperature. The position of the Nd magnet is illustrated as inset in Figure 3.18b. Suspended solids (SS) concentration, in mg/L, in the supernatant was evaluated by converting turbidity (in formazin turbidity unit) using a calibration curve prepared from solutions with known SS concentrations. As seen in Figure 3.18b, the concentration of SS slowly decreased in the absence of magnet for both samples, in which the magnetic RHAS-BEA sedimented more slowly because of its smaller aggregate sizes. The SS level could not meet the SS standard value for rivers set in the Japan Environmental Quality Standards for Protecting the Living Environment (25 mg/L) [56] even after waiting for an hour. Meanwhile, when a magnet was applied, the SS for non-magnetic RHAS-BEA slowly decreased at similar rate to the test without magnetic field while that for magnetic RHAS-BEA sharply decreased to below 25 mg/L. These results reveal that the co-existing weakly

magnetic phase, i.e., α-Fe_2O_3, did not show severe adverse effect on the separation of the magnetic RHAS-BEA adsorbent. Therefore, compositing RHAS-BEA zeolite with magnetic particles greatly facilitated the collection of adsorbents after paraquat removal.

3.7 Reusability and ions leached from the adsorbents during adsorption

Economic feasibility was considered in terms of reusability in addition to adsorption performance and magnetic separability. This is an important aspect in practical water treatments. In most studies, the adsorption of paraquat on adsorbents is mainly ion exchange, which is inhibited in acidic media or at high salinity. Therefore, salt solutions [50] and acid solutions [4,41,49] were previously used as desorption solvents for regenerating adsorbents after paraquat adsorption. However, handling of washing solutions after adsorbent regeneration was of concern. Thus, thermal treatment of the spent adsorbent was considered in this work. After paraquat adsorption, using 500 mg/L-paraquat solutions, the paraquat-adsorbed RHAS-BEA and magnetic RHAS-BEA adsorbents were collected and calcined in air at 450 C for 6 h. This temperature is above the thermal degradation temperature of paraquat, i.e., 300 °C [57]. The thermal treated adsorbents were then reused in the following adsorption cycle.

Figure 3.19 presents the q_e values obtained from each adsorption/regeneration cycle. The regenerated adsorbents show lower q_e values by approximately 40 and 30% for RHAS-BEA and magnetic RHAS-BEA, respectively, than the pristine ones. After the first reuse, the adsorbents show unchanged q_e values for additional three re-adsorption/regeneration cycles. The lower adsorption performance after the first cycle can be attributed to the incomplete removal of adsorbed paraquat. The residue may remain at the least accessible sites, hindering the access of paraquat in the following cycles.

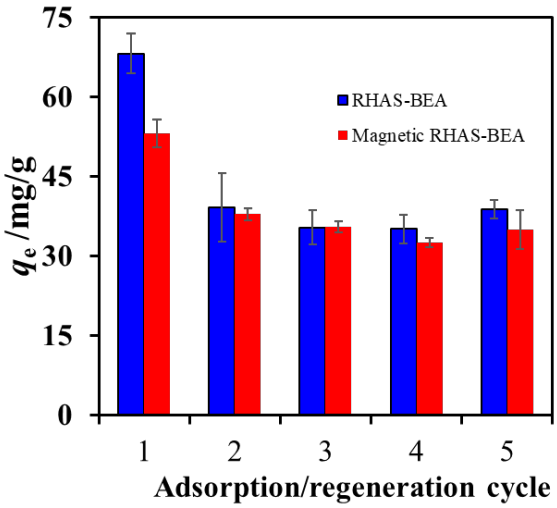

Figure 3.19 q_e values for RHAS-BEA and magnetic RHAS-BEA obtained after five consecutive adsorption/thermal regeneration cycles (error bars represent the standard deviation, n=2) [25].

Regardless of the initial use, the adsorbents could be reused for at least four cycles without showing degradation in their performance, i.e., the q_e values were in the range 37.08 ± 7.95 and 35.21 ± 4.04 mg/g for used RHAS-BEA and magnetic RHAS-BEA, respectively. These levels are still acceptable and comparable to those of fresh adsorbents reported previously (Table 3.3), given the advantages of using DGC method, and magnetic separability. Moreover, the similar adsorption amounts among the four-time regeneration revealed that there was no negative impact on the adsorption due to the inclusion of Fe_3O_4 particles in the BEA zeolite.

Stability of the synthesized adsorbents were evaluated by investigating the ions leached from the adsorbents during the adsorption tests, i.e., Si, Al and Fe. Suspension of adsorbents (1 g/L) in water and paraquat solution (1 mg/L) was shaken for 3 h at 26 °C. The solutions were collected for measuring the potential leached elements using ICP-AES. It was found that Si slightly leached from the adsorbents while Al was not detected in the solutions after 3-h shaking time at pH ≈ 6. The detected concentration of Si in RHAS-BEA and magnetic RHAS-BEA suspension were 1 mg/L and 0.4 mg/L, respectively, which were

approximately 0.1 and 0.04 wt% of the pristine RHAS-BEA and magnetic RHAS-BEA adsorbents, respectively. The leaching of Si at this level was considerably negligible which indicates that the developed adsorbents are stable under the tested conditions. For the magnetic RHAS-BEA, Fe was not detected in the adsorption solution, which also supports the idea that the magnetic particles were incorporated inside the zeolite particles.

3.8 Co-adsorption tests

3.8.1 Paraquat adsorption with co-existing of blue dye

Aqueous paraquat solutions are generally colorless. Additives, i.e, dyes, are therefore used in commercial herbicides in order to avoid accidental poisoning [8,38]. This experiment is carried out to examine the paraquat adsorption selectivity in the presence of a representative blue dye, i.e., Cibacron blue 3G-A (CB), in practical applications. Paraquat and CB aqueous solutions were prepared individually and mixed. Fixed concentration of paraquat at 40 µmol/L (equivalent to 10 mg/L) in both single and mixed solutions was used, while CB concentration was examined at two different levels, i.e., 4 and 40 µmol/L (neglected the purity). Single and binary adsorption tests were performed using the adsorbent concentration of 1 g/L, contact time of 24 h at 26 °C, and non-adjusted pH values. The UV–Visible spectrophotometer was used to measure the concentration of paraquat and CB.

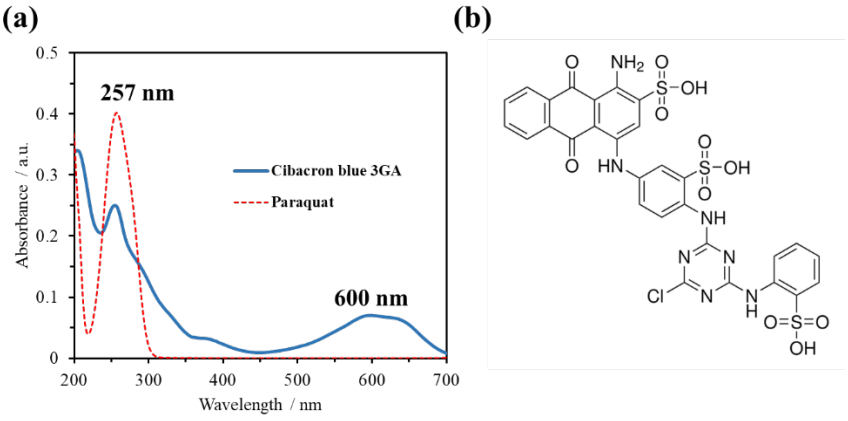

Figure 3.20 (a) UV–Visible absorption spectra of paraquat and CB [25], (b) Chemical structure of CB.

The UV–visible absorption spectra of paraquat and CB, presented in Figure 3.20a, showed the strong absorption band at 600 nm for CB and the co-absorption peaks of paraquat and CB at 257 nm which hindered the quantification of paraquat. The co-absorption effect was subtracted in the binary mixture using the constant ratio between the absorbance at 257 and 600 nm of a single CB. The results in Figure 3.21 show that paraquat removal efficiencies of more than 99% in the single adsorption and with the presence of CB at two different levels. This means that CB did not suppress the adsorption of paraquat, whereas the adsorbents only adsorbed a small amount of CB since its molecular size is much larger than that of paraquat (see the chemical structure of CB in Figure 3.20b). The results implies that the synthesized RHAS-BEA and magnetic RHAS-BEA have high potential in selective removal of paraquat from commercial herbicides.

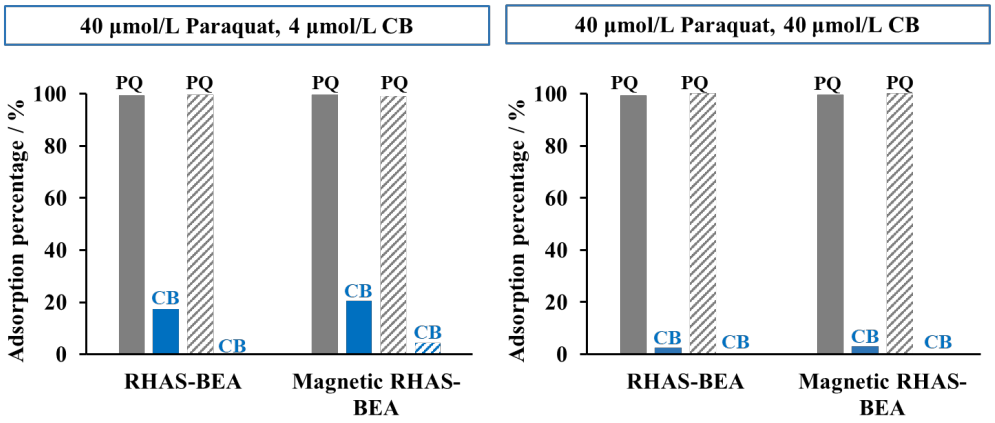

Figure 3.21 Paraquat (PQ) removal efficiency of RHAS-BEA and magnetic RHAS-BEA tested without (solid-fill bars) and with co-existing of CB (pattern fill bars) systems [25].

3.8.2 Paraquat adsorption with co-existing of diquat

Herbicides that have similar structures to paraquat might also be adsorbed on the developed adsorbents through similar mechanisms. Diquat is one of the commonly used herbicides along with paraquat [58] and also shows negative effects to human health [59]. Both paraquat and diquat should be therefore removed from water. Paraquat and diquat aqueous solutions were prepared individually and mixed at fixed concentration of 40 µmol/L. Single and binary adsorption tests were performed using the adsorbent

concentration of 1 g/L, contact time of 24 h at 26 °C, and non-adjusted pH values (≈ 5.8). UV absorption spectra of paraquat and diquat were recorded and compared using the UV–Visible spectrophotometer.

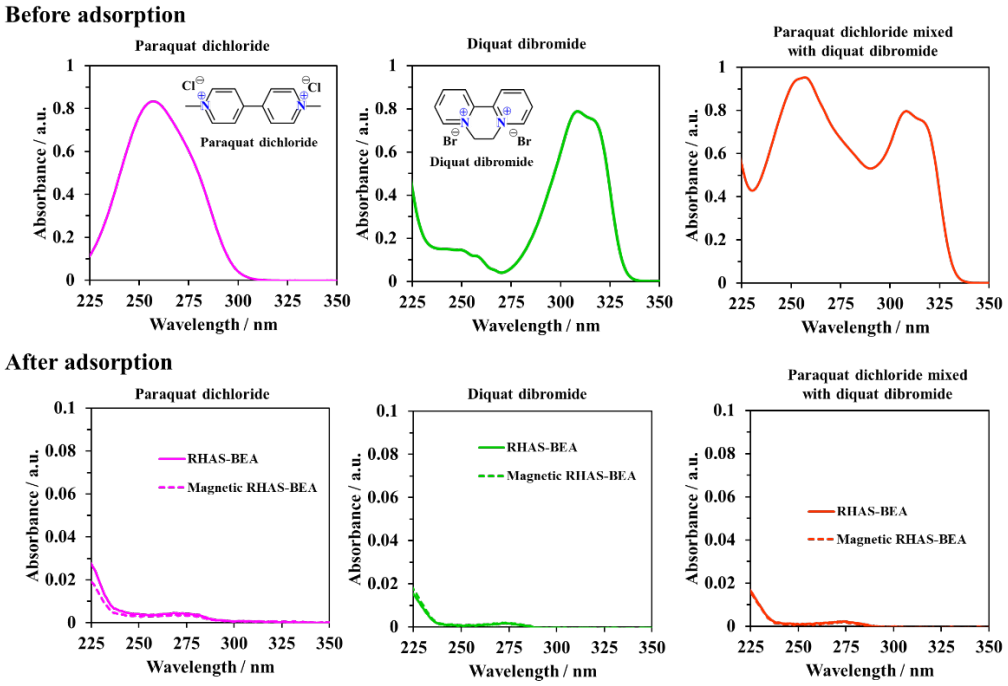

Figure 3.22 UV absorption spectra of paraquat and diquat before and after adsorption on RHAS-BEA and magnetic RHAS-BEA tested using single and mixed systems [25].

Before adsorption, paraquat and diquat showed strong UV absorption peaks at 257 and 322 nm, respectively, in both single and mixed solutions as shown in Figure 3.22. After adsorption using RHASBEA and magnetic RHAS-BEA, their UV absorption intensities decreased below the detection limit of the spectrophotometer for both single and mixed systems. This means that diquat is also adsorbed onto the synthesized adsorbents and did not interfere the adsorption of paraquat. Therefore, the developed RHAS-BEA and magnetic RHAS-BEA show another advantage of being applicable for simultaneous removal of more than one herbicide from contaminated waters.

3.9 Comparison of adsorption performance of this work with other adsorbents

The difference in experimental conditions and adsorbent natures make direct comparison of adsorption performance among various types of adsorbents rather difficult. However, the Langmuir maximum adsorption capacities (q_m) of various adsorbents, summarized in Table 3.3, are compared per equal weight of each adsorbent, i.e., 1 g adsorbent. The developed adsorbents in this work showed lower q_m values than the low-SiO_2 zeolites reported in several papers, including the BEA zeolite prepared by conventional hydrothermal synthesis using RHAS [8], but higher adsorption performance than those of several types of adsorbents, such as mesoporous SiO_2, clays, graphene oxide, and H-LTL zeolites. Despite the moderate adsorption performance, the developed RHAS-BEA and magnetic RHAS-BEA adsorbents show following advantages: they are synthesized through the use of agricultural waste–derived ingredients; the magnetic adsorbent can be easily collected through magnetic separation; and they both can also be reused. Additionally, our adsorbents exhibited a paraquat removal efficiency of more than 99% in the presence of blue dye. Thus, RHAS-BEA and magnetic RHAS-BEA could be used as alternative candidates for paraquat removal from contaminated waters.

Table 3.3 Langmuir maximum paraquat adsorption capacities of the adsorbents in this study and previous studies [25].

Adsorbents	Adsorption test conditions					q_m (mg/g)	Reported number of reuses (cycle)	Ref.
	C_0 (mg/L)	Adsorbent dosage (g/L)	Contact time (min)	pH	Temp. (°C)			
k-carrageenan modified Fe_3O_4@SiO_2 nanosorbent	30–900	0.50	60	7.3	25	257	4*	[5]
FAU (NaY) zeolite (Si/Al = 2.40)	100–1500	2.5	60	5	25	234.40	NR	[46]
FAU (NaY) zeolite (Si/Al = 3.5)	100–750	2.5	60	NR	RT	204.1	NR	[47]
FAU (NaY) zeolite (Si/Al = 2.2)	80–1000	2.5	60	NR	RT	185.2	NR	[8]
K-LTL zeolite (Si/Al = 3.14)	50–500	2.0	1440	11	30	166.71	NR	[45]
FAU (NaY) zeolite /SBA-15 composite (Si/Al = 4.7)	100–750	2.5	60	NR	RT	144.9	NR	[47]
BEA zeolite (Si/Al = 14.2)	80–1000	2.5	60	NR	RT	122.0	NR	[8]
FAU (NaX) zeolite (Si/Al = 1.27)	80–720	2.5	60	NR	RT	120.3	NR	[48]
Poly (vinyl alcohol)-cyclodextrin nanosponges	25–300	2	180	6.5	30	112.2	5*	[60]
2,2,6,6-tetramethylpiperidine 1-oxyl oxidized cellulose nanofibers	NR	0.10	120	7	30	108	NR	[51]

NR = not reported; RT = Room temperature; * = number of reuses with no significant change in adsorption performance, including the first use.

Table 3.3 (Continued) [25].

Adsorbents	Adsorption test conditions					q_m (mg/g)	Reported number of reuses (cycle)	Ref.
	C_0 (mg/L)	Adsorbent dosage (g/L)	Contact time (min)	pH	Temp. (°C)			
Algerian bentonite	50–300	2.0	1440	NR	25	100	NR	[50]
FAU (HY) zeolite (Si/Al = 50)	50–250	1.0	1440	11	30	92.59	NR	[37]
RHAS-BEA zeolite (Si/Al = 48.8)	10–750	1.0	1440	5.8	26	75.64	4	This study
SDS-modified FAU (HY) zeolite (Si/Al = 50)	50–250	1.0	1440	11	30	71.42	NR	[37]
25%Al-MCM-41	80–560	2.5	60	NR	RT	65.6	NR	[48]
Magnetic RHAS-BEA zeolite (Si/Al = 45.0)	10–750	1.0	1440	5.8	26	54.71	4	This study
Graphene oxide/SiO_2	4–24	0.40	2	7	25	31.34	4	[49]
H_LTL zeolite (Si/Al = 5.10)	50–500	2.0	1440	11	30	25.67	NR	[45]
Polyester textile coated with cyclodextrin	10–250	2	420	6.5	30	24.2	6*	[52]
MCM-41	80–1000	2.5	60	NR	RT	21.3	NR	[8]
Rice husk ash-SiO_2	80–1000	2.5	60	NR	RT	18.9	NR	[8]

NR = not reported; RT = Room temperature; * = number of reuses with no significant change in adsorption performance, including the first use.

Table 3.3 (Continued) [25].

Adsorbents	Adsorption test conditions					q_m (mg/g)	Reported number of reuses (cycle)	Ref.
	C_0 (mg/L)	Adsorbent dosage (g/L)	Contact time (min)	pH	Temp. (°C)			
Ketoenol–pyrazole receptor functionalized SiO_2	NR	2	NR	11.0	25±0.1	17.63	5*	[41]
SBA-3-SO_3H decorated Fe_3O_4/SiO_2 core shell nanoparticles	5–75	2.4	60	7.0	RT	14.73	6*	[4]
Bentonite/SiO_2	4–24	1.6	2	7	NR	11.75	NR	[44]
Acid activated bentonite	4–24	1.6	2	NR	NR	5.93	NR	[44]

NR = not reported; RT = Room temperature; * = number of reuses with no significant change in adsorption performance, including the first use.

3.10 Conclusion

This work succeeded in developing a sustainable, environmentally friendly and cost-effective approach for preparation of magnetic BEA zeolite. Bulky solid rice husk ash-SiO_2 was possibly used in the preparation of a uniform dry precursor gel with the assistance of ultrasonic waves before converting to magnetic zeolite composite via DGC method. The inclusion of Fe_3O_4 particles by using this method showed no adverse effects to the surface morphologies of BEA zeolite. The prepared composite also showed sustainability as an adsorbent for fast adsorption of paraquat in aqueous solutions with quick magnetic separability, and excellent reusability. This work contributes to sustainable circulation of materials in agriculture owing to the utilization of agricultural waste–derived materials for treating of agrochemical contaminated water.

Additionally, this study has proved that the prepared magnetic BEA zeolite in this study is a potential adsorbent for cationic pollutants. In the next chapter, adsorption of inorganic cations, i.e., heavy metals, using the synthesized RHAS-BEA and magnetic RHAS-BEA are studied.

Acknowledgement

Material from: Arabian Journal of Chemistry, 2023, 16, 104959. Published by Elsevier B.V. on behalf of King Saud University. https://doi.org/10.1016/j.arabjc.2023.104959.

References

[1] S.S. Mohanty, H.M. Jena, A systemic assessment of the environmental impacts and remediation strategies for chloroacetanilide herbicides, J. Water Process Eng. 31 (2019) 100860. https://doi.org/https://doi.org/10.1016/j.jwpe.2019.100860.

[2] I.A. Badroo, H.P. Nandurkar, A.H. Khanday, Toxicological impacts of herbicide paraquat dichloride on histological profile (gills, liver, and kidney) of freshwater fish Channa punctatus (Bloch), Environ. Sci. Pollut. Res. 27 (2020) 39054–39067. https://doi.org/10.1007/s11356-020-09931-6.

[3] Y. Huang, H. Zhan, P. Bhatt, S. Chen, Paraquat degradation from contaminated environments: current achievements and perspectives, Front, Microbiol. 10 (2019). https://doi.org/10.3389/fmicb.2019.01754.

[4] R. Kouchakinejad, S. Shariati, J. Abolhasani, E.G. Kalhor, M.T. Vardini, Core-shells of magnetite nanoparticles decorated by SBA-3-SO_3H mesoporous silica for magnetic solid phase adsorption of paraquat herbicide from aqueous solutions, Colloids Surf. A Physicochem. Eng. Asp. 643 (2022). https://doi.org/10.1016/j.colsurfa.2022.128709.

[5] T. Fernandes, S.F. Soares, T. Trindade, A.L. Daniel-Da-silva, Magnetic hybrid nanosorbents for the uptake of paraquat from water, Nanomaterials. 7 (2017). https://doi.org/10.3390/nano7030068.

[6] I.A. Saleh, N. Zouari, M.A. Al-Ghouti, Removal of pesticides from water and wastewater: Chemical, physical and biological treatment approaches, Environ. Technol. Innov. 19 (2020). https://doi.org/10.1016/j.eti.2020.101026.

[7] D.S.P. Franco, J. Georgin, E.C. Lima, L.F.O. Silva, Advances made in removing paraquat herbicide by adsorption technology: a review, J. Water Process Eng. 49 (2022). https://doi.org/10.1016/j.jwpe.2022.102988.

[8] W. Rongchapo, O. Sophiphun, K. Rintramee, S. Prayoonpokarach, J. Wittayakun, Paraquat adsorption on porous materials synthesized from rice husk silica, Water Sci. Technol. 68 (2013) 863–869. https://doi.org/10.2166/wst.2013.311.

[9] X. Peng, Y. Jiang, Z. Chen, A.I. Osman, M. Farghali, D.W. Rooney, P.-S. Yap, Recycling municipal, agricultural and industrial waste into energy, fertilizers, food and construction materials, and economic feasibility: a review, Environ. Chem. Lett. 21 (2023) 765–801. https://doi.org/10.1007/s10311-022-01551-5.

[10] L.I. Xuan, D. Baotong, Y.E. Hua, The research based on the 3-R principle of agro-circular economy model-the Erhai Lake basin as an example, Energy Procedia. 5 (2011) 1399–1404. https://doi.org/https://doi.org/10.1016/j.egypro.2011.03.242.

[11] FAO, Food and Agriculture Organization of the United Nations, (2022). https://www.fao.org/faostat/en/#data/QCL/visualize (accessed October 13, 2022).

[12] S. Steven, E. Restiawaty, Y. Bindar, Routes for energy and bio-silica production from rice husk: a comprehensive review and emerging prospect, Renew. Sust. Energ. Rev. 149 (2021). https://doi.org/10.1016/j.rser.2021.111329.

[13] S. Chandrasekhar, K.G. Satyanarayana, P.N. Pramada, P. Raghavan, T.N. Gupta, Review Processing, properties and applications of reactive silica from rice husk—an overview, J. Mater. Sci. 38 (2003) 3159–3168. https://doi.org/10.1023/A:1025157114800.

[14] P.U. Nzereogu, A.D. Omah, F.I. Ezema, E.I. Iwuoha, A.C. Nwanya, Silica extraction from rice husk: comprehensive review and applications, Hybrid Adv. 4 (2023) 100111. https://doi.org/https://doi.org/10.1016/j.hybadv.2023.100111.

[15] L. Khouchaf, K. Boulahya, P.P. Das, S. Nicolopoulos, V.K. Kis, J.L. Lábár, Study of the microstructure of amorphous silica nanostructures using high-resolution electron microscopy, electron energy loss spectroscopy, X-ray powder diffraction, and electron pair distribution function, Materials. 13 (2020) 1–14. https://doi.org/10.3390/ma13194393.

[16] T. Shams, G. Schober, D. Heinz, S. Seifert, Rice husk ash as a silica source for the production of autoclaved aerated concrete – a chance to save energy and primary resources, J. Build. Eng. 57 (2022). https://doi.org/10.1016/j.jobe.2022.104810.

[17] A.G. Gebretatios, A.R. Kadiri Kanakka Pillantakath, T. Witoon, J.-W. Lim, F. Banat, C.K. Cheng, Rice husk waste into various template-engineered mesoporous silica materials for different applications: a comprehensive review on recent developments, Chemosphere. 310 (2023). https://doi.org/10.1016/j.chemosphere.2022.136843.

[18] S. Sivalingam, S. Sen, Rice husk ash derived nanocrystalline ZSM-5 for highly efficient removal of a toxic textile dye, J. Mater. Res. Technol. 9 (2020) 14853–14864. https://doi.org/10.1016/j.jmrt.2020.10.074.

[19] Y. Wang, T. Du, H. Jia, Z. Qiu, Y. Song, Synthesis, characterization and CO_2 adsorption of NaA, NaX and NaZSM-5 from rice husk ash, Solid State Sci. 86 (2018) 24–33. https://doi.org/10.1016/j.solidstatesciences.2018.10.003.

[20] C.M.C. Tolentino, M.D.G. de Luna, C.M. Futalan, A.E.S. Choi, F.G. Manegdeg, N. Grisdanurak, Influence of hydrocarbons on hydrogen chloride removal from refinery off-gas by zeolite NaY derived from rice husks, Sci. Total Environ. 728 (2020). https://doi.org/10.1016/j.scitotenv.2020.138782.

[21] C.G. Flores, H. Schneider, J.S. Dornelles, L.B. Gomes, N.R. Marcilio, P.J. Melo, Synthesis of potassium zeolite from rice husk ash as a silicon source, Clean. Eng. Technol. 4 (2021). https://doi.org/10.1016/j.clet.2021.100201.

[22] S. Banerjee, S. Barman, G. Halder, Sorptive elucidation of rice husk ash derived synthetic zeolite towards deionization of coalmine waste water: a comparative study, Groundw. Sustain. Dev. 5 (2017) 137–151. https://doi.org/10.1016/j.gsd.2017.06.004.

[23] D. Prasetyoko, Z. Ramli, S. Endud, H. Hamdan, B. Sulikowski, Conversion of rice husk ash to zeolite beta, Waste Manag. 26 (2006) 1173–1179. https://doi.org/10.1016/j.wasman.2005.09.009.

[24] J.A. Santana Costa, C.M. Paranhos, Systematic evaluation of amorphous silica production from rice husk ashes, J. Clean. Prod. 192 (2018) 688–697. https://doi.org/10.1016/j.jclepro.2018.05.028.

[25] V. Phouthavong, T. Hagio, J.-H. Park, S. Nijpanich, T. Srihirunthanon, N. Chantanurak, K. Duangkhai, R. Rujiravanit, V. Chounlamany, K. Phomkeona, L. Kong, L. Li, R. Ichino, Utilization of agricultural waste to herbicide removal: magnetic BEA zeolite adsorbents prepared by dry-gel conversion using rice husk ash–derived SiO_2 for paraquat removal, Arab. J. Chem. 16 (2023) 104959. https://doi.org/https://doi.org/10.1016/j.arabjc.2023.104959.

[26] M. Criado, A. Fernández-Jiménez, A.G. de la Torre, M.A.G. Aranda, A. Palomo, An XRD study of the effect of the SiO_2/Na_2O ratio on the alkali activation of fly ash, Cem. Concr. Res. 37 (2007) 671–679. https://doi.org/10.1016/j.cemconres.2007.01.013.

[27] L.V. Dang, S.T. Le, R.F. Lobo, T.D. Pham, Hydrothermal synthesis of alkali-free chabazite zeolites, J. Porous Mater. 27 (2020) 1481–1489. https://doi.org/10.1007/s10934-020-00923-y.

[28] I.H.A.E. Maksod, A. Al-Shehri, S. Bawaked, M. Mokhtar, K. Narasimharao, Structural and photocatalytic properties of precious metals modified TiO_2/BEA zeolite composites, Mol. Catal. 441 (2017) 140–149. https://doi.org/10.1016/j.mcat.2017.08.012.

[29] A. Fauzi, R. Ratnawulan, The effect of calcination temperature on the structure of iron oxide phase from west Sumatra, in: J. Phys. Conf. Ser., 2021. https://doi.org/10.1088/1742-6596/1876/1/012028.

[30] T. Hagio, S. Nijpanich, H. Kunishi, K. Yamaoka, V. Phouthavong, Y. Kamimoto, R. Ichino, K. Iwai, Synthesis of MOR zeolite/magnetite composite via seed assisted method, J. Nanosci. Nanotechnol. 19 (2019) 6841–6848. https://doi.org/10.1166/jnn.2019.17123.

[31] S. Miao, P. She, X. Chang, C. Zhao, Y. Sun, Z. Lei, S. Sun, W. Zhang, M. Jia, Synthesis of beta nanozeolite aggregates with hierarchical pores via steam-assisted conversion of dry gel and their catalytic properties for Friedel-Crafts acylation, Microporous Mesoporous Mater. 334 (2022). https://doi.org/10.1016/j.micromeso.2022.111777.

[32] M. Matsukata, T. Osaki, M. Ogura, E. Kikuchi, Crystallization behavior of zeolite beta during steam-assited crystallization of dry gel, Microporous Mesoporous Mater. 56 (2002) 1–10. https://doi.org/10.1016/S1387-1811(02)00412-2.

[33] S. Inagaki, K. Nakatsuyama, Y. Saka, E. Kikuchi, S. Kohara, M. Matsukata, Elucidation of medium-range structure in a dry gel-forming *BEA-type zeolite, J. Phys. Chem. C. 111 (2007) 10285–10293. https://doi.org/10.1021/jp0668044.

[34] J. Li, M. Gao, W. Yan, J. Yu, Regulation of the Si/Al ratios and Al distributions of zeolites and their impact on properties, Chem. Sci. 14 (2022) 1935–1959. https://doi.org/10.1039/d2sc06010h.

[35] T. Brar, P. France, P.G. Smirniotis, Control of crystal size and distribution of zeolite A, Ind. Eng. Chem. Res. 40 (2001) 1133–1139. https://doi.org/10.1021/ie000748q.

[36] J. Warzywoda, A.G. Dixon, R.W. Thompson, A. Sacco, S.L. Suib, The role of the dissolution of silicic acid powders in aluminosilicate synthesis mixtures in the crystallization of large mordenite crystals, Zeolites. 16 (1996) 125–137. https://doi.org/https://doi.org/10.1016/0144-2449(95)00101-8.

[37] Y. Pukcothanung, T. Siritanon, K. Rangsriwatananon, The efficiency of zeolite Y and surfactant-modified zeolite Y for removal of 2,4-dichlorophenoxyacetic acid and 1,1″-dimethyl-4,4″-bipyridinium ion, Microporous Mesoporous Mater. 258 (2018) 131–140. https://doi.org/10.1016/j.micromeso.2017.08.035.

[38] H. Nur, A.F.N.A. Manan, L.K. Wei, M.N.M. Muhid, H. Hamdan, Simultaneous adsorption of a mixture of paraquat and dye by NaY zeolite covered with alkylsilane, J. Hazard. Mater. 117 (2005) 35–40. https://doi.org/10.1016/j.jhazmat.2004.07.015.

[39] A. Walcarius, R. Mouchotte, Efficient *in vitro* paraquat removal via irreversible immobilization into zeolite particles, Arch. Environ. Contam. Toxicol. 46 (2004) 135–140. https://doi.org/10.1007/s00244-003-2242-3.

[40] K.L. Tan, B.H. Hameed, Insight into the adsorption kinetics models for the removal of contaminants from aqueous solutions, J. Taiwan Inst. Chem. Eng. 74 (2017) 25–48. https://doi.org/10.1016/j.jtice.2017.01.024.

[41] S. Jodeh, G. Hanbali, S. Tighadouini, S. Radi, O. Hamed, D. Jodeh, Removal and extraction efficiency of quaternary ammonium herbicides paraquat (PQ) from aqueous solution by ketoenol- pyrazole receptor functionalized silica hybrid adsorbent (SiNPz), BMC Chem. 13 (2019). https://doi.org/10.1186/s13065-019-0599-2.

[42] S.E. Moradi, Microwave assisted preparation of sodium dodecyl sulphate (SDS) modified ordered nanoporous carbon and its adsorption for MB dye, J. Ind. Eng. Chem. 20 (2014) 208–215. https://doi.org/10.1016/j.jiec.2013.04.005.

[43] M. Özacar, Equilibrium and kinetic modelling of adsorption of phosphorus on calcined alunite, Adsorption. 9 (2003) 125–132. https://doi.org/10.1023/A:1024289209583.

[44] A. Rasaie, M.M. Sabzehmeidani, M. Ghaedi, M. Ghane-Jahromi, A. Sedaratian-Jahromi, Removal of herbicide paraquat from aqueous solutions by bentonite modified with mesoporous silica, Mater. Chem. Phys. 262 (2021). https://doi.org/10.1016/j.matchemphys.2021.124296.

[45] W. Insuwan, K. Rangsriwatananon, Removal of paraquat from aqueous solutions onto zeolite LTL, Eng. J. 21 (2017) 15–23. https://doi.org/10.4186/ej.2017.21.2.15.

[46] C. Keawkumay, W. Rongchapo, N. Sosa, S. Suthirakun, I.Z. Koleva, H.A. Aleksandrov, G.N. Vayssilov, J. Wittayakun, Paraquat adsorption on NaY zeolite at various Si/Al ratios: a combined experimental and computational study, Mater. Chem. Phys. 238 (2019). https://doi.org/10.1016/j.matchemphys.2019.121824.

[47] N. Osakoo, C. Pansakdanon, N. Sosa, K. Deekamwong, C. Keawkumay, W. Rongchapo, N. Chanlek, J. Jitcharoen, S. Prayoonpokarach, J. Wittayakun, Characterization and comprehension of zeolite NaY/mesoporous SBA-15 composite as adsorbent for paraquat, Mater. Chem. Phys. 193 (2017) 470–476. https://doi.org/10.1016/j.matchemphys.2017.03.002.

[48] W. Rongchapo, K. Deekamwong, S. Loiha, S. Prayoonpokarach, J. Wittayakun, Paraquat adsorption on NaX and Al-MCM-41, Water Sci. Technol. 71 (2015) 1347–1353. https://doi.org/10.2166/wst.2015.100.

[49] Z. Dehghani, M. Sedghi-Asl, M. Ghaedi, M.M. Sabzehmeidani, E. Adhami, Ultrasound-assisted adsorption of paraquat herbicide from aqueous solution by graphene oxide/ mesoporous silica, J. Environ. Chem. Eng. 9 (2021). https://doi.org/10.1016/j.jece.2021.105043.

[50] D. Ait Sidhoum, M.M. Socías-Viciana, M.D. Ureña-Amate, A. Derdour, E. González-Pradas, N. Debbagh-Boutarbouch, Removal of paraquat from water by an Algerian bentonite, Appl. Clay Sci. 83–84 (2013) 441–448. https://doi.org/10.1016/j.clay.2013.07.007.

[51] C.-F. Huang, C.-W. Tu, R.-H. Lee, C.-H. Yang, W.-C. Hung, K.-Y. Andrew Lin, Study of various diameter and functionality of TEMPO-oxidized cellulose nanofibers on paraquat adsorptions, Polym. Degrad. Stab. 161 (2019) 206–212. https://doi.org/10.1016/j.polymdegradstab.2019.01.023.

[52] J. Junthip, N. Jumrernsuk, P. Klongklaw, W. Promma, S. Sonsupap, Removal of paraquat herbicide from water by textile coated with anionic cyclodextrin polymer, SN Appl. Sci. 1 (2019). https://doi.org/10.1007/s42452-018-0102-z.

[53] J. Mokrzycki, M. Fedyna, M. Marzec, J. Szerement, R. Panek, A. Klimek, T. Bajda, M. Mierzwa-Hersztek, Copper ion-exchanged zeolite X from fly ash as an efficient adsorbent of phosphate ions from aqueous solutions, J. Environ. Chem. Eng. 10 (2022). https://doi.org/10.1016/j.jece.2022.108567.

[54] W. Rongchapo, C. Keawkumay, N. Osakoo, K. Deekamwong, N. Chanlek, S. Prayoonpokarach, J. Wittayakun, Comprehension of paraquat adsorption on faujasite zeolite X and Y in sodium form, Adsorpt. Sci. Technol. 36 (2018) 684–693. https://doi.org/10.1177/0263617417715394.

[55] H. Zhang, Y. Kim, P.K. Dutta, Controlled release of paraquat from surface-modified zeolite Y, Microporous Mesoporous Mater. 88 (2006) 312–318. https://doi.org/https://doi.org/10.1016/j.micromeso.2005.09.026.

[56] Ministry of the Environment Government of Japan, Environmental quality standards for water pollution, https://www.env.go.jp/content/900454947.pdf (accessed September 25, 2023).

[57] T.J. Haley, Review of the toxicology of paraquat (1, 1′dimethyl-4, 4′bipyridinium chloride), Clin. Toxicol. 14 (1979) 1–46. https://doi.org/10.3109/15563657909030112.

[58] M. Ronnen, B. Klin, S. Suster, Mixed diquat/paraquat-induced burns, Int. J. Dermatol. 34 (1995) 23–25. https://doi.org/10.1111/j.1365-4362.1995.tb04371.x.

[59] Y. Uematsu, F. Ogata, N. Nagai, C. Saenjum, T. Nakamura, N. Kawasaki, *In vitro* removal of paraquat and diquat from aqueous media using raw and calcined basil seed, Heliyon. 7 (2021). https://doi.org/10.1016/j.heliyon.2021.e07644.

[60] E. Martwong, S. Chuetor, J. Junthip, Adsorption of paraquat by poly(Vinyl alcohol)-cyclodextrin nanosponges, Polymers (Basel). 13 (2021). https://doi.org/10.3390/polym13234110.

CHAPTER 4

Removal of heavy metals by magnetic BEA zeolite prepared using rice husk ash–SiO_2 in dry-gel conversion method

4.1 Background

4.1.1 Heavy metals: potential sources and environmental effects

Metals and metalloids that have densities above 5 g/cm^3 and atomic weight in the range 63.5–200.6 g/mol are classified as heavy metals [1]. Most heavy metals such as cadmium (Cd), chromium (Cr), lead (Pb), mercury (Hg), nickel (Ni), copper (Cu) and zinc (Zn) are highly toxic elements, unless some of them are considered as essential micro-nutrient elements such as Cr, Cu, Ni [2] and Zn [3] owing to their important roles in giving positive effect to growth of plants, animals and human. Therefore, heavy metals can be either found as the active ingredients, i.e., Cu, Zn, in fungicides and fertilizers [4] or as contaminants in fertilizers and pesticides, i.e., Pb, Cr, Cd [5]. Heavy metals have been known to be one of the leading harmful contaminants worldwide for decades. Contamination of heavy metals that are released from diverse sources in water, as shown in Figure 4.1, can be bioaccumulated in aquatic animals, i.e., fishes, which are further consumed by human and leads to potential health risks [6]. Agricultural activities become a main source of heavy metal contamination through the utilizing fertilizers and pesticides [7,8]. Consequently, long-term overuse of agrochemicals become an anthropogenic source of water pollution. Removal of heavy metals from polluted water is therefore still of necessary to return cleaner resource to society.

Long-term exposure to heavy metals causes toxicity in human body systems such as nervous, skin, cardiovascular, and reproductive systems. Intake of heavy metals can also lead to genotoxicity in which human DNA is damaged [9]. Many diseases such as Alzheimer's, Parkinson's, muscle dystrophy, and multiple sclerosis, etc., are the results of heavy metal toxicities in vital organs [10]. Pb, Cu, and Zn are commonly found in agrochemicals and as contaminants in environment, i.e., soil and water [11,12]. According to the Agency for Toxic Substances and Disease Registry, these heavy metals have been

ranked 2nd, 74th, and 120th, respectively, in the 275 substances priority list that have most significant potential threat to human health [13]. Circulatory and nervous system-related diseases can be caused by Pb, whereas ingestion of Cu causes damage to liver and kidney and lung cancer. The adverse effect of Zn is to cause dehydration, depression, and anemia [14]. Removal of these three representative heavy metals is of necessary.

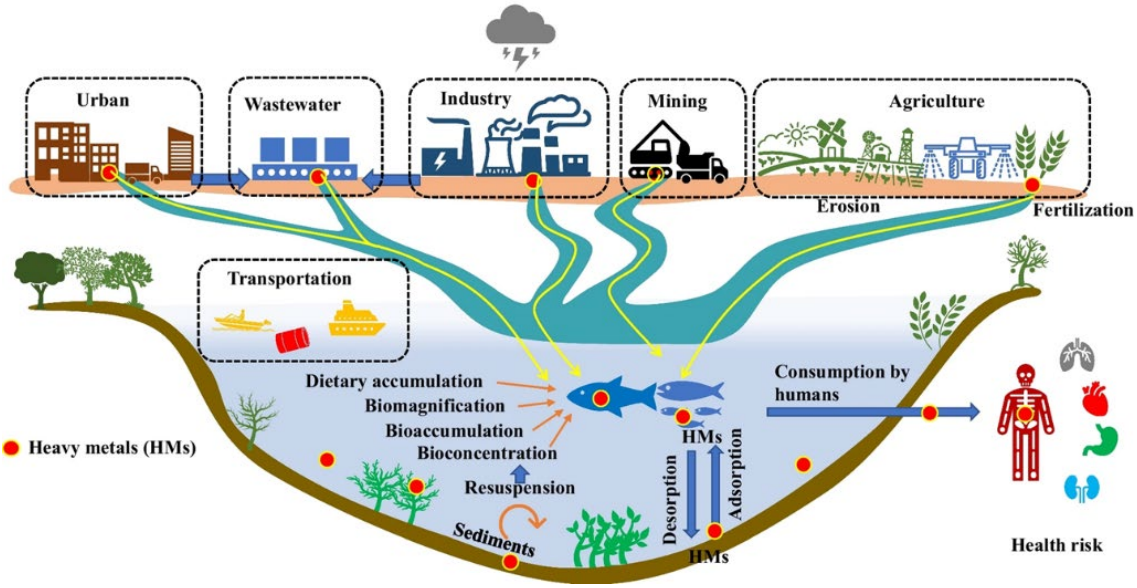

Figure 4.1 Heavy metals released from different sources to water and their bioaccumulation by aquatic animals. Reprinted with permission from Ajala et al. [6]., Environmental Science and Pollution Research, 29, 82660–82680, 2022, Springer Nature.

4.1.2 Adsorption of heavy metals using zeolitic adsorbents

Adsorption is among several physical water treatment methods that is the simplest, robust, and cost-effective method. After the treatment process, the adsorbents that are used to remove pollutants can be collected and reused, whereas the effective chemical methods, i.e., chemical precipitation, leave behind sludge as secondary waste [15,16]. There are diverse types of adsorbents used for removal of heavy metals from water which generally rely on the chelation between the hydrophilic surface, containing carboxylic acid, amino-carbonyl, hydroxyl, and sulfonic acid groups, of the adsorbents and heavy metal ions. Such adsorbents, e.g., graphene oxide, activated carbon, functionalized mesoporous SiO_2,

chitosan, biosorbents, etc., are mostly reported in heavy metal adsorption [17]. Ion exchange is another process that is utilized for removal of heavy metals by using materials that possess cation exchange properties such as zeolites, sodium titanates, metal sulfides, layered double hydroxides, metal tungstates, etc. [18].

Among those materials, zeolites have been utilized in wastewater treatment for a long time. Zeolites are a group of crystalline aluminosilicates that are available in nature and as synthetics with various uniform micropore sizes. Three-dimensional connection of primary $SiO_{4/2}$ and $[AlO_{4/2}]^-$ tetrahedra units results in various zeolitic framework types [19]. In addition to their various pore sizes, the exchangeable counter cations at the $[AlO_{4/2}]^-$ sites allow zeolites themselves being cation exchanger. The most abundant natural zeolite, i.e., clinoptilolite (HEU), has been intensively used in many studies on heavy metal adsorption [20]. Other small to medium pore natural zeolites, such as erionite (ERI), chabazite (CHA), and mordenite (MOR) also showed cation exchange properties to several heavy metal ions [21]. However, the impurity of natural zeolites might have limited their cation exchange capacities [22]. Synthetic zeolites therefore became emerging alternative adsorbents for removal of heavy metals. Large pore zeolites, e.g., NaX and NaY (i.e., that belong to FAU-type), also have high capacities towards adsorption of heavy metals [23,24].

BEA zeolite is a large pore 12-membered ring zeolite and possesses high hydrothermal stability and high acidity [25]. Most of BEA zeolites were easily synthesized with Si/Al ratios in the range 10–30 [26], which are considered as high SiO_2 zeolites [27]. However, its low negatively charged $[AlO_{4/2}]^-$ content sufficiently allows for attraction to cationic species such as cationic organic dyes [28–30], and herbicides [31,32]. The application of high-SiO_2 BEA zeolite as adsorbent in removal of heavy metals is rarely reported [33,34], more studies on utilizing this type of adsorbent is beneficial in environmental protection. In most studies, combination of different properties from different materials as composites succeeds in improving heavy metal adsorption performance and collectability of zeolites [22]. Magnetic zeolite composites are easier to collect after the adsorption process which are beneficial in practical manipulation. Recently, magnetic BEA zeolite was successfully synthesized in this thesis research using agricultural

waste-derived materials, rice husk ash-SiO_2, in an environmentally friendly DGC method, (Chapter 3). The magnetic composite shows high potential as a sustainable adsorbent for removal of cationic herbicide from agricultural affected water. Ion exchange of the cationic herbicide was assumed on this magnetic BEA zeolite and is thus anticipated to be able to adsorb cationic heavy metals as well.

4.2 Objective

This chapter investigates the adsorption performance of magnetic BEA zeolite that was prepared using solid rice husk ash–SiO_2 in DGC method towards removal of heavy metal ions, i.e., Pb(II), Cu(II), and Zn(II) that are mostly derived from using fertilizers. This work aims to show the extension of utilizing sustainable adsorbent synthesized by using agricultural waste in the treatment of wastewater affected by the use of agrochemicals.

4.3 Materials

Chemicals and equipment used in this chapter are listed in Table 4.1 and 4.2, respectively. BEA and magnetic BEA zeolite (RHAS-BEA and magnetic RHAS-BEA) prepared using rice husk ash-SiO_2 and dry-gel conversion method in Chapter 3 were used as adsorbents.

Table 4.1 Chemicals

Name (Formula, purity)	Manufacturer, country
Lead (II) nitrate ($Pb(NO_3)_2$, 99.9%)	Fujifilm Wako Pure Chemical Corp., Japan
Copper (II) nitrate trihydrate ($Cu(NO_3)_2 \cdot 3H_2O$, 77.0~80.0 wt% as $Cu(NO_3)_2$)	Nacalai Tesque, Japan
Zinc sulfate heptahydrate ($ZnSO_4 \cdot 7H_2O$, 99.5 wt%)	Nacalai Tesque, Japan
Sodium nitrate ($NaNO_3$, 99.0 wt%)	Nacalai Tesque, Japan
Lead standard solution (Pb, 1000 mg/L)	Fujifilm Wako Pure Chemical Corp., Japan
Copper standard solution (Cu, 999 mg/L)	Fujifilm Wako Pure Chemical Corp., Japan
Zinc standard solution (Zn, 1001 mg/L)	Fujifilm Wako Pure Chemical Corp., Japan
Silicon standard solution (Si, 1.00 mgSi/mL)	Nacalai Tesque, Japan
Aluminum standard solution (Al, 1002 mgAl/L)	Fujifilm Wako Pure Chemical Corp., Japan
Iron standard solution (Fe, 1001 mgFe/L)	Fujifilm Wako Pure Chemical Corp., Japan

Table 4.2 Equipment

Name	Model	Manufacturer, country
Convection oven	SOFW-300SB	AS ONE Corporation, Japan
Horizontal shaker	MK161	Yamato Scientific, Japan
Field emission-scanning electron microscope (FE-SEM)	JSM-6330F	JEOL, Japan
Inductively coupled plasma-Atomic emission spectrometer (ICP-AES)	SK-II	Seiko Instrument, Japan
X-ray photoelectron spectrometer (XPS, Al-kα (1486 eV))	ESCALAB 250Xi	Thermo Fisher Scientific, USA

4.4 Adsorption of heavy metals

The adsorption studies generally were carried out using batch adsorption. Fixed conditions were used throughout the experiments, i.e., adsorbent concentration (1 g/L), a shaking speed (80 rpm) and temperature (26 °C), unless otherwise stated. Aqueous solutions of the heavy metals were prepared using distilled water and used without pH adjustment. The initial pH values of Pb(II), Cu(II), and Zn(II) solutions were in the range 5.2–5.9, 5.2–5.7, and 5.7–6.6, respectively. After adsorption, the solutions were filtered through PTFE syringe filters (0.22 μm) before measuring the concentration of heavy metal ions using ICP-AES. The adsorption amount of each heavy metal was calculated using Equation 2.2 as shown in Chapter 2.

4.4.1 Effect of Si/Al ratio of the synthesized magnetic RHAS-BEA

Before further studies on adsorption kinetic and isotherm, effect of Si/Al ratio of the magnetic RHAS-BEA synthesized in Chapter 3 using RHA-SiO_2 and DGC method was examined. The adsorption tests were conducted using equal molarity of each heavy metal. Magnetic RHAS-BEA with two different Si/Al ratios of 23.3 and 48.8 were used in this study, which was found to affect the adsorption capacity of the heavy metals, as shown in

Figure 4.2. The lower Si/Al ratio shows higher adsorbed amount of each heavy metal ion. This supports the anticipation that more negatively charged $[AlO_{4/2}]^-$ sites are available for ion exchange with the cationic metal ions when the Si/Al ratio of the BEA zeolite is lower [33]. The magnetic RHAS-BEA with lower Si/Al ratio was subsequently used for the evaluation of heavy metal adsorption performance. The studies were also carried out for non-magnetic RHAS-BEA for comparison.

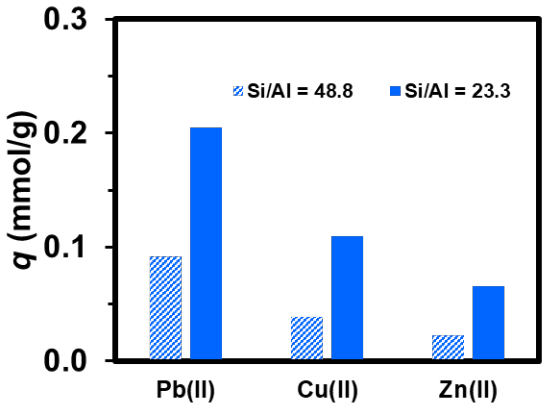

Figure 4.2 Effect of Si/Al ratio of magnetic RHAS-BEA on the adsorption amount of Pb(II), Cu(II), and Zn(II) [35].

4.4.2 Adsorption kinetics

Adsorption kinetics of Pb(II), Cu(II), and Zn(II) in single system were studied in order to examine the metal ions uptake rate for scaling up the process in practical use, and also to predict the adsorption mechanism. The experiments were carried out by examining the adsorption amount over varied shaking time from 1 min to 180 min at a fixed initial metal ion concentration (≈ 0.75 mmol/L). The change in q values for each heavy metal as a function of time (q_t) is shown in Figure 4.3. Adsorption of Cu (II) and Zn(II) quickly reached saturation within 5 min whereas that of Pb(II) was continuously increased and became slower from 30 min before approaching saturation at 1 h. Pb(II) was found to have higher equilibrium adsorbed amount than Cu(II) and Zn(II). The adsorption kinetic trend was identically observed for both RHAS-BEA and magnetic RHAS-BEA.

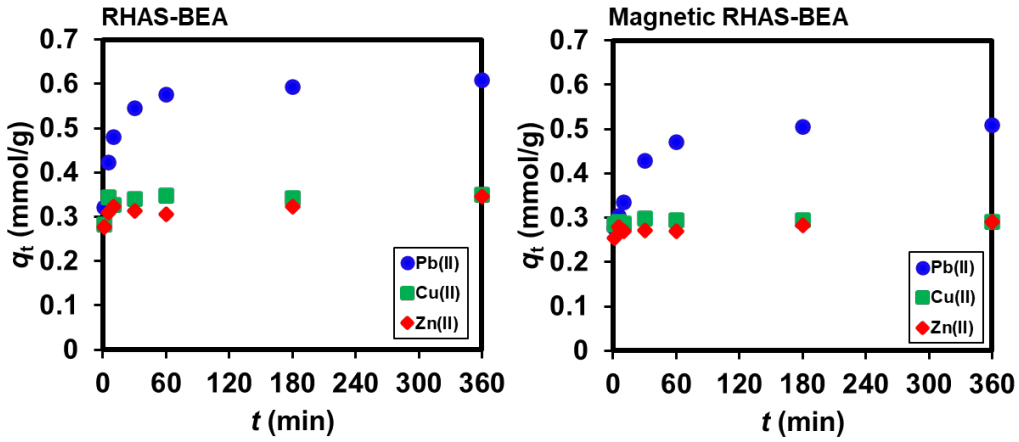

Figure 4.3 Adsorption kinetics of Pb(II), Cu(II), and Zn(II) on RHAS-BEA and magnetic RHAS-BEA [35].

The obtained change in adsorbed amount as a function of time data was plugged in four linear forms of PFO, PSO, Elovich, and IPD adsorption kinetic models. The linear equations of PFO, PSO, and IPD are shown in Equation 3.1–3.3, respectively, in Chapter 3, and that of Elovich is shown in Equation 4.1.

$$\text{Elovich:} \quad q_t = \frac{1}{\beta}\ln(\alpha\beta) + \frac{1}{\beta}\ln t \qquad \text{Equation 4.1}$$

where α and β are the initial adsorption rate (mmol/g min) and the constant related to the extent of surface coverage and activation energy for chemisorption (g/mmol) in the Elovich model, respectively [36].

Considering the higher R^2 values (> 0.999), the adsorption kinetics of the three types of heavy metal ions best fitted to the PSO model. PFO also showed good fit to some extent; however, the R^2 values were much lower compared to that of the PSO model (Figure 4.4). Elovich and IPD models were found to be inappropriate (Figure 4.5). The IPD model plots for most cases were divided into two regions in which their trend lines did not pass through the origin, indicating the inapplicability of this model to describe the adsorption in this case. The good fit of the data to the PSO model indicates that the surface adsorption might have been the rate-limiting step, involving chemisorption of the metal ions onto the adsorbent surface [37]. This assumption was mostly found suitable to describe the uptake kinetic of

divalent heavy metals on zeolite-based adsorbents [22] and various types of adsorbents such as metal oxide nanoparticles [38,39], carbon-based materials [40], metal-organic frameworks [41], biosorbent [42], and biopolymer-based materials [43].

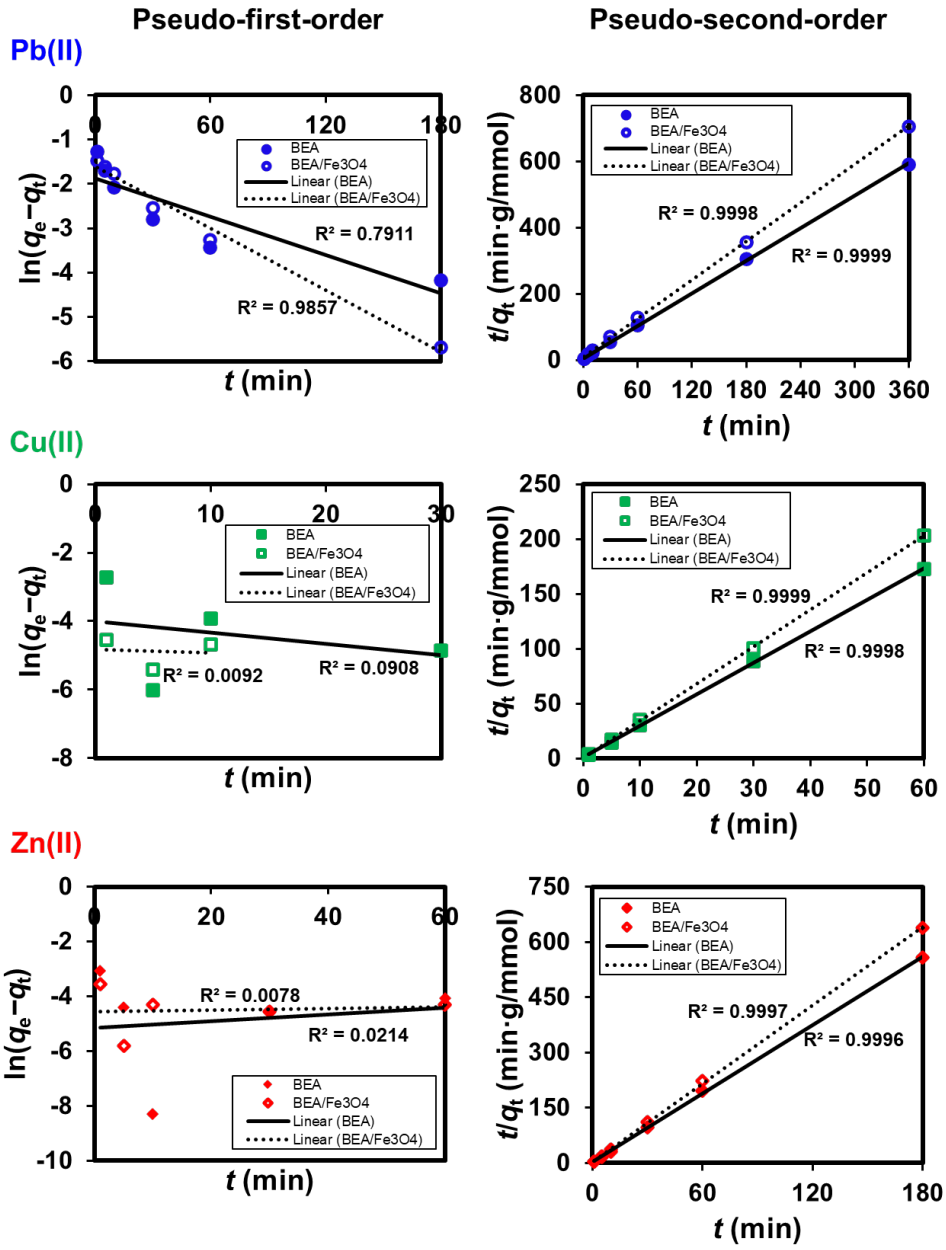

Figure 4.4 PFO and PSO adsorption kinetics model plots of Pb(II), Cu(II), and Zn(II) on RHAS-BEA and magnetic RHAS-BEA. BEA and BEA/Fe_3O_4 in the figure represent RHAS-BEA and magnetic RHAS-BEA, respectively [35].

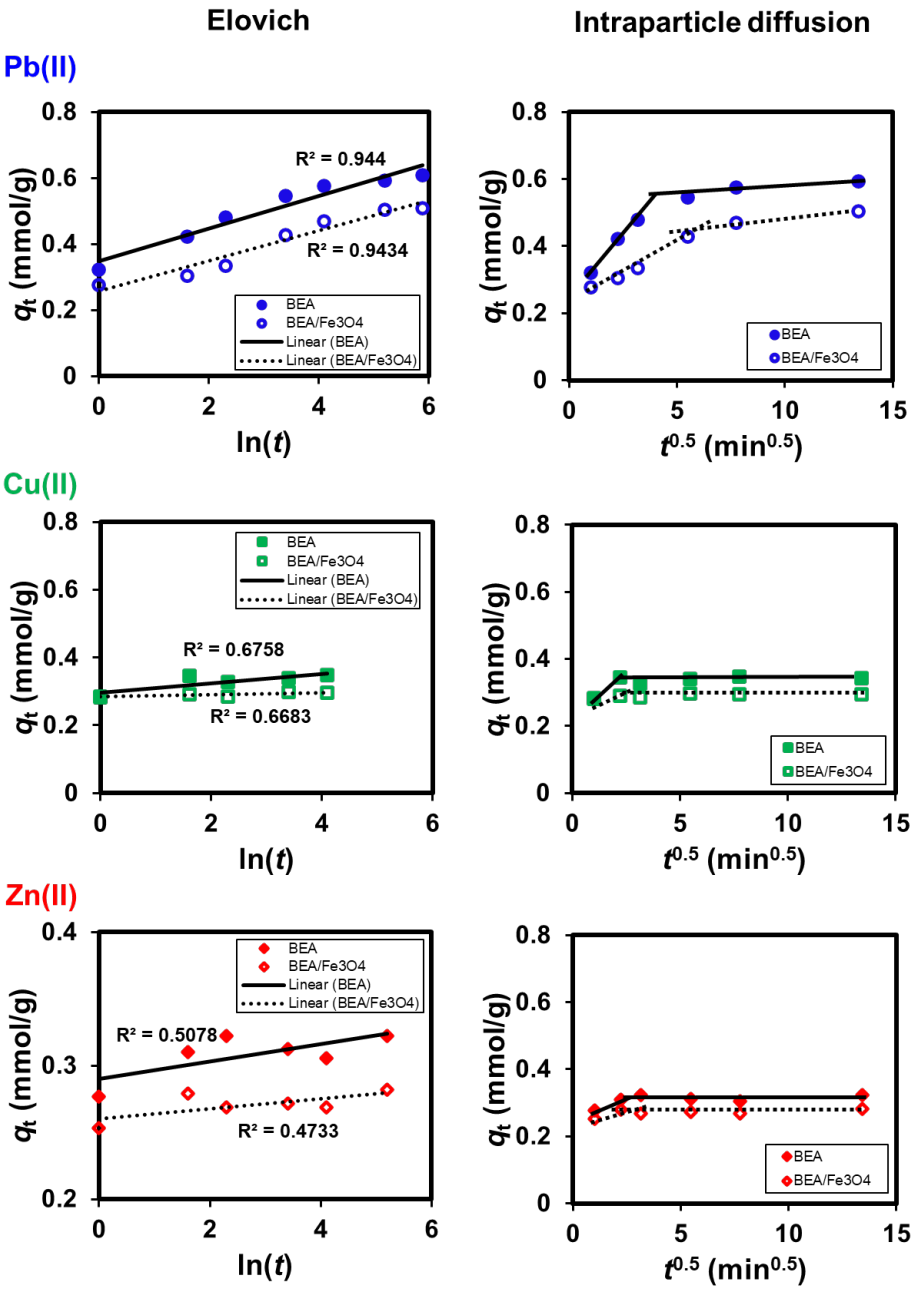

Figure 4.5 Elovich and IPD adsorption kinetics model plots of Pb(II), Cu(II), and Zn(II) on RHAS-BEA and magnetic RHAS-BEA. BEA and BEA/Fe_3O_4 in the figure represent RHAS-BEA and magnetic RHAS-BEA, respectively [35].

4.4.3 Adsorption isotherm

For evaluation of the adsorption behavior, adsorption isotherm studies of the heavy metals were carried out using different initial metal ion concentrations in the range 0.15~1.5 mmol/L, at room temperature (26 °C). The change of q values at equilibrium as a function of equilibrium concentration of metal ion (C_e) for each heavy metal ion was shown in Figure 4.6.

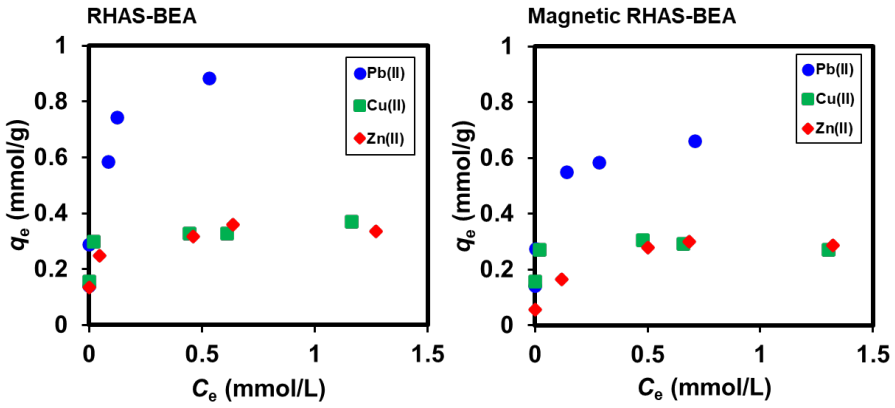

Figure 4.6 Adsorption isotherms of Pb(II), Cu(II), and Zn(II) on RHAS-BEA and magnetic RHAS-BEA at 26 °C [35].

The highest adsorbed amount was found for Pb(II) in the whole concentration range while Cu(II) and Zn(II) showed similar saturated adsorbed amount for both RHAS-BEA and magnetic RHAS-BEA. Again, the Langmuir and Freundlich adsorption isotherm models (Equation 2.4 and 2.5 in Chapter 2) were used to investigate the adsorption behavior and the maximum uptake capacity of the metal ions on the synthesized adsorbents.

Figure 4.7 indicates that Langmuir model was more suitable to describe the adsorption behavior and predict the maximum adsorption capacity. Fitting of the adsorption to the Langmuir model implies that adsorption of those heavy metals was monolayer-type on a homogeneous surface [1].

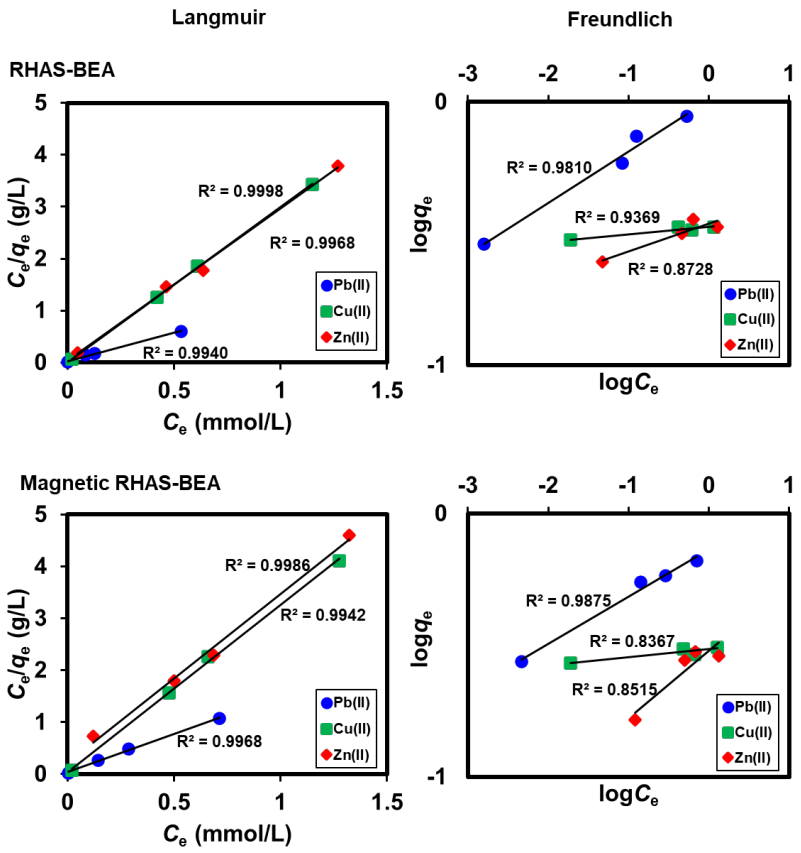

Figure 4.7 Langmuir and Freundlich adsorption isotherm model plots of Pb(II), Cu(II), and Zn(II) on RHAS-BEA and magnetic RHAS-BEA [35].

The q_m values calculated from the Langmuir plots of the heavy metal are in the order Pb(II) > Cu(II) ≈ Zn(II) for both RHAS-BEA and magnetic RHAS-BEA (Table 4.3), which indicate moderate performance among other types of zeolites e.g. FAU (NaX [23,24], illite clay-derived Y-type zeolite [44], rice husk ash-derived FAU [45], coal fly ash-derived FAU [46], Egyptian boiler ash residue and kaolin-based FAU zeolite [47], magnetic NaY [48]), GIS (P-type zeolite [49], fly ash-derived NaP1 [50], NaP1 [23]), LTA (mesoporous LTA [51], Lithium leach residue-derived NaA [52]), MOR (mordenite [53], Japanese zeolite that mainly contains gypsum, bassanite, calcite and mordenite [54]), BEA (β-zeolite [33,34]), HEU (Na-clinoptilolite [55], natural clinoptilolite [56], Romanian zeolitic volcanic tuff-derive Ca-clinoptilolite [57], magnetic Na-clinoptilolite [55], magnetic EDI (magnetic

nano Linde F (K) [58]), and some magnetic zeolites that their framework types were not reported [59,60].

Table 4.3 Comparison of Langmuir q_m for Pb(II), Cu(II), and Zn(II) among various types of zeolites [35]

Metal ion	Zeolitic adsorbent	Langmuir q_m (mg/g)	Reference
Pb(II)	NaX	676.594	[23]
	P-type zeolite (NASO)	649	[49]
	Mesoporous LTA	510	[51]
	NaX	492.1	[24]
	Lithium leach residue-derived NaA	487.805	[52]
	Magnetic nanozeolite (Linde F (K) zeolite/$KAlSiO_4 \cdot 1.5H_2O$)	476.1	[58]
	Fly ash derived NaP1 zeolite	432.572	[50]
	NaP1	432.572	[23]
	Illite clay-derived Y-type zeolite	372.16	[44]
	Rice husk ash derived FAU	342.5	[45]
	Japanese zeolite	286	[54]
	Fly ash derived NaP1 zeolite	192	[61]
	RHAS-BEA	190.0 (0.917 mmol/g)	This study
	Mordenite	151.256	[53]
	Magnetic RHAS-BEA	139.9 (0.675 mmol/g)	This study
	Magnetic zeolite	123	[59]
	Coal fly ash-derived FAU	109.89	[46]
	β-zeolite	91.74	[34]
	Magnetically modified zeolite	85.62	[55]
	Na zeolite	66.96	[55]
	Egyptian boiler ash residue and kaolin-based zeolite	15.96	[47]
	NaX	14.22	[62]
	Romanian zeolitic volcanic tuff	0.393	[57]

Table 4.3 (Continued) [35]

Metal ion	Zeolitic adsorbent	Langmuir q_m (mg/g)	Reference
Cu(II)	Mesoporous LTA	170	[51]
	NaX	118.7	[24]
	P-type zeolite (NASO)	90	[49]
	Magnetic NaY	87	[48]
	Magnetic nanozeolite (Linde F (K) zeolite/$KAlSiO_4 \cdot 1.5H_2O$)	59.9	[58]
	Coal fly ash-derived FAU	57.803	[46]
	Illite clay-derived Y-type zeolite	53.46	[44]
	Mordenite	31.773	[53]
	BEA (Si/Al 6.3)	29.5	[33]
	RHAS-BEA	21.3 (0.335 mmol/g)	This study
	Magnetic RHAS-BEA	19.7 (0.310 mmol/g)	This study
	BEA (Si/Al 7.9)	14.1	[33]
	Egyptian boiler ash residue and kaolin-based zeolite	12.247	[47]
	Clinoptilolite (particle size 20 mm)	2.3518	[56]
	Clinoptilolite (particle size 50 mm)	1.6745	[56]
	Romanian zeolitic volcanic tuff	0.129	[57]

Table 4.3 (Continued) [35]

Metal ion	Zeolitic adsorbent	Langmuir q_m (mg/g)	Reference
Zn(II)	NaX	639.289	[23]
	NaP1	144.062	[23]
	Fly ash derived NaP1 zeolite	114.062	[50]
	Magnetic NaY	114	[48]
	NaX	109.8	[24]
	P-type zeolite (NASO)	88	[49]
	Coal fly ash-derived FAU	36.765	[46]
	Fly ash derived NaP1 zeolite	34.2	[61]
	Coal fly ash-derived magnetic zeolite	30	[60]
	RHAS-BEA	22.4 (0.342 mmol/g)	This study
	Magnetic RHAS-BEA	20.1 (0.308 mmol/g)	This study
	BEA (Si/Al 6.3)	17.3	[33]
	Egyptian boiler ash residue and kaolin-based zeolite	12.025	[47]
	BEA (Si/Al 7.9)	11.1	[33]
	Clinoptilolite (particle size 20 mm)	1.1541	[56]
	Clinoptilolite (particle size 50 mm)	0.3928	[56]
	Romanian zeolitic volcanic tuff	0.094	[57]

4.4.4 Adsorption in mixed-ion system and possible adsorption mechanism

The adsorption isotherm studies reveal that Pb(II) was better adsorbed on RHAS-BEA and magnetic RHAS-BEA than Cu(II) and Zn(II) in the single system. Then, a mixed ion adsorption test was carried out to investigate the effect of competitive adsorption at initial concentrations of ≈ 0.3 mmol/L, where the q_e value for Pb(II) did not much differ from the others (second data point of each heavy metal in Figure 4.6). The results shown in Figure 4.8 indicate that the adsorption amounts of all heavy metals were obviously lower than those in the single system, indicating a competitive adsorption among them. Pb(II) still showed the highest adsorption amount whereas Cu(II) was adsorbed slightly more than

Zn(II) in the mixed system, indicating that adsorption of Pb(II) is more preferable on RHAS-BEA or magnetic RHAS-BEA over Cu(II) and Zn(II).

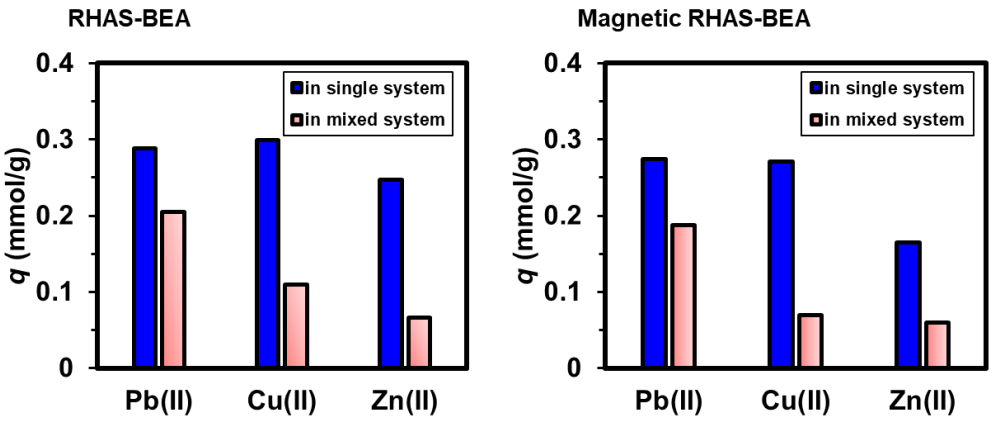

Figure 4.8 Adsorption amount of Pb(II), Cu(II), and Zn(II) on RHAS-BEA and magnetic RHAS-BEA in single and mixed systems [35].

Table 4.4 Hydrated ionic diameters, hydration energy, and Pauling electronegativity of the studied heavy metals

Metal ion	Hydrated ionic diameter (nm) [24]	Hydration energy (kJ/mol) [63]	Pauling electronegativity [24]
Pb(II)	0.802	−1481	2.33
Cu(II)	0.838	−2100	1.9
Zn(II)	0.860	−2024	1.65

The hydrated ionic diameters of Pb(II), Cu(II), and Zn(II), shown in Table 4.4, are slightly bigger than the pore size of BEA, i.e., 0.76 × 0.64 nm. To enter the zeolite pore, the hydrated metal ions should have lost their water molecules to some extent. Exothermic hydration free energy of Pb(II) is much lower than that of Cu(II) and Zn(II). Therefore, hydration shell of Pb(II) ions is softer which should have stripped easier than that of Cu(II) and Zn(II) [64]. This means that hydrated ionic size of Pb(II) became sufficiently smaller to diffuse through the zeolite pore easily. The hydration energy of Zn(II) is slightly lower

than that of Cu(II), that means adsorbed amount of Zn(II) should have been little higher than that of Cu(II) in the mixed system. However, the experiments show the opposite result. This could be explained by the greater affinity between cationic charge center of hydrated Cu(II) and negatively charged adsorption site of zeolite due to the higher Pauling electronegativity of Cu(II) than that of Zn(II). Moreover, the greatest Pauling electronegativity of Pb(II) also supports this anticipation as it shows the highest adsorbed amount among them. In previous literatures, higher adsorption selectivity to Pb(II) over Cu(II) or Zn(II), and other divalent metal ions was also found in similar order for other zeolites including MOR [65], HEU [65], GIS [49,61], EDI [58], LTA [52], and FAU [24,44].

The interaction between metal ions and adsorbent surface was investigated using XPS. Figure 4.9, presents the survey scan that shows the detected binding energy (BE) of the main elemental composition of the pristine BEA and BEA/Fe_3O_4 composite such as Si2s, Si2p, Al2s, O1s, Na1s, and Fe2p. After adsorption, the peak of Na1s, that appeared at 1073 eV before adsorption, disappeared while that of Pb4f, Cu2p, and Zn2p were obviously found on the surface. This significantly reveals the evidence of the ion change between Na ions and those three metal ions that is predominant on the surface in the single and mixed ion systems.

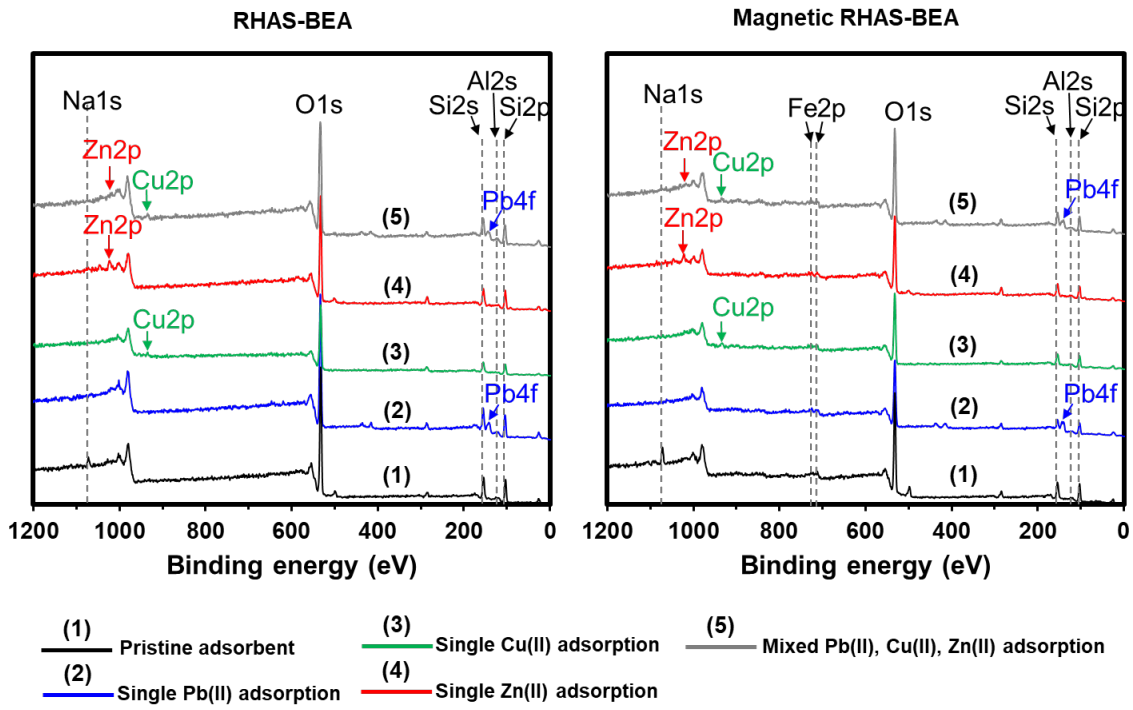

Figure 4.9 XPS Survey scan spectra of the pristine and Pb(II), Cu(II), and Zn(II) adsorbed RHAS-BEA and magnetic RHAS-BEA in single and mixed systems [35].

Higher resolution-XPS spectra (Figure 4.10) of the samples obtained from mixed ion system adsorption show two photoelectron peaks of Pb4f (i.e., $Pb4f_{7/2}$ and $Pb4f_{5/2}$ with BE values of ≈139 and 144 eV, respectively), two peaks of Cu2p (i.e., $Cu2p_{3/2}$ and $Cu2p_{1/2}$ with BE values of ≈932 and 953 eV, respectively), and one peak of $Zn2p_{3/2}$ with BE value of ≈1022 eV. These BE values indicate the evidence of +2 oxidation state of Pb [66], Cu [67], and Zn [68] adsorbed on the surface of RHAS-BEA and magnetic RHAS-BEA. According to the Si/Al ratios, the calculated available negatively charged Al amount of RHAS-BEA and magnetic RHAS-BEA were 0.68±0.01 and 0.65±0.01 mmol/g, respectively, which are theoretically equivalent to the adsorption capacity of ≈ 0.3 mmol/g for each divalent cation through ion exchange. The estimated value well matches with the Langmuir q_m values for Cu(II) and Zn(II) (Table 4.3). This suggested that the calculated ion exchange sites could have fully occupied by Cu(II) or Zn(II) ions through ion exchange, which accounts for the main adsorption mechanism for Cu(II) and Zn(II). However, the estimated Langmuir q_m values for Pb(II) was much lower than actual q_e value. In case of Pb(II), two main cationic

species, i.e, Pb^{2+} and $PbOH^{+}$ that probably exist at approximately 60 and 40% (pH ≈ 6), respectively [69], in the solution might involve in the ion exchange. Because the valance of $PbOH^{+}$ is reduced from +2 to +1, the adsorption amount can be doubled. However, even when we take into account the existence of this cation, it only contributes to ca. 50–60% of the actual q_e value of Pb(II), indicating that an additional different mechanisms to ion exchange is taking place. The found photoelectron peaks of Pb4f (≈ 139 and 144 eV) were also assigned to $Pb(OH)_2$ [23], implying that Pb(II) precipitated on the surface at certain amount. Moreover, BE values of Si2p and O1s shifted to the same direction after adsorption (Figure 4.11), indicating the interaction between metal ions and Si and O containing groups, probably, through surface complexation of the metal ions with silanol groups (–Si–OH) on zeolite [70]. Adsorption capacities of Pb(II) on RHAS-BEA and magnetic RHAS-BEA in this study were greater than that of Cu(II) and Zn(II) possibly owing to the effect of ionic species and precipitation.

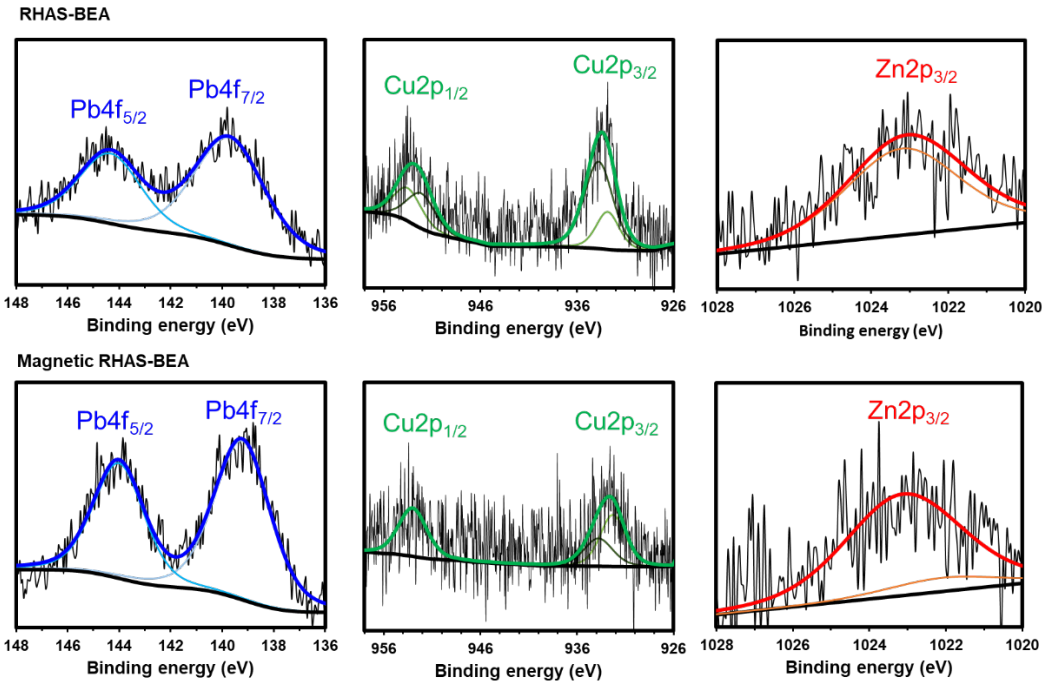

Figure 4.10 Higher resolution-XPS spectra of RHAS-BEA and magnetic RHAS-BEA obtained after mixed ion system adsorption of Pb(II), Cu(II), and Zn(II) [35].

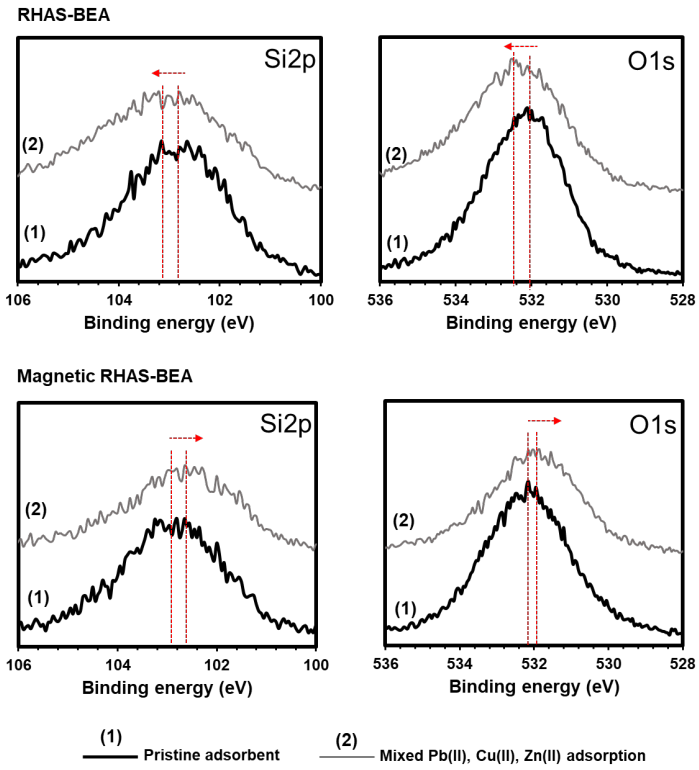

Figure 4.11 The Si2p and O1s XPS spectra of RHAS-BEA and magnetic RHAS-BEA obtained after mixed ion system adsorption of Pb(II), Cu(II), and Zn(II) [35].

4.5 Reusability and stability of the adsorbents

Ion exchange is believed to mainly occur during the adsorption; therefore, reusability of the adsorbents was studied by regenerating the used adsorbents using Na ion-containing solution. The used adsorbents were collected, dried (60 °C, 24 h), and subsequent washed using 5 mol/L $NaNO_3$ solution. After 48-h washing, the adsorbents were collected and washed with distilled water before drying at 60 °C for 24 h before reuse. Na ion solutions were commonly used in removal of exchanged cation from ion exchanger [33,45,49]. The reusability study was conducted in mixed ion system, containing 0.3 mmol/L of each heavy metal. Removal efficiency percentage calculated by

$$\text{Removal efficiency} = \frac{(C_0 - C_e) \times 100}{C_0}$$

where C_0 and C_e are the concentration of the heavy metal (mmol/L) before and after adsorption, respectively. Figure 4.12 shows the heavy metal removal efficiency in % of RHAS-BEA and magnetic RHAS-BEA in mixed ion system that were regenerated and reused for three cycles. The used RHAS-BEA and magnetic RHAS-BEA performance was found to significantly decrease after the first cycle; however, it still exhibited heavy metal removal efficiency to some extent for, at least, other three cycles.

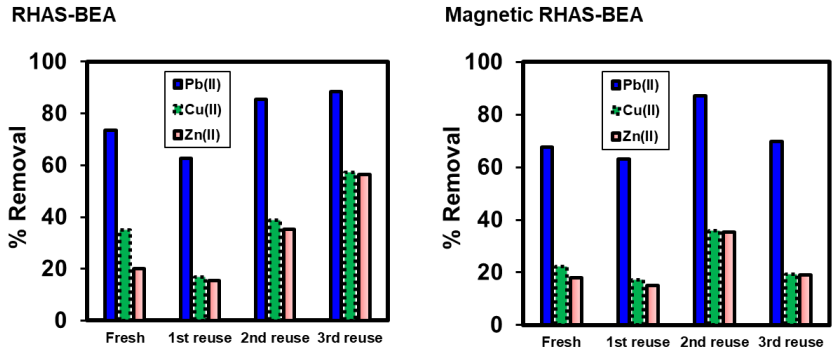

Figure 4.12 Pb(II), Cu(II), and Zn(II) removal efficiencies of RHAS-BEA and magnetic RHAS-BEA after 3-time reuses in mixed ion system [35].

Stability of the adsorbents was evaluated by analyzing Si, Al, and Fe leached to the solutions that were collected after some adsorption tests, using ICP-AES. Leaching of Si from the RHAS-BEA and magnetic RHAS-BEA was found after the first mixed ion system adsorption test by 0.7 and 0.4 wt% of the adsorbent mass, respectively, and slightly decreased in the following cycles. Detectable leaching of Al was found by 0.03 wt% of the adsorbent mass only after the first use of the RHAS-BEA sample before it became non-detectable in the following cycles. Leaching of Al was also found below the detection limit of ICP-AES after each adsorption cycle of the magnetic RHAS-BEA. However, the Si leaching was investigated more by measuring Si concentration in the final solutions collected after single ion adsorption (C_0 = 0.75 mmol/L). Concentration of Si found in the final Pb(II), Cu(II), and Zn (II) solution was 19.4, 6.3, and 7.2 mg/L, respectively for RHAS-BEA, and 9.5, 3.9, and 4.3 mg/L, respectively for magnetic RHAS-BEA. As seen that Si amount was found at higher concentration in the final Pb(II) solutions, while that for

Cu(II) and Zn(II) were at similar level. The measurement was additionally carried out in some of the final solutions obtained from the isotherm studies of Pb(II) and Zn(II) as the representatives. As shown in Figure 4.12, the increase and saturation trend of Si leached amount tended to be similar to that of the *q* values for both Pb(II) and Zn(II). Adsorption amount of Pb(II) was higher than that of Zn(II) and the Si leached amount was found in the same trend. From the results, leached amount of Si was likely to be consistent with the amount of metal ion adsorbed. Peric et al. [71] also reported the detected amount of Si during Pb(II), Cu(II), and Zn(II) adsorption on natural clinoptilolite which showed a similar trend to our finding. The leaching of Si corresponded to broken negatively charged Si–O–Al bonds due to their amphoteric property where cationic metal ion attached [71]. The dissolution was pronounced when Pb(II) was adsorbed in that Pb(II) has high Pauling ionic electronegativity (2.33) compared to Si (1.90) and Al (1.61) which destabilized Si–O–Al bonds by strongly pulling the electron of negatively charged O [24]. The leaching of Si from the adsorbents might have affected to the surface homogeneity and variation of Si/Al ratio to some extent, which might have caused the fluctuation in heavy metal removal efficiency of the reused adsorbents. For BEA/Fe_3O_4 composite sample, Fe was not detectable in the adsorption solution after each cycle.

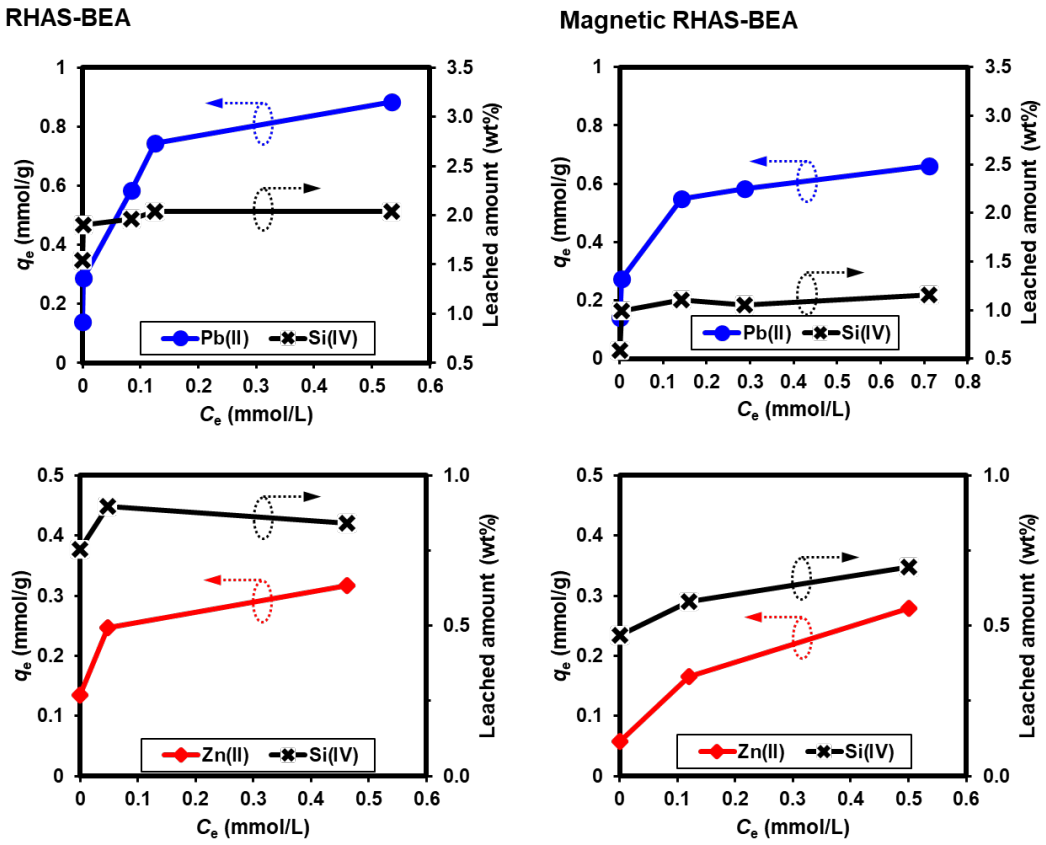

Figure 4.12 Leached amount of Si from the adsorbents and the q_e values of Pb(II) and Zn(II) [35].

Additionally, BE values of the two photoelectron peaks of Fe2p did not change after adsorption, revealing no interaction with the metal ions occurred. This implies that the magnetic particle was protected inside the BEA particles, preserving the magnetic properties of the adsorbent. Difference in the morphology at microscopic view of the adsorbents after first and fourth adsorption from the pristine ones, reobserved using FE-SEM, was hardly seen (Figure 4.13). The leaching amounts of Si and Al from the adsorbents were considered almost negligible which can be compensated by their reusability and the stable magnetic content.

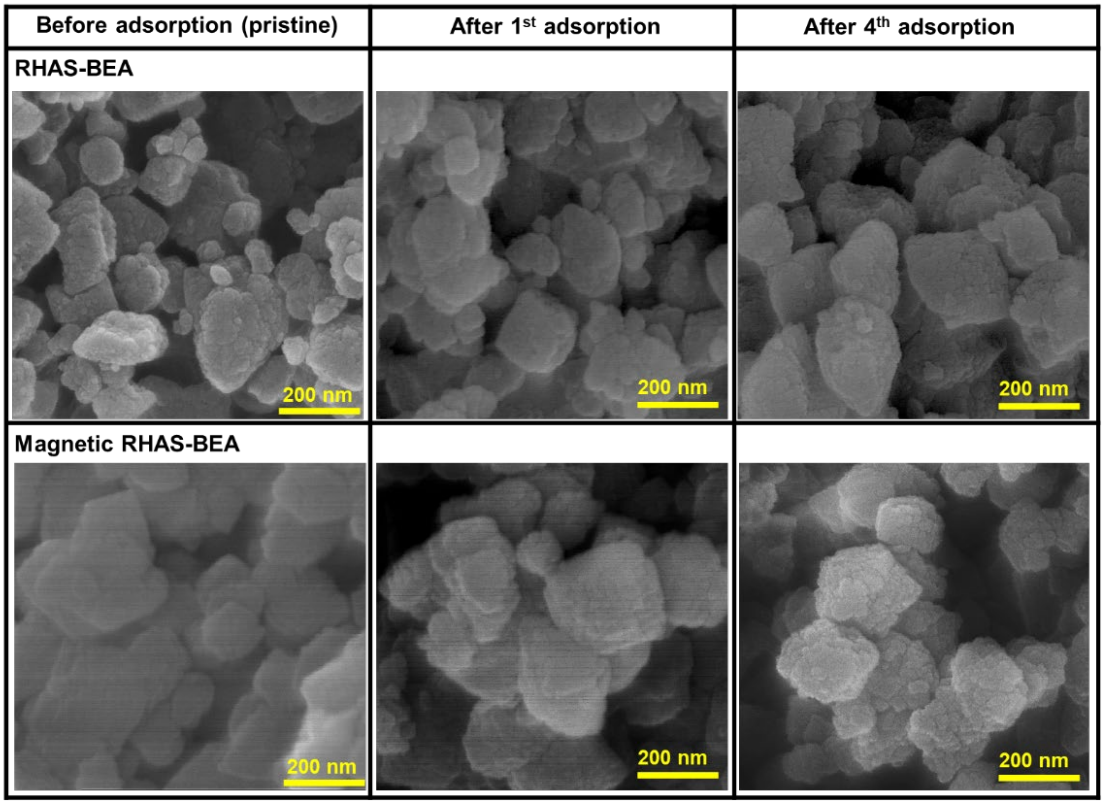

Figure 4.13 FE-SEM images of RHAS-BEA and magnetic RHAS-BEA observed before and after adsorption [35].

4.6 Conclusion

This work investigated the adsorption performance of magnetic RHAS-BEA that was synthesized using RHA-SiO_2 and DGC method for removal of heavy metals from water. The adsorption studies reveal moderate adsorption capacities compared to other reported zeolites for adsorption of three representative toxic heavy metals, i.e., Pb(II), Cu(II), Zn(II), that were mostly found in agrochemicals. The composite showed reusability to some extent with negligible changes in surface morphologies. This work may contribute to the sustainable utilization of magnetic zeolitic adsorbent that was synthesized using agricultural waste-derived materials and an environmentally friendly method in removal of cationic pollutants from agricultural wastewater.

Acknowledgement

This chapter was published in Solid State Sciences, 149, Vanpaseuth Phouthavong, Takeshi Hagio, Jae-Hyeok Park, Supinya Nijpanich, Kanchanok Duangkhai, Ratana Rujiravanit, Piyatida Thaveemas, Vanseng Chounlamany, Long Kong, Liang Li, Ryoichi Ichino, Removal of heavy metals by BEA zeolite/Fe_3O_4 composite prepared via dry-gel conversion method using agrowaste-derived raw material, 107473, Copyright Elsevier (2024). https://doi.org/10.1016/j.solidstatesciences.2024.107473.

References

[1] T.N. Dharmapriya, D.Y. Li, Y.C. Chung, P.J. Huang, Green synthesis of reusable adsorbents for the removal of heavy metal ions, ACS Omega 6 (2021) 30478–30487. https://doi.org/10.1021/acsomega.1c03879.

[2] A. Selvi, A. Rajasekar, J. Theerthagiri, A. Ananthaselvam, K. Sathishkumar, J. Madhavan, P.K.S.M. Rahman, Integrated remediation processes toward heavy metal removal/recovery from various environments-A review, Front. Environ. Sci. 7 (2019). https://doi.org/10.3389/fenvs.2019.00066.

[3] R. Sharma, P.R. Agrawal, R. Kumar, G. Gupta, Ittishree, Current scenario of heavy metal contamination in water, in: Contamination of Water: Health Risk Assessment and Treatment Strategies, Elsevier, 2021: pp. 49–64. https://doi.org/10.1016/B978-0-12-824058-8.00010-4.

[4] J.-Z. Ma, M. Zhang, Z.-G. Liu, M. Wang, Y. Sun, W.-K. Zheng, H. Lu, Copper-based-zinc-boron foliar fertilizer improved yield, quality, physiological characteristics, and microelement concentration of celery (*Apium graveolens L.*), Env. Pollut. Bioavail. 31 (2019) 261–271. https://doi.org/10.1080/26395940.2019.1668859.

[5] M.N.E. Alam, M.M. Hosen, A.K.M.A. Ullah, M.A. Maksud, S.R. Khan, L.N. Lutfa, T.R. Choudhury, S.B. Quraishi, Pollution characteristics, source identification, and health risk of heavy metals in the soil-vegetable system in two districts of

Bangladesh, Biol. Trace Elem. Res. 201 (2023) 4985–4999. https://doi.org/10.1007/s12011-023-03558-7.

[6] O.A. Ajala, M.R. Oke, T.F. Ajibade, F.O. Ajibade, B. Adelodun, J.O. Ighalo, M.O. Ajala, P. Kumar, H. Demissie, A.Y. Ugya, I.D. Sulaymon, L.F.O. Silva, Concentrations, bioaccumulation, and health risk assessments of heavy metals in fishes from Nigeria's freshwater: a general overview, , Environ. Sci. Pollut. Res. 29 (2022) 82660–82680. https://doi.org/10.1007/s11356-022-23390-1.

[7] J. Mateo-Sagasta, S.M. Zadeh, H. Turral, J. Burke, Water pollution from agriculture: a global review, The Food and Agriculture Organization of the United Nations (FAO), The International Water Management Institute (IWMI) (2017). https://www.fao.org/3/i7754e/i7754e.pdf (accessed September 18, 2023).

[8] E.C. Emenike, K.O. Iwuozor, S.U. Anidiobi, Heavy metal pollution in aquaculture: sources, impacts and mitigation techniques, Biol. Trace Elem. Res. 200 (2022) 4476–4492. https://doi.org/10.1007/s12011-021-03037-x.

[9] S. Mitra, A.J. Chakraborty, A.M. Tareq, T. Bin Emran, F. Nainu, A. Khusro, A.M. Idris, M.U. Khandaker, H. Osman, F.A. Alhumaydhi, J. Simal-Gandara, Impact of heavy metals on the environment and human health: novel therapeutic insights to counter the toxicity, J. King Saud Univ. Sci. 34 (2022) 101865. https://doi.org/https://doi.org/10.1016/j.jksus.2022.101865.

[10] M. Zaynab, R. Al-Yahyai, A. Ameen, Y. Sharif, L. Ali, M. Fatima, K.A. Khan, S. Li, Health and environmental effects of heavy metals, J. King Saud Univ. Sci. 34 (2022) 101653. https://doi.org/https://doi.org/10.1016/j.jksus.2021.101653.

[11] A. Alengebawy, S.T. Abdelkhalek, S.R. Qureshi, M.Q. Wang, Heavy metals and pesticides toxicity in agricultural soil and plants: Ecological risks and human health implications, Toxics 9 (2021) 1–34. https://doi.org/10.3390/toxics9030042.

[12] T. Adhikari, R.C. Gowda, R.H. Wanjari, M. Singh, Impact of continuous fertilization on heavy metals content in soil and food grains under 25 years of long-

term fertilizer experiment, Commun. Soil Sci. Plant Anal. 52 (2021) 389–405. https://doi.org/10.1080/00103624.2020.1854290.

[13] Agency for Toxic Substances and Disease Registry (ATSDR), U.S. Department of Health and Human Services, ATSDR's Substance Priority List, (2022). https://www.atsdr.cdc.gov/spl/index.html#2022spl (accessed September 8, 2023).

[14] R. Chakraborty, A. Asthana, A.K. Singh, B. Jain, A.B.H. Susan, Adsorption of heavy metal ions by various low-cost adsorbents: a review, Int. J. Environ. Anal. Chem. 102 (2022) 342–379. https://doi.org/10.1080/03067319.2020.1722811.

[15] R. Rashid, I. Shafiq, P. Akhter, M.J. Iqbal, M. Hussain, A state-of-the-art review on wastewater treatment techniques: the effectiveness of adsorption method, Environ. Sci. Pollut. Res. 28 (2021) 9050–9066. https://doi.org/10.1007/s11356-021-12395-x.

[16] M. Kumar, A. Seth, A.K. Singh, M.S. Rajput, M. Sikandar, Remediation strategies for heavy metals contaminated ecosystem: A review, Environ. Sustain. Indic. 12 (2021) 100155. https://doi.org/https://doi.org/10.1016/j.indic.2021.100155.

[17] Renu, M. Agarwal, K. Singh, Heavy metal removal from wastewater using various adsorbents: a review, J. Water Reuse Desalin. 7 (2016) 387–419. https://doi.org/10.2166/wrd.2016.104.

[18] A. Bashir, L.A. Malik, S. Ahad, T. Manzoor, M.A. Bhat, G.N. Dar, A.H. Pandith, Removal of heavy metal ions from aqueous system by ion-exchange and biosorption methods, Environ. Chem. Lett. 17 (2019) 729–754. https://doi.org/10.1007/s10311-018-00828-y.

[19] T. Derbe, S. Temesgen, M. Bitew, A short review on synthesis, characterization, and applications of zeolites, Adv. Mater. Sci. Eng. 2021 (2021). https://doi.org/10.1155/2021/6637898.

[20] E. Erdem, N. Karapinar, R. Donat, The removal of heavy metal cations by natural zeolites, J. Colloid Interface Sci. 280 (2004) 309–314. https://doi.org/https://doi.org/10.1016/j.jcis.2004.08.028.

[21] K.D. Mondale, R.M. Carland, F.F. Aplan, The comparative ion exchange capacities of natural sedimentary and synthetic zeolites, Miner. Eng. 8 (1995) 535–548. https://doi.org/https://doi.org/10.1016/0892-6875(95)00015-I.

[22] L. Roshanfekr Rad, M. Anbia, Zeolite-based composites for the adsorption of toxic matters from water: A review, J. Environ. Chem. Eng. 9 (2021). https://doi.org/10.1016/j.jece.2021.106088.

[23] M. Medykowska, M. Wiśniewska, K. Szewczuk-Karpisz, R. Panek, Interaction mechanism of heavy metal ions with the nanostructured zeolites surface – Adsorption, electrokinetic and XPS studies, J. Mol. Liq. 357 (2022) 119144. https://doi.org/https://doi.org/10.1016/j.molliq.2022.119144.

[24] X. Fan, H. Liu, E. Anang, D. Ren, Effects of electronegativity and hydration energy on the selective adsorption of heavy metal ions by synthetic nax zeolite, Materials 14 (2021). https://doi.org/10.3390/ma14154066.

[25] T.O. Bok, E.P. Andriako, E.E. Knyazeva, I.I. Ivanova, Engineering of zeolite BEA crystal size and morphology: via seed-directed steam assisted conversion, RSC Adv. 10 (2020) 38505–38514. https://doi.org/10.1039/d0ra07610d.

[26] A. Marino, E. Catizzone, M. Migliori, G. Ferrarelli, A. Aloise, D. Chillè, G. Papanikolaou, P. Lanzafame, S. Perathoner, G. Centi, G. Giordano, Hydrothermal synthesis and catalytic assessment of high-silica (B,Fe)-beta zeolites, Cryst. Growth Des. 23 (2023) 2988–3001. https://doi.org/10.1021/acs.cgd.3c00085.

[27] J. Li, M. Gao, W. Yan, J. Yu, Regulation of the Si/Al ratios and Al distributions of zeolites and their impact on properties, Chem. Sci. 14 (2022) 1935–1959. https://doi.org/10.1039/d2sc06010h.

[28] V. Phouthavong, M. Hiraiwa, T. Hagio, S. Nijpanich, V. Chounlamany, T. Nishihama, Y. Kamimoto, R. Ichino, Magnetic BEA-type zeolites: preparation by dry-gel conversion method and assessment of dye removal performance, J. Mater. Cycles Waste Manag. 22 (2020) 375–382. https://doi.org/10.1007/s10163-020-00994-8.

[29] Z.-L. Cheng, Y. Li, Z. Liu, Study on adsorption of rhodamine B onto Beta zeolites by tuning SiO_2/Al_2O_3 ratio, Ecotoxicol. Environ. Saf. 148 (2018) 585–592. https://doi.org/https://doi.org/10.1016/j.ecoenv.2017.11.005.

[30] M. Rakanović, A. Vukojević, M.M. Savanović, S. Armaković, S. Pelemiš, F. Živić, S. Sladojević, S.J. Armaković, Zeolites as adsorbents and photocatalysts for removal of dyes from the aqueous environment, Molecules 27 (2022). https://doi.org/10.3390/molecules27196582.

[31] V. Phouthavong, T. Hagio, J.-H. Park, S. Nijpanich, T. Srihirunthanon, N. Chantanurak, K. Duangkhai, R. Rujiravanit, V. Chounlamany, K. Phomkeona, L. Kong, L. Li, R. Ichino, Utilization of agricultural waste to herbicide removal: Magnetic BEA zeolite adsorbents prepared by dry-gel conversion using rice husk ash–derived SiO2 for paraquat removal, Arab. J. Chem. 16 (2023) 104959. https://doi.org/https://doi.org/10.1016/j.arabjc.2023.104959.

[32] W. Rongchapo, O. Sophiphun, K. Rintramee, S. Prayoonpokarach, J. Wittayakun, Paraquat adsorption on porous materials synthesized from rice husk silica, Water Sci. Technol. 68 (2013) 863–869. https://doi.org/10.2166/wst.2013.311.

[33] L.M. Pratti, G.M. Reis, F.S. dos Santos, G.R. Gonçalves, J.C.C. Freitas, M.K. de Pietre, Effects of textural and chemical properties of β-zeolites on their performance as adsorbents for heavy metals removal, Environ. Earth Sci. 78 (2019). https://doi.org/10.1007/s12665-019-8568-6.

[34] S. Motlagh Bahadory Esfahani, H. Faghihian, Modification of synthesized β-zeolite by ethylenediamine and monoethanolamine for adsorption of Pb^{2+}, J. Water Process Eng. 3 (2014) 62–66. https://doi.org/https://doi.org/10.1016/j.jwpe.2014.05.007.

[35] V. Phouthavong, T. Hagio, J.-H. Park, S. Nijpanich, K. Duangkhai, R. Rujiravanit, P. Thaveemas, V. Chounlamany, L. Kong, L. Li, R. Ichino, Removal of heavy metals by BEA zeolite/Fe_3O_4 composite prepared via dry-gel conversion method using agrowaste-derived raw material, Solid State Sci. 149 (2024) 107473. https://doi.org/https://doi.org/10.1016/j.solidstatesciences.2024.107473.

[36] L. Largitte, R. Pasquier, A review of the kinetics adsorption models and their application to the adsorption of lead by an activated carbon, Chem. Eng. Res. Des. 109 (2016) 495–504. https://doi.org/https://doi.org/10.1016/j.cherd.2016.02.006.

[37] D. Robati, Pseudo-second-order kinetic equations for modeling adsorption systems for removal of lead ions using multi-walled carbon nanotube, J. Nanostructure Chem. 3 (2013) 55. https://doi.org/10.1186/2193-8865-3-55.

[38] T. Sheela, Y.A. Nayaka, R. Viswanatha, S. Basavanna, T.G. Venkatesha, Kinetics and thermodynamics studies on the adsorption of Zn(II), Cd(II) and Hg(II) from aqueous solution using zinc oxide nanoparticles, Powder Technol. 217 (2012) 163–170. https://doi.org/https://doi.org/10.1016/j.powtec.2011.10.023.

[39] A.E.D. Mahmoud, K.M. Al-Qahtani, S.O. Alflaij, S.F. Al-Qahtani, F.A. Alsamhan, Green copper oxide nanoparticles for lead, nickel, and cadmium removal from contaminated water, Sci. Rep. 11 (2021) 12547. https://doi.org/10.1038/s41598-021-91093-7.

[40] C. Duan, T. Ma, J. Wang, Y. Zhou, Removal of heavy metals from aqueous solution using carbon-based adsorbents: A review, J. Water Process Eng. 37 (2020) 101339. https://doi.org/https://doi.org/10.1016/j.jwpe.2020.101339.

[41] G. Lin, B. Zeng, J. Li, Z. Wang, S. Wang, T. Hu, L. Zhang, A systematic review of metal organic frameworks materials for heavy metal removal: Synthesis, applications and mechanism, Chem. Eng. J. 460 (2023) 141710. https://doi.org/https://doi.org/10.1016/j.cej.2023.141710.

[42] J. Febrianto, A.N. Kosasih, J. Sunarso, Y.-H. Ju, N. Indraswati, S. Ismadji, Equilibrium and kinetic studies in adsorption of heavy metals using biosorbent: a

summary of recent studies, J. Hazard. Mater. 162 (2009) 616–645. https://doi.org/https://doi.org/10.1016/j.jhazmat.2008.06.042.

[43] A.N. Doyo, R. Kumar, M.A. Barakat, Recent advances in cellulose, chitosan, and alginate based biopolymeric composites for adsorption of heavy metals from wastewater, J. Taiwan Inst. Chem. Eng. 151 (2023) 105095. https://doi.org/https://doi.org/10.1016/j.jtice.2023.105095.

[44] K.J. Shah, J. Yu, T. Zhang, Z. You, Y-Type Zeolite synthesized from an illite applied for removal of Pb(II) and Cu(II) ions from aqueous solution: Box-Behnken design and kinetics, Water (Switzerland). 15 (2023). https://doi.org/10.3390/w15061171.

[45] R. Chanda, M. Hosain, S.A. Sumi, M. Sultana, S. Islam, B.K. Biswas, Removal of chromium (VI) and lead (II) from aqueous solution using domestic rice husk ash-(RHA-) based zeolite faujasite, Adsorpt. Sci. Technol. 2022 (2022) 4544611. https://doi.org/10.1155/2022/4544611.

[46] I. V Joseph, L. Tosheva, A.M. Doyle, Simultaneous removal of Cd(II), Co(II), Cu(II), Pb(II), and Zn(II) ions from aqueous solutions via adsorption on FAU-type zeolites prepared from coal fly ash, J. Environ. Chem. Eng. 8 (2020) 103895. https://doi.org/https://doi.org/10.1016/j.jece.2020.103895.

[47] A.H. Ibrahim, X. Lyu, A.B. ElDeeb, Synthesized zeolite based on Egyptian boiler ash residue and kaolin for the effective removal of heavy metal ions from industrial wastewater, Nanomaterials. 13 (2023). https://doi.org/10.3390/nano13061091.

[48] L.C.A. Oliveira, D.I. Petkowicz, A. Smaniotto, S.B.C. Pergher, Magnetic zeolites: a new adsorbent for removal of metallic contaminants from water, Water Res. 38 (2004) 3699–3704. https://doi.org/https://doi.org/10.1016/j.watres.2004.06.008.

[49] M. Chen, S. Nong, Y. Zhao, M.S. Riaz, Y. Xiao, M.S. Molokeev, F. Huang, Renewable P-type zeolite for superior absorption of heavy metals: isotherms, kinetics, and mechanism, Sci. Total Environ. 726 (2020) 138535. https://doi.org/https://doi.org/10.1016/j.scitotenv.2020.138535.

[50] R. Panek, M. Medykowska, K. Szewczuk-Karpisz, M. Wisniewska, Comparison of physicochemical properties of fly ash precursor, Na-P1(C) zeolite–carbon composite and Na-P1 zeolite—adsorption affinity to divalent Pb and Zn cations, Materials. 14 (2021). https://doi.org/10.3390/ma14113018.

[51] M. Hong, L. Yu, Y. Wang, J. Zhang, Z. Chen, L. Dong, Q. Zan, R. Li, Heavy metal adsorption with zeolites: the role of hierarchical pore architecture, Chem. Eng. J. 359 (2019) 363–372. https://doi.org/https://doi.org/10.1016/j.cej.2018.11.087.

[52] Y. Lv, B. Ma, Y. Liu, C. Wang, Y. Chen, Adsorption behavior and mechanism of mixed heavy metal ions by zeolite adsorbent prepared from lithium leach residue, Microporous Mesoporous Mater. 329 (2022) 111553. https://doi.org/https://doi.org/10.1016/j.micromeso.2021.111553.

[53] K. Nakamoto, M. Ohshiro, T. Kobayashi, Mordenite zeolite—Polyethersulfone composite fibers developed for decontamination of heavy metal ions, J. Environ. Chem. Eng. 5 (2017) 513–525. https://doi.org/https://doi.org/10.1016/j.jece.2016.12.031.

[54] G.M.P. Kumara, K. Kawamoto, Use of natural zeolite and its mixtures to refine high-concentrated heavy metal-contaminated wastewater: an investigation of simultaneous removal of Cd (II) and Pb (II) by batch adsorption method, Water Air Soil Pollut. 232 (2021) 463. https://doi.org/10.1007/s11270-021-05420-9.

[55] M. Yuan, T. Xie, G. Yan, Q. Chen, L. Wang, Effective removal of Pb2+ from aqueous solutions by magnetically modified zeolite, Powder Technol. 332 (2018) 234–241. https://doi.org/https://doi.org/10.1016/j.powtec.2018.03.043.

[56] T. Bakalár, H. Pavolová, K. Kyšeľa, Z. Hajduová, Characterization of Cu(II) and Zn(II) sorption onto zeolite, Crystals (Basel). 12 (2022). https://doi.org/10.3390/cryst12070908.

[57] M. Senila, E. Neag, O. Cadar, E.D. Kovacs, I. Aschilean, M.H. Kovacs, Simultaneous removal of heavy metals (Cu, Cd, Cr, Ni, Zn and Pb) from aqueous

solutions using thermally treated Romanian zeolitic volcanic tuff, Molecules. 27 (2022). https://doi.org/10.3390/molecules27123938.

[58] X. Zhang, T. Cheng, C. Chen, L. Wang, Q. Deng, G. Chen, C. Ye, Synthesis of a novel magnetic nano-zeolite and its application as an efficient heavy metal adsorbent, Mater. Res. Express. 7 (2020) 085007. https://doi.org/10.1088/2053-1591/abab43.

[59] I.W. Nah, K.-Y. Hwang, C. Jeon, H.B. Choi, Removal of Pb ion from water by magnetically modified zeolite, Miner. Eng. 19 (2006) 1452–1455. https://doi.org/https://doi.org/10.1016/j.mineng.2005.12.006.

[60] D.A. Fungaro, J.E.A. Graciano, Adsorption of zinc ions from water using zeolite/iron oxide composites, Adsorpt. Sci. Technol. 25 (2007) 729–740. https://doi.org/10.1260/026361707785284185.

[61] A.F. Ankrah, B. Tokay, C.E. Snape, Heavy metal removal from aqueous solutions using fly-ash derived zeolite NaP1, Int. J. Environ. Res. 16 (2022) 17. https://doi.org/10.1007/s41742-022-00395-9.

[62] P.K. Pandey, S.K. Sharma, S.S. Sambi, Removal of lead(II) from waste water on zeolite-NaX, J. Environ. Chem. Eng. 3 (2015) 2604–2610. https://doi.org/https://doi.org/10.1016/j.jece.2015.09.008.

[63] M. Panayotova, B. Velikov, Kinetics of heavy metal ions removal by use of natural zeolite, J. Environ. Sci. Health A. 37 (2002) 139–147. https://doi.org/10.1081/ESE-120002578.

[64] O. Allahdin, N. Poumaye, M. Wartel, A. Boughriet, Correlation analysis between cationic metal characteristics and ion-exchange performance of brick-derived zeolites: A comprehensive mechanistic explanation, Mater. Chem. Phys. 276 (2022) 125353. https://doi.org/https://doi.org/10.1016/j.matchemphys.2021.125353.

[65] G. Yuan, H. Seyama, M. Soma, B.K.G. Theng, A. Tanaka, Adsorption of some heavy metals by natural zeolites: XPS and batch studies, J. Environ. Sci. Health A. 34 (1999) 625–648. https://doi.org/10.1080/10934529909376856.

[66] Y. Adachi, N. Hatada, A. Kuramitsu, T. Uda, Exploration of dopant species for lanthanum polyphosphate, J. Electrochem. Soc. 162 (2015) F596. https://doi.org/10.1149/2.0821506jes.

[67] D.M. de los Santos, S. Chahid, R. Alcántara, J. Navas, T. Aguilar, J.J. Gallardo, R. Gómez-Villarejo, I. Carrillo-Berdugo, C. Fernández-Lorenzo, MoS2/Cu/TiO_2 nanoparticles: synthesis, characterization and effect on photocatalytic decomposition of methylene blue in water under visible light, Water Sci. Technol. 2017 (2018) 184–193. https://doi.org/10.2166/wst.2018.101.

[68] Y. Kim, S. Kim, K. Nahm, M. Kang, Dynamic rapid synthesis of bis(2,2'-bipyridine)nitrato zinc (II) nitrate using a microwave method and its application to Dye-Sensitized Solar Cells (DSSC), Bull. Korean Chem. Soc. 31 (2010) 2923–2928. https://doi.org/10.5012/bkcs.2010.31.10.2923.

[69] Y. Liang, M. Jun, W. Liu, Enhanced removal of lead(II) and cadmium(II) from water in alum coagulation by ferrate(VI) pretreatment, Water Environ. Res. 79 (2007) 2420–2426. https://doi.org/https://doi.org/10.2175/106143007X212148.

[70] N.S. Inchaurrondo, J. Font, Clay, Zeolite and oxide minerals: natural catalytic materials for the ozonation of organic pollutants, Molecules. 27 (2022). https://doi.org/10.3390/molecules27072151.

[71] J. Perić, M. Trgo, N. Vukojević Medvidović, Removal of zinc, copper and lead by natural zeolite - a comparison of adsorption isotherms, Water Res. 38 (2004) 1893–1899. https://doi.org/10.1016/j.watres.2003.12.035.

CHAPTER 5

Conclusion

This dissertation demonstrated the sustainable circulation of materials in agricultural activities. Agricultural waste-derived materials, RHAS, was utilized as a low-cost and alternative source of SiO_2 in DGC method for developing a sustainable and environmentally friendly synthesis method of magnetic BEA zeolite composite. Performance of the composite for removing diverse pollutants from water that are potentially released from utilization of agrochemicals, i.e., antibiotics, herbicides, and heavy metals, during agricultural activities were studied. The following findings were obtained.

(i) **Dry-gel conversion synthesis of magnetic BEA zeolite: optimization of synthesis conditions and assessment of antibiotic adsorption.** The optimal DGC conditions, i.e., H_2O/gel ratio, crystallization temperature and time, were studied for preparation of magnetic BEA zeolite. Effect of template removal temperature on the magnetic properties of the composite were also investigated. By using the optimal conditions, magnetic BEA zeolite was obtained without the adverse effect from the incorporation of magnetic particles. The magnetic zeolite composite prepared by DGC method was tested for removal of antibiotics, i.e., sulfadiazine, from water, which potentially shows high feasibility for removal of antibiotics from agricultural wastewater.

(ii) **Using rice husk ash–SiO_2 in dry-gel conversion synthesis of magnetic BEA zeolite: assessment of herbicide removal.** The studied optimal DGC conditions were applied in this work for direct utilization of solid-state RHAS in the synthesis of magnetic RHAS-BEA. With the assistance of ultrasonic waves in the preparation of gel precursor, magnetic RHAS-BEA was successfully obtained. The inclusion of magnetic particles (Fe_3O_4) did not significantly change that surface morphology of the zeolite. The method shows sustainability and environmentally friendliness in the preparation of magnetically collectable and reusable magnetic BEA zeolite for removal of cationic herbicides, i.e., paraquat, from water.

(iii) **Removal of heavy metals from water using magnetic BEA zeolite prepared using rice husk ash-SiO_2 via DGC method.** This work evaluated the adsorption performance of the synthesized magnetic RHAS-BEA for removal of heavy metals from water, i.e., Pb(II), Cu(II), and Zn(II). The magnetic composite shows moderate adsorption capacities of the representative heavy metals with potential numbers of reuse and stability after several adsorption cycles. This work emphasizes the sustainability of using magnetic RHAS-BEA in the remediation of wastewater affected from the use of heavy metal-contained agrochemicals.

In conclusion, agricultural waste-derived materials can be directly used in DGC route for developing a sustainable and environmentally friendly synthesis method of magnetic zeolite composite. The synthesized magnetic zeolite composite showed good adsorption ability, magnetic separability, and reusability in minimizing diverse agrochemical contamination in water, i.e., antibiotics, herbicides, and heavy metals. This work shall pave the way for realizing sustainable material circulation in agriculture which can be hopefully implemented, not only in Laos or Japan but in entire global communities, in practical minimization of water pollution.

ACHIEVEMENTS

1. Main achievements

Publications

1) **V. Phouthavong**, R. Yan, S. Nijpanich, T. Hagio, R. Ichino, L. Kong, L. Li, Magnetic adsorbents for wastewater treatment: advancements in their synthesis methods, Materials 15 (2022) 1053. (Review article, Published)
2) **V. Phouthavong**, T. Hagio, S. Nijpanich, J.H. Park, M. Hiraiwa, T. Srihirunthanon, N. Chantanurak, R. Rujiravanit, Y. Kamimoto, X. Li, L. Kong, L. Li, R. Ichino, Dry-gel conversion synthesis of magnetic BEA-type zeolites for antibiotics adsorption, J. Sol-Gel Sci. Technol. 105 (2023) 511–524. (Original article, Published)
3) **V. Phouthavong**, T. Hagio, J.H. Park, S. Nijpanich, T. Srihirunthanon, N. Chantanurak, K. Duangkhai, R. Rujiravanit, V. Chounlamany, K. Phomkeona, L. Kong, L. Li, R. Ichino, Utilization of agricultural waste to herbicide removal: Magnetic BEA zeolite adsorbents prepared by dry-gel conversion using rice husk ash–derived SiO_2 for paraquat removal, Arab. J. Chem. 16 (2023) 104959. (Original article, Published)
4) **V. Phouthavong**, T. Hagio, J.H. Park, S. Nijpanich, K. Duangkhai, R. Rujiravanit, P. Thaveemas, V. Chounlamany, L. Kong, L. Li, R. Ichino, Removal of heavy metals by BEA zeolite/Fe_3O_4 composite prepared via dry-gel conversion method using agrowaste-derived raw material, Solid State Sci. 149 (2024) 107473. (Original article, Published)

Conferences

1) **V. Phouthavong**, S. Nijpanich, T. Hagio, M. Hiraiwa, T. Srihirunthanon, N. Chantanurak, K. Duangkhai, R. Rujiravanit, Y. Kamimoto, R. Ichino, Magnetic zeolites prepared by dry-gel conversion method and their possibilities for environmental remediation applications. Japan, INTERFINISH2020, September 6-8, 2021. (Online oral presentation)
2) **V. Phouthavong**, T. Hagio, S. Nijpanich, M. Hiraiwa, T. Srihirunthanon, N. Chantanurak, R. Rujiravanit, L. Kong, L. Li, Y. Kamimoto, R. Ichino, Magnetic BEA-

type zeolite synthesized via dry-gel conversion method: studies on its synthesis conditions and antibiotics adsorption performance. The 8th 3R International Scientific Conference (3RINCs2022), held Online, March 14-18, 2022. (Online oral presentation).

3) **V. Phouthavong**, T. Hagio, S. Nijpanich, M. Hiraiwa, T. Srihirunthanon, N. Chantanurak, R. Rujiravanit, L. Kong, L. Li, Y. Kamimoto, R. Ichino, Environmental remediation by application of zeolite/magnetite composites prepared by dry-gel conversion. The 1st Campus Asia Workshop, organized by Nagoya University, Nagoya, Japan, March 22-23, 2022. (Online poster presentation)
4) **V. Phouthavong**, T. Hagio, J.H. Park, S. Nijpanich, T. Srihirunthanon, N. Chantanurak, K. Duangkhai, R. Rujiravanit, V. Chounlamany, K. Phomkeona, L. Kong, L. Li, R. Ichino, Agrowaste-derived magnetic zeolite prepared by dry-gel conversion: herbicide removal. The 33rd Annual Meeting of MRS-Japan 2023, Yokohama, Japan, November 14-16, 2023. (On-site poster presentation)

Awards

Student Award from the oral presentation at the 20th Interfinish World Congress, 2020, Japan.

2. Other achievements

Publications

1) **V. Phouthavong**, J.H. Park, T. Nishihama, S. Yoshida, T. Hagio, Y. Kamimoto, R. Ichino, Amine-modified small pore mesoporous silica as potential adsorbent for Zn removal from plating wastewater. Coatings 12 (2022) 1258. (Published)
2) J.H. Park, Y. Fujita, T. Hagio, **V. Phouthavong**, Y. Kamimoto, T. Bessho, R. Ichino, Preliminary study on electrodeposition of copper platings and codeposition of carbon nanotubes from organic solvent, Coatings 13 (2023) 802. (Published)
3) S. Wada, T. Hagio, H. Kunishi, **V. Phouthavong**, J.H. Park, Y. Yamada, T. Terao, X. Li, S. Nijpanich, R. Ichino, Gas permeation properties of c-plane aligned hexagonal tungsten oxide membranes formed by multi-stage synthesis. J. Korean Ceram. Soc. 60 (2023) 967–978. (Published)

4) T. Hagio, H. Kunishi, S. Wada, T. Terao, S. Kinoshita, **V. Phouthavong**, S. Nijpanich, J.H. Park, R. Ichino, Potential of C-plane aligned hexagonal tungsten oxide film as a molecular sieve-type separation membrane. Zeolite 41 (2024) 9–19. (Article in Japanese, Published)

Conferences

1) R. Ichino, H. Suzuki, **V. Phouthavong**, Removal of zinc from multi-cation systems using magnetic layered sodium titanates. Strategic International Collaborative Research Program (SICORP), International Joint Research Innovation Center, Japan-China Energy-Environmental CORE: Japan-China E2C with Campus Asia (for education), Joint Symposium 2022. Nagoya University Green Vehicle Materials Research Center, September 12-13, 2022. (Online oral presentation)

ACKNOWLEDGEMENT

Firstly, I would like to deeply express my sincere gratitude to the most important people, Prof. Ryoichi ICHINO, my academic supervisor, and Assist. Prof. Takeshi HAGIO for their unlimited support, reviewing my progress constantly, and unconditional guidance during my doctoral course. Without them I will not be here.

Again, I would like to additionally thank Assist. Prof. Takeshi HAGIO for his super kind help and patience not only on my studies but my daily life as well. My life and study in Japan would be definitely difficult without his help.

A special thanks to Assist. Prof. Jae-Hyeok PARK for his generous assistance and guidance on operating advanced instruments.

I would like to gratefully acknowledge Yoshida Scholarship Foundation for the doctoral scholarship and Kyosho Hatta Foundation for the grant support during my PhD studies.

Finally, I would like to thank my parents for their continued love and support.